QUANTIFICATION OF ENERGY DEMAND FOR BUCKLING-RESTRAINED BRACES

by

Muhib Muazzam

B.Sc., Ahsanullah University of Science and Technology, 2013

A THESIS SUBMITTED IN PARTIAL FULFILLMENT OF

THE REQUIREMENTS FOR THE DEGREE OF

MASTER OF APPLIED SCIENCE

in

THE FACULTY OF GRADUATE AND POSTDOCTORAL STUDIES

(Civil Engineering)

THE UNIVERSITY OF BRITISH COLUMBIA

(Vancouver)

November 2019

The following individuals certify that they have read, and recommend to the Faculty of Graduate and Postdoctoral Studies for acceptance, a thesis/dissertation entitled:

Quantification of Energy Demand for Buckling-Restrained Braces

submitted by Muhib Muazzam in partial fulfillment of the requirements for

the degree of Master of Applied Science

in Civil Engineering

Examining Committee:

Dr. Tsung-Yuan Yang
Supervisor

Dr. Svetlana Brzev
Additional Examiner

Abstract

Buckling Restrained Brace (BRB) is a novel energy dissipation device that was developed in the 1980s. Past experimental investigations were performed by using deformation-related parameters such as drift and ductility-based loading history to evaluate the performance of the BRBs. The outcome of the performance evaluation of the BRBs was based on either the ability of the BRBs against the fracture or its ability to sustain axial deformation, as opposed to evaluating the energy demand of the BRBs during earthquake excitation. A novel approach was proposed to explicitly quantify the energy demand of the BRBs during earthquakes. First, an equation was proposed to determine energy demand from the site-specific design spectrum. After that, floor-wise energy distribution was proposed based on empirical equations. Finally, equations to obtain rise time for the energy demand for the BRB were proposed. Engineers can use the equations to quantify the energy demand for BRBs at different floors at different site locations. The empirical equations were obtained by studying a range of single-degree-of-freedom systems and a series of prototype buildings with 3, 6 and 8 storeys. The proposed equations were used to quantify the seismic demand of the BRBs in a 5-storey configuration. The results show that the energy demand obtained by applying the proposed method is similar to the median demand obtained from the time history analysis. The results show that the proposed procedure is effective and efficient for quantifying the energy demand for buildings with BRBs.

Lay Summary

Buckling Restrained Braces (BRBs) are commonly used in buildings to resist the consequences of earthquake shaking. In this study, a novel approach was proposed to quantify energy demand in BRBs for buildings with different configurations at different site locations. The proposed empirical equations were verified on a typical 5-storey building. The results show that the proposed equations can be used to calculate the BRB demand in different site locations.

Preface

This thesis is original, unpublished work by Muhib Muazzam. The author was responsible for implementing, analyzing, documenting, and discussing all aspects of the presented research except where noted otherwise. Parts of this thesis are being reworked into a peer-reviewed journal paper.

Table of Contents

List of Tables

List of Figures

List of Symbols

A = Area

E = Modulus of Elasticity

F_y = Yield Strength (Stress) of Steel

b = Strain Hardening Ratio

ε_y = Yield Strain of Steel

P_y = Global Yield Force

Δ_y = Global Yield Deformation

Δ_{mon} = Deformation at Failure from Monotonic Test

Δ_m = Maximum Deformation

Δ_o = Smallest Deformation

q = Force

δ = Deformation

q_y = Local Yield Force or BRB Yield Force

δ_y = Local Yield Deformation or BRB Yield Deformation

θ = Angle or Story Drift Angle

m = Mass

M_w = Moment Magnitude

R_{jb} = Closest Distance to Surface Projection of Rupture

S_{DS} = The Design Spectral Response Acceleration Parameter in the Short Period Range

S_{D1} = The Design Spectral Response Acceleration Parameter at 1 second Period

S_a = Spectral Acceleration from Site-specific Spectrum

S_d = Spectral Displacement from Site-specific Spectrum

T = Fundamental Period of a System

R = Response Modification Coefficient

γ_{lp} = Energy Quantification Factor

t_R = Rise Time

E_i = Input Energy

E_d = Dissipated Energy

List of Abbreviations

AISC = American Institute of Steel Construction

ASCE = American Society of Civil Engineers

ATC = Applied Technology Council

BRB = Buckling-Restrained Brace

CP = Collapse Prevention

CUREE = Consortium of Universities for Research in Earthquake Engineering

CUREe = California Universities for Research in Earthquake Engineering

DBE = Design-Basis Earthquake

EEDP = Equivalent Energy Design Procedure

ESFP/ELFP = Equivalent Static Force Procedure/ Equivalent Lateral Force Procedure

HSF = Honeycomb Structural Fuse

HSS = Hollow Steel Section

IO = Immediate Occupancy

MCE = Maximum Considered Earthquake

MDOF = Multiple Degree of Freedom

MRF = Moment Resisting Frame

OpenSees = Open System for Earthquake Engineering Simulation

PBPD = Performance-Based Plastic Design

PEER = Pacific Earthquake Engineering Research

RR = Rapid Return

SAC = Joint venture of **S**EAOC, **A**TC and **C**UREe

SDOF = Single Degree of Freedom

SEAOC = Structural Engineers Association of California

SFRS = Seismic Force-Resisting System

SLE = Service Level Earthquake

WWFF = Welded Wide Flange Fuse

Acknowledgements

Any thesis requires contributions from one's parents, friends, colleagues, and faculty. The progression of this research is also the result of many such contributors. I would like to thank all those individuals who helped me complete it.

First and foremost, I would like to thank my research supervisor, Dr. Tony T.Y. Yang. His wisdom and patience have guided me throughout this research project. I am grateful to Dr. Svetlana Brzev for her guidance. Without her time and consideration, I would not be able to learn how to develop a research document. Finally, I am grateful to thousands of discussions with my research colleagues, Dr. Dorian Tung, Behtash Javed Sharifi, Fabrício Bagatini-Cachuço and Xiao Pan.

I owe special thanks which are owed to my parents, who constantly supported me both morally and financially and kept me motivated throughout my studies at UBC. I am grateful to my younger brother for being there as a support to my parents so that I could focus on my studies. Finally, I am appreciative of my friends back in Bangladesh who kept me motivated on the weakest days of my studies.

Dedication

To My Parents and My Brother

For their encouragement and patience

Chapter 1: Introduction

It has been well-established that to improve performance in damaging earthquakes, the structures need to be earthquake resilient. Towards that resiliency, high-importance structures are designed to be functional immediately or shortly after strong earthquake shaking. This is achieved by using structural fuses. Fuses are designed to dissipate earthquake energy and protect the remaining structural components from damages. Examples of structural fuses, which have been developed in previous studies, include viscous fluid, viscoelastic and friction dampers, and metallic fuses (Makris and Constantinou 1990, Symans, et al. 2002, Wang, et al. 2018, Zhou, et al. 2019, Qian, et al. 2016, Lu, et al. 2018). Structural fuses have also been incorporated in moment-resisting frames (Koetaka, et al. 2005, Shen, et al. 2011), concentrically braced frames (Gray, et al. 2014, Tena-Colunga and Hernández-Ramirez 2017, Tremblay, et al. 2011, Vargas and Bruneau 2009a), eccentrically braced frames (EBF) (Malakoutian 2012), rocking and self-centered structures (Ma, et al. 2013) and precast concrete walls (Kurama 2000). These investigations were carried out to study their well-known stable and advanced hysteresis performance. However, there is a lack of research related to predicting the performance of the fuses before experimental investigation. An efficient and effective approach of experimental investigation requires that the designers and researchers alike would be able to predict the performance of a structural fuse at any site location and floor. Such an approach has been proposed in this study where the performance demand in terms of energy dissipation and floor-wise distribution can be predicted without performing numerical analysis. The most commonly used energy dissipation device (structural fuse), known as Buckling-Restrained Brace (BRB), has been selected for this study.

The existing performance evaluation procedure for structural fuses prescribes that a component should be tested experimentally until it either fractures or sustains large inelastic deformations.

This is known as the loading protocol. Examples of loading protocols include SAC basic loading protocol (Clark, et al. 1997) and AISC loading protocol (ANSI/AISC 341-16 2016). These loading protocols were developed based on deformation-related demand parameters such as drift and ductility. Other loading protocols were developed for steel moment connections, wood-frame shear walls, reinforced concrete shear walls, BRBs, short links in EBFs and displacement-sensitive non-structural components (ATC-24 1992, CUREE-Caltech 2001, SPD 1987, Richards and Uang 2003, Dehghani and Tremblay 2012a, Mergos and Beyer 2014, Lanning, et al. 2016, Shafei and Zareian 2008, FEMA 2007). Energy dissipation in loading protocols for structural components has not been accounted for explicitly. This study presents a detailed derivation of the approach to quantify energy dissipation demand and application of the approach on BRB.

1.1 Objectives and Scope

An efficient and effective testing program requires to determine seismic energy demand beforehand without conducting any nonlinear time history analysis in order to evaluate the performance of a structural component. The objectives of this study were to:

1. Investigate the concept of obtaining total dissipated energy demand in a structure with structural fuses from site-specific design spectrum, and
2. Provide recommendations to obtain system-specific energy demand and floor-wise distribution of the demand.

This study is focused on the application of the recommended quantification approach on BRB, a novel energy dissipation device that overcomes the sudden degradation in stiffness and strength due to buckling of conventional steel brace. The buckling of the ductile steel core in a BRB is restrained by steel casing and concrete filling. By suppressing buckling the device exhibits stable and balanced hysteretic behavior and achieves considerable ductility. Up-to-date investigations of

BRBs have been mostly concentrated on developing the physical features of BRB. However, consideration of energy dissipation capability of the BRB to evaluate its seismic performance has not been studied yet. This realization paves the way for the scopes of the current research, which includes the following tasks:

1. Propose an equation for Energy Quantification Factor required for estimating energy demand based on a design spectrum;
2. Propose equations for Rise Time to obtain the rate at which energy will be dissipated in an energy dissipation device;
3. Propose a floor-wise distribution procedure to distribute the energy demand, and
4. Apply the procedure to a building equipped with BRBs.

1.2 Organization

Development of the proposed quantification approach has been outlined in the following chapters:

- Chapter 2 reviews previous studies on the development of BRBs. The concept and application of BRBs are also documented. The description of the development of existing testing protocols is also described in this chapter.
- Chapter 3 presents the parametric study on a range of equivalent nonlinear single degree of freedom (SDOF) systems. The purpose was to propose an equation to obtain the energy factor to determine energy demand from the site-specific design spectrum. Moreover, equations were proposed to quantify the rate at which energy is dissipated in the system.
- Chapter 4 proposes an empirical equation for the floor-wise distribution of energy demand along the floors of a building equipped with BRB. Also, equations were proposed to quantify coefficients which were used to determine the energy distribution and control the shape of the

distribution. The empirical equation and the equations for the coefficients were developed based on numerical analysis conducted on 3-, 6- and 8-storey prototype frames.

- Chapter 5 presents the application of the proposed approach to a prototype building equipped with BRB. It includes the quantification and distribution of energy demand for the BRBs in the building. Predicted energy demand is compared with energy demand from nonlinear dynamic analysis of the two-dimensional numerical model of a 5-storey prototype frame.
- Chapter 6 summarizes the framework for the proposed approach and research findings and identifies future scopes and application in the experimental quantification.

Chapter 2: Literature Review

2.1 Introduction

This chapter provides a brief review of past investigations and the development of Buckling-Restrained Brace (BRB) devices. In Section 2.2, components of typical BRBs are discussed. Applications of BRBs in Japan and the US are presented in Section 2.3. A brief description of past experimental studies is documented in Section 2.4. Section 2.5 discusses testing protocols for experimental studies on BRBs and other components. Finally, in Section 2.6, the theory behind the current quantification approach is discussed.

2.2 Buckling-Restrained Brace

Buckling-Restrained Brace (BRB) is a novel energy dissipation device which has several advantages when compared to the conventional steel brace. Conventional braces exhibit sudden degradation in stiffness and strength due to buckling under compression loading. To prevent the buckling due to compression loading, a ductile steel core in BRB is placed inside a steel casing and then filled with concrete. Transfer of axial force from steel core to concrete filling is minimized by providing an air gap or by unbonding material.

A typical BRB made of yielding steel core encased in a steel tube with mortar is shown in Figure 2.1 (a). BRB exhibits stable and balanced hysteretic behavior while conventional brace buckles. The difference between the hysteretic performance of conventional brace and BRB is shown in Figure 2.1 (b).

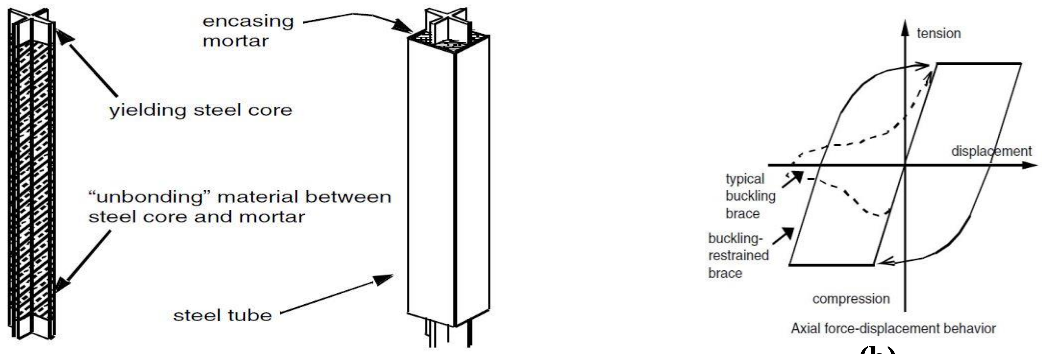

(a) (b)

Figure 2.1 Features of BRB: (a) Key components; (b) hysteresis curves for conventional (buckling) braces versus BRBs (Uang and Nakashima 2004)

2.3 Worldwide Applications of Buckling-Restrained Braces

BRBs have been applied in the construction of new buildings as well as retrofitting of both steel and reinforced concrete (RC) buildings worldwide, especially in Japan and the US. The new constructions were mostly concentrically braced frames (CBFs) equipped with BRBs, however, in retrofitting application BRBs had been used both in moment resisting frames (MRFs) and CBFs.

2.3.1 Applications in Japan

Several attempts were made to achieve the practical application of the concept of BRB in Japan between 1970 and 1990. Initial success was achieved by Wada in 1988 (Takeuchi 2018). After that, BRBs were applied to two steel frame office buildings by Nippon Steel Corporation in 1989 (Takeuchi and Wada 2018). However, the popularity of BRB in Japan increased after the 1995 Kobe earthquake and the application was not limited to new construction, but also retrofitting of existing structures. An example of new construction in Japan is shown in Figure 2.2 (a) and a retrofit of an existing RC building (Midorigaoka, Tokyo Institute of Technology) is shown in Figure 2.2 (b).

(a)

(b)

Figure 2.2 Application of BRB in Japan: (a) construction of Osaka International Convention Centre (Ko and Field) and (b) retrofitting of Midorigaoka, Tokyo (Takeuchi, et al. 2009)

2.3.2 Applications in the USA

After the 1994 Northridge Earthquake BRBs gained access in the USA (Aiken and Kimura 2001). The first application in the USA was reported in 1998 at the University of California (UC), Davis Campus as shown in Figure 2.3 (a) (Ko and Field). The popularity of BRB extended the application of this device in retrofitting of an existing building in UC, Berkeley shown in Figure 2.3 (b) (Comerio, et al. 2006).

(a)

(b)

Figure 2.3 Application of BRB in the USA: (a) construction of UC Davis Plant & Environmental Facility, California (Ko and Field) and (b) retrofitting of a building at UC Berkeley Campus, California (Credit: S. Brzev)

2.4 Experimental Studies on BRBs

The stable and desired energy dissipation capacity of BRBs was confirmed by many experimental investigations around the globe. The first experimental tests were reported in Japan. Soon after that, researchers in the USA, Canada, India, and other countries also studied BRB performance. However, only research findings from studies performed in Japan and the USA are discussed here.

2.4.1 Experimental Studies in Japan

Experimental studies in Japan were spearheaded by Wada (Fujimoto, et al. 1990). He led the first experimental study on BRBs which had been used in the Nippon Steel Frame Office buildings project in Tokyo. Five BRB specimens were tested in that experiment by placing them diagonally in a frame and by applying alternating loads. The test setup of this experiment is shown in Figure 2.4 (a). It was observed in the experimental results that the BRBs exhibited stable symmetrical hysteresis. The hysteresis curve of one of the specimens is presented in Figure 2.4 (b). The maximum displacement from the result is 1.57 in. (40 mm).

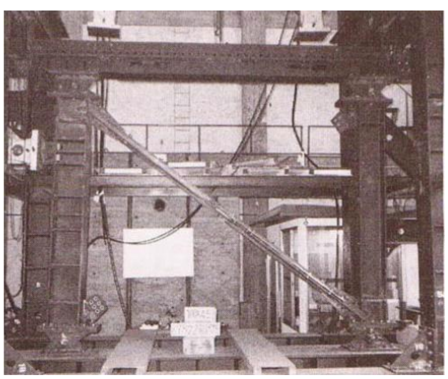

(a)

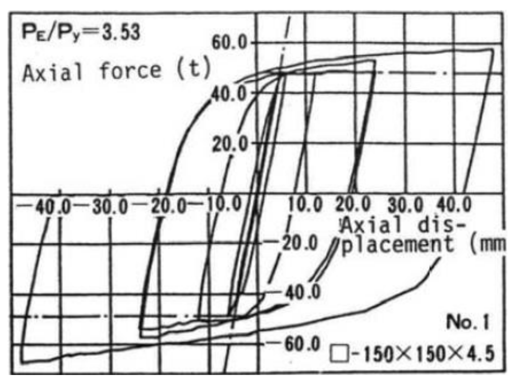

(b)

Figure 2.4 Experimental study in Japan: (a) test setup, and (b) hysteresis curves for BRB No. 1 (Fujimoto, et al. 1990)

In another experimental study, Wada (1990) confirmed that frames equipped with BRBs exhibited high energy absorption capacity and earthquake resistance. BRBs were placed in an inverted V-braced frame test specimen as shown in Figure 2.5 (a). Three models were prepared namely, Model A, Model B and Model C. Models A and B were equipped with braces while Model C was tested without braces. The results obtained in those tests are shown in Figure 2.5 (b) where the hysteresis curve of Model A was shown with envelope curves of Model B and Model C. Similar hysteresis characteristics were observed with a maximum displacement of 0.60 in. (15 mm) by Iwata (2000). However, Iwata employed strain-based loading protocol and the testing was continued until either a significant strength degradation was observed or the BRB fractured.

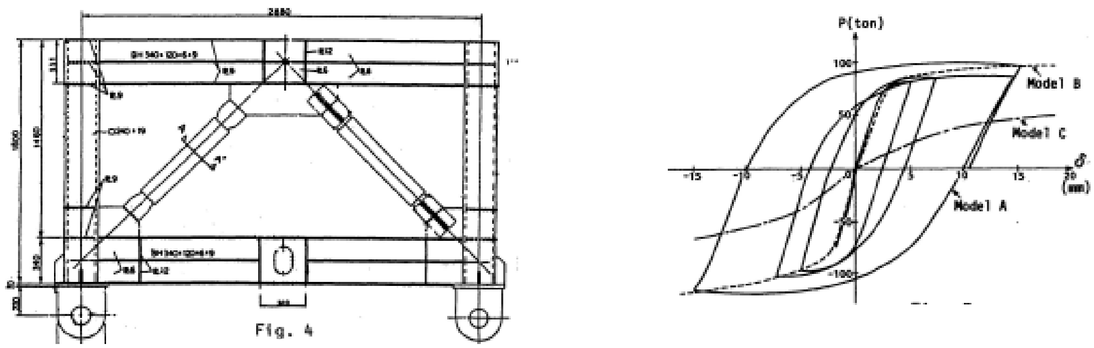

(a) (b)

Figure 2.5 Experimental study in Japan: (a) test setup, and (b) hysteresis curves (Wada, et al. 1990)

2.4.2 Experimental Studies in the USA

In the United States, the first tests of the BRB were carried out at UC Berkeley for the UC Davis project (Clark, et al. 1999). The braces were tested with loading histories specified by the SAC loading protocol as shown in Figure 2.6 (a). However, this loading protocol was converted to an equivalent strain history and applied to the test braces. Three braces, each of them having different cross-sectional areas, were tested. The test result as shown in Figure 2.6 (b) demonstrated stable and repeated hysteretic behavior which verified the theoretical prediction (Clark, et al. 2000). It can be observed from the figure that the specimen sustained a maximum displacement of 2.38 in. (60.45 mm).

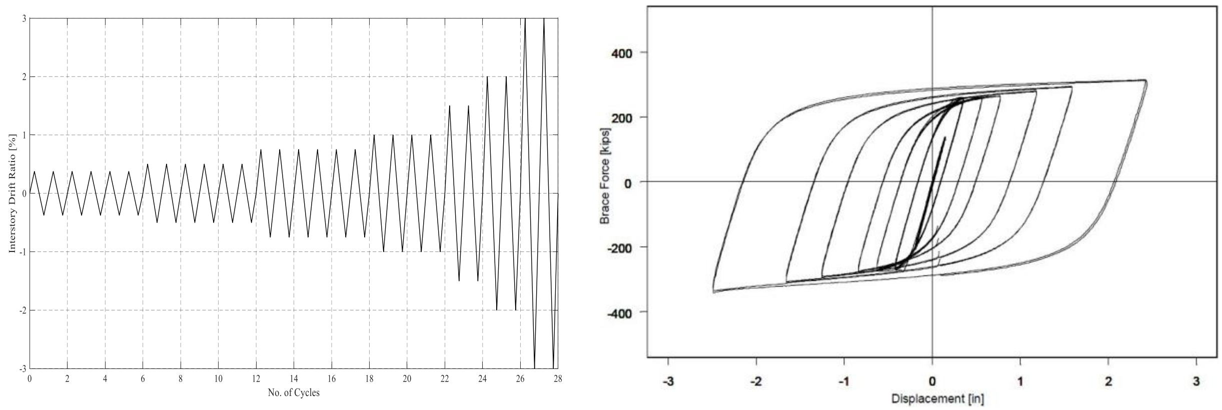

Figure 2.6 Experimental study in UC Berkeley: (a) test loading history, and (b) hysteretic behavior of the brace (Clark, et al. 1999)

SAC loading protocol used in the UC Berkeley test was developed based on nonlinear dynamic analysis conducted on SAC steel moment frame building. Later, the SEAOC-AISC task group included a provision for cyclic testing of either brace or subassembly specimen based on a series of nonlinear dynamic analysis conducted on moment frames equipped with BRBs by Sabelli (2001), as reported by Uang and Nakashima (2004). Using the loading protocol mentioned in that provision shown in Figure 2.7 (a), Merritt, Uang and Benzoni (2003) implemented a sub-assemblage testing program at UC San Diego on eight full-scale BRBs provided by Star Seismic, LLC, a BRB manufacturer in the US. The specimen sustained a maximum deformation of 4.01 in. (101.85 mm). Even though the objective was to investigate the cumulative inelastic axial deformation, the hysteresis curve of one of the specimens as shown in Figure 2.7 (b) complemented the findings in terms of stable hysteresis by Wada (1990) and Clark (1999).

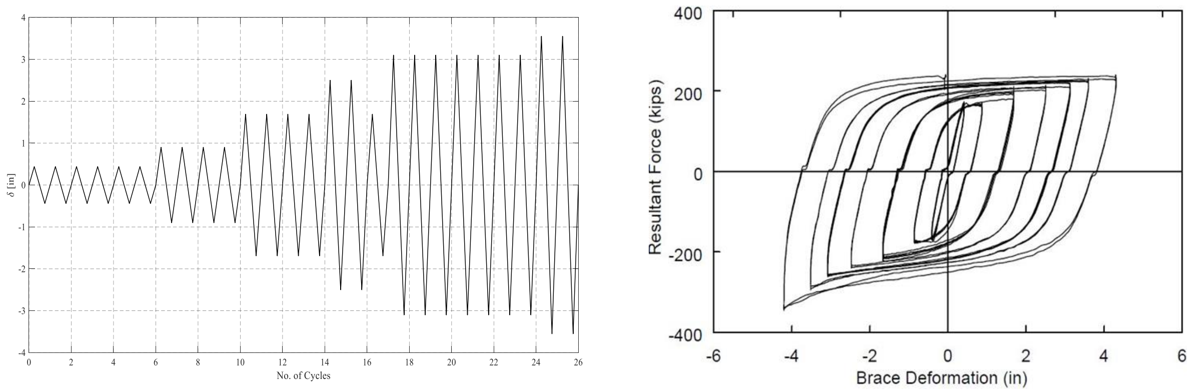

Figure 2.7 Experimental study in UC San Diego: (a) test loading history, and (b) hysteresis curve of one of the eight braces (Merritt, et al. 2003)

2.5 Existing Testing Protocols

Over the last four decades, a lot of efforts have been made to develop a reversed cyclic loading protocols for experimental investigations of both BRBs and other components. The development of those protocols adopted a conservative approach without a rational basis.

2.5.1 Standard Testing Protocol for BRB in Japan

Even though earlier experimental programs adopted force-based loading sequence, deformation-based namely, strain loading histories were used in later experiments conducted by researchers in Japan. For example, Iwata (2004, 2006) employed a reversed cyclic loading sequence which started with one cycle of 1/3 and 2/3 of yield strain and continued after yielding with 0.25%, 0.50%, 0.75%, 1.00%, 1.50%, 2.00% and 2.5% of maximum strain obtained from dynamic analysis of 10-storey prototype building consisted of moment-resisting frames with BRBs. Each load was applied for two cycles, except for 0.25% and 1.00% strain which were applied for 1 and 5 cycles respectively. The test was further continued with additional cycles of 3.00% strain until significant strength degradation was observed or the steel core fractured. Takeuchi (2010, 2012, 2014, 2016) applied a similar strain-based reversed loading sequence in his study on local buckling and out-of-plane stability of BRBs. The loading sequence, in this case, differed in the number of cycles and strain amplitudes. Takeuchi applied 3 cycles of 0.10%, 0.50%, 1.00%, 2.00% of plastic strain which is the ratio of displacement and length of plastic zone of the core plate and continued the test with additional cycles of 3.00% plastic strain, until either core plate fractured or instability in the BRB and connections was observed. Building Center of Japan (BCJ) has adopted a testing protocol in their Specifications for BRB Certification (BCJ-16) which is identical to the one which Takeuchi used except that the BCJ recommended that loading starts with 3 cycles of yielding strain (Takeuchi and Wada 2018). The testing protocol is shown in Figure 2.8 (a) where amplitudes are plotted against the number of cycles.

2.5.2 Standard Testing Protocol for BRB in the USA

Current AISC (2016) has recommended adopting deformation-based loading sequences shown in Figure 2.8 (b) where amplitudes were plotted against the number of cycles. AISC recommended continuing the testing of brace with $\Delta_b = 1.50 \times \Delta_{bm}$ until a cumulative inelastic axial deformation of at least 200 times the yield deformation is achieved. Here, Δ_b can be the steel core axial deformation for the test specimen and the rotational deformation demand for the sub-assemblage test specimen. AISC has also permitted other testing protocols if they were capable of imposing equal or greater severity in terms of maximum and cumulative inelastic deformation. The foundation of this protocol was laid back in 2001 when the SEAOC-AISC task group included requirements for cyclic testing of either braces or subassembly specimens in the draft of their proposed *Recommended Provisions for Buckling-Restrained Braced Frames* (Uang and Nakashima 2004). The SEAOC-AISC provision for testing was developed based on the seismic demands observed in a series of nonlinear dynamic analyses on frames equipped with BRBs conducted by Sabelli (2001) and further adopted in the AISC 341-05, as reported by Wijanto

(2012). The differences between current AISC testing protocol (2016) and AISC 341-05 are related to the number of cycles and loading sequence, and critical criteria to be achieved by additional cycles. For example, the AISC 341-05 loading protocol required to achieve cumulative inelastic axial deformation of 140 times the yield deformation, as reported by Uang and Nakashima (2004). This demand is lower than the one recommended in AISC 341-16. However, a rational basis behind these demands has not been mentioned in any of the AISC editions.

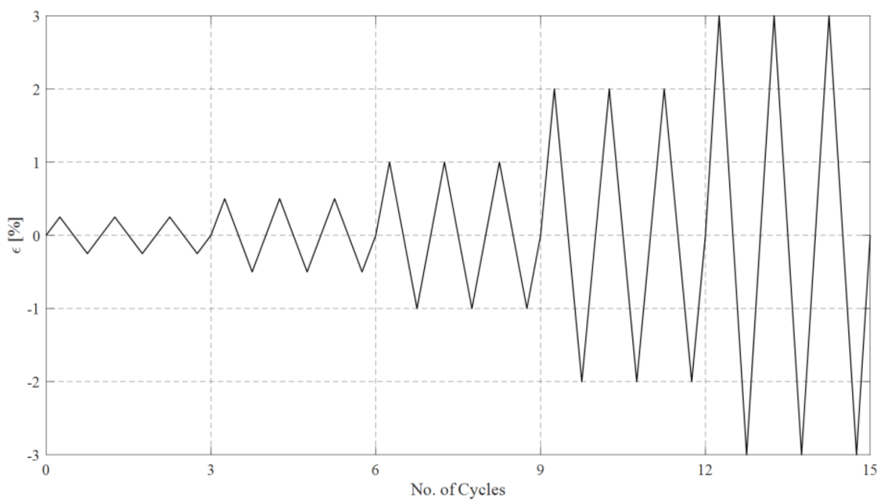

(a)

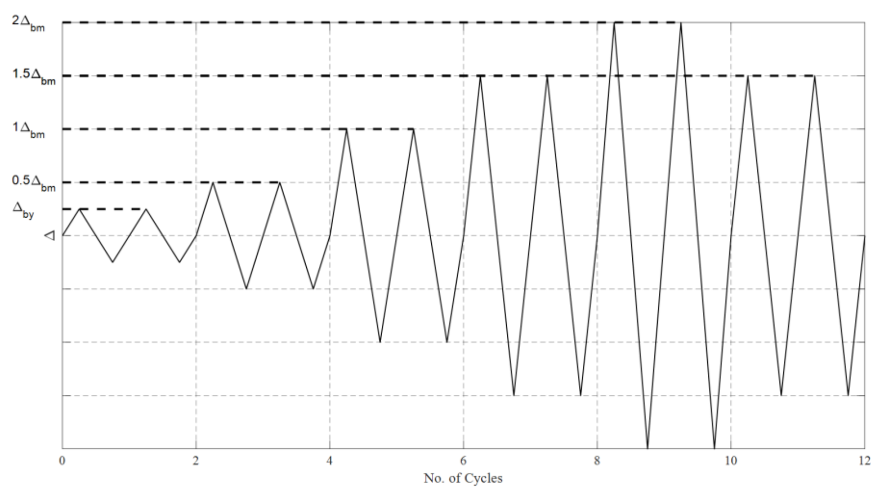

(b)

Figure 2.8 Standard loading protocols: (a) Japanese practice, and (b) the USA practice

The differences in the protocols shown in Figure 2.8 are in the number of load steps and cycles and demand parameters as presented in Table 2.1. For example, the basic feature of the loading protocol in Japanese practice has 5 load steps while one in the USA practice has 6 load steps. Furthermore, the number of cycles in Japanese and The USA standard loading protocol are 3 and 2 respectively. The demand parameters are different as well. However, the parameters, namely strain and deformation, are interrelated. An experimental program on a specimen should be employed to have a comprehensive overview of the differences in the performance evaluation using the protocols. Both loading protocols recommend continuing the testing until the specimen fractured.

Table 2.1 Comparison of loading protocols in standards

Load Steps	**Japanese Standard: BCJ-16**		**USA Standard: AISC 341-16**	
	Cycles	**Strain, ε (%)**	**Cycles**	**Deformation, Δ in (mm)**
1	3	0.25	2	Δ_{by}
2	3	0.50	2	$0.50 \times \Delta_{bm}$
3	3	1.00	2	$1.00 \times \Delta_{bm}$
4	3	2.00	2	$1.50 \times \Delta_{bm}$
5	3	3.00[1]	2	$2.00 \times \Delta_{bm}$
6			2	$1.50 \times \Delta_{bm}$[2]

Note:

Δ_{by} = deformation quantity at first yield of the test specimen;

Δ_{bm} = deformation quantity corresponding to the design story drift; this drift should not be less than 0.01 times the story height.

1. BCJ-16 recommends continuing with this loading step until the specimen fractured;

2. AISC 341-16 recommends continuing with this loading step until the specimen fractured;

2.5.3 Testing Protocols for BRBs and Other Components

Apart from the recommended testing protocols in Japanese and the USA standards, individual researchers in Canada, USA and other countries have developed loading protocols for the qualification of BRBs based on demand parameters such as ductility and cumulative energy dissipation. In Canada, the testing protocol specified in CSA S16-09 is identical to the one recommended in AISC 341-05 (Dehghani 2016). Dehghani and Tremblay (2012a) developed a dynamic loading protocol for the qualification of BRBs considering western and eastern seismic regions of Canada. The demand parameters, which played key roles in the development of the protocol, were ductility, ductility rates and effective durations of a damaged brace. The most damaged brace was identified based on demand indices, such as peak ductility, maximum ductility excursions, maximum ductility range, cumulative ductility, maximum ductility rate and normalized hysteresis energy (Dehghani and Tremblay 2012b). Consequently, three loading protocols representing intra-plate (east and west) and inter-plate (west) events were proposed. In Appendix A.1, loading protocol for the west intra-plate event was shown in Figure A.1 where ductility amplitudes are plotted against time. Then, in the USA, the development of loading protocols for the qualification of BRBs besides the code was found in the works of Lanning (2014). In that work, Lanning proposed a testing protocol for BRBs specifically used in a bridge. Two protocols, namely VTB (Vincent Thomas Bridge) Proof Protocol and Near Fault Protocol were developed to represent conservative near-fault seismic demands. In the first protocol, the peak demands on BRB, located between side spans and cable bents, had been taken as prototypical response considering only one ground motion (Lanning, Benzoni and Uang 2016). The second protocol was developed based on the statistical representation of maximum inelastic strain amplitudes. In this work, a rainflow cycle counting algorithm was employed to filter out elastic events. Moreover, by incorporating time in those pseudo-static VTB protocols and using sinusoidal waves with frequencies reflecting time steps, the dynamic version of those protocols was developed, as shown in Figure A.2 (b), where amplitudes are plotted against the number of load steps. Contrary to the ductility-based and strain-based loading protocol by Dehghani and Lanning, Aguaguiña (2019) proposed loading protocols with strain amplitudes which are representative of reference cumulative distribution of hysteretic energy. This parameter was obtained from analytical studies conducted on BRBs for five different loading histories. The BRBs were sub-divided into Yield Length Ratio (YLR) of 0.50 and 0.60. The two divisions of YLR were based on a database composed of 35 BRB specimens selected from 16 experimental tests prepared by the authors. Hence, two quasi-static loading protocols were proposed. In Figure A.3, the loading protocol for YLR of 0.50 is shown where strain amplitudes are plotted against the number of cycles.

Besides these loading protocols for BRBs, qualification procedure for other components such as wood-frame shear walls, RC shear walls, RC frames, steel moment connections and so on, were also developed in the last four decades. These protocols were developed based on deformation-related demand parameters such as drift and rotation. The demands imposed by the developers of those loading protocols were outcomes of nonlinear time history analysis conducted on either single-degree-of-freedom (SDOF) systems which were representative of structural systems such as wood-frame shear walls, RC frames and so others, or two-dimensional numerical models of prototype frames. For example, loading protocols developed from demand on a range of SDOF systems are ATC (1992) and CUREE-Caltech (2001). A similar procedure has been adopted in developing loading protocols for European earthquake regions (Mergos and Beyer 2014) and displacement-sensitive non-structural components (Shafei and Zareian 2008). On the other hand, SPD (1987) and SAC (1997) loading protocols were developed based on demands obtained from analysis results of numerical models representing timber or masonry structures and steel moment-resisting frames respectively. Similarly, Richards and Uang (2003) proposed a loading protocol for short links where demands were obtained from links equipped in eccentrically braced frames (EBFs). FEMA-461 (2007) developed loading protocols for the qualification of structural and non-structural components. The performance of the components investigated by these loading protocols was based on the ability to sustain cumulative damage, which according to Krawinkler (1983) is the rate at which a component loses its capacity. The amplitudes of loading protocols are plotted against the number of cycles and presented in Table A.1 of Appendix A.2. Overall, the loading protocols discussed above assess performance without a predefined performance standard for the comparison of experimental results.

2.6 Energy Demand Quantification Approach

It was realized that the experimental qualification of components by traditional testing protocols did not have predefined quantification demand for a comparison. Without an appropriate demand, it will be difficult to evaluate the performance of such components effectively and efficiently. It is crucial to select a demand which takes the performance objective of the component into consideration. For example, a structural fuse dissipates energy and protects the structure from damage and for that reason, the fuse needs to yield before the structural system. Hence, a testing protocol for the qualification of such fuse should take hazard-specific dissipated energy demand into account. In this study, as an energy dissipation device such as BRB was investigated, so a novel approach to quantify dissipated energy demand for BRBs in different floors of a building located in different sites was proposed.

The proposed quantification approach is inspired by an Equivalent Energy Design Procedure (EEDP) notion, developed by Yang (2018) based on energy-balanced design concepts. The concept was originally developed by Housner (1956). Housner explained that a huge portion of the earthquake input energy, E_i, into a structure will be dissipated through damping, E_ξ, and the remainder of the energy will be stored in the structure in the form of kinetic, E_k, and strain, E_a, energies. While E_a will be stored as strain energy, E_S, in an elastic structure, it will be divided into strain, E_S and hysteresis, E_h, energies (provided that the structure yields). E_h is the most crucial of all energy components as it indicates energy dissipation induced following structural damage. E_h can be decomposed into components and calculated as the sum of the products of force and deformation for each component. The EEDP design philosophy was based on approximation of the force-deformation relationship using an equivalent nonlinear SDOF (ENLSDOF) system without conducting a nonlinear dynamic analysis. A similar approach was adopted herein for the development of the quantification of the energy demand of BRBs.

2.7 Concluding Remarks

BRBs are novel devices with potentials for a wide range of application which have been studied and developed for decades. So far, progress has been made in the development of the physical features of BRBs. The conventional approach of performance evaluation does not consider the hazard intensity of a site in the analysis. A recent development in design procedure specifies the performance of components based on different hazard levels such as Service Level Earthquake (SLE), Design-Basis Earthquake (DBE) or Maximum Considered Earthquake (MCE). However, in this study, an approach was proposed to quantify energy demand for BRBs from the design spectrum. The approach consists of two quantification parameters, namely Energy Quantification Factor (γ_{lp}) and Rise Time (t_R), and a procedure for floor-wise distribution of energy demand in a building. The equations for quantification parameters and floor-wise distributions are discussed in Chapters 3 and 4 respectively.

Chapter 3: Energy Quantification Factor and Rise Time

3.1 Introduction

The development of the proposed equations is presented in this chapter. At first, in Section 3.2, the development of numerical models of equivalent nonlinear single-degree-of-freedom (ENLSDOF) systems is discussed. Finally, based on the numerical analysis conducted on those systems equations for energy quantification factor and rise time are proposed in Section 3.3.

3.2 Development of Numerical Models

An efficient quantification method should be simple where energy demand in an energy dissipation device can be approximated using an ENLSDOF system without conducting a dynamic time history analysis. Such a method has been proposed in this study to quantify the energy demand for BRBs in different floors and site locations. At first, the total energy demand is obtained from the design spectrum and modified using an energy quantification factor. After that, the energy demand of the BRB over time can be determined using a series of equations. A range of SDOF systems has been analyzed to propose equations as a function of the fundamental period of a building to determine the energy quantification factor and the rise time.

3.2.1 Properties of the Numerical Models

Twelve ENLSDOF models were developed to investigate the effect of fundamental periods and yield strengths of a system on the quantification parameters in OpenSees Navigator (2013). The elastic periods of the ENLSDOF models were 0.25 sec., 0.50 sec., 1.00 sec. and 2.00 sec. A building is designed with reduced yield force corresponding to Response Modification Coefficient (also known as the R-factors) in accordance with the US practice (ASCE/SEI 7-16 2017), hence a range of R-factors were considered in this study. The yield strength of each ENLSDOF was modified using R-factors of 4, 6 and 8. R-value of 8 was considered, as the proposed equations were applied to a building that was designed according to the ASCE 7-10 (2010) standard which requires R = 8 for buildings with BRBs. The hysteresis of the ENLSDOF systems was modeled by Giuffré-Menegotto-Pinto material (Filippou, Popov and Bertero 1983), also known as Steel02 material in OpenSees platform. Moreover, the comparison of force-deformation hysteresis curves against the experimental results from the test conducted on BRB by Clark (1999) is shown in Figure 3.1. The numerical analyses were conducted assuming 2% damping to impose higher energy dissipation demand than the typical code practice of 5% damping.

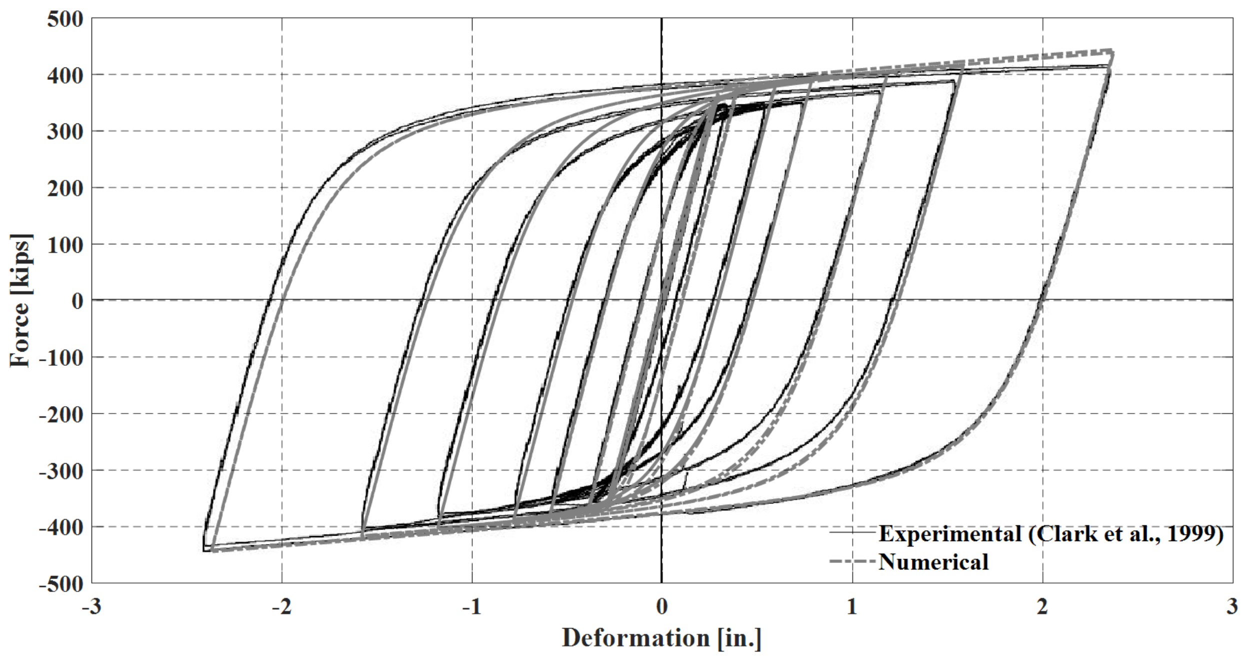

Figure 3.1 Giuffré-Menegotto-Pinto material (Steel02 material) model calibration

In the development of the ENLSOF model, the stiffness was kept constant while the masses were varied to obtain different fundamental periods. The masses corresponding to the fundamental periods of the systems are shown in Table 3.1. Yield strengths of the brace material were determined to represent R factors of 4.0, 6.0 and 8.0 as shown in the table. The changes in yield forces due to changes in yield strength are further illustrated in Figure 3.2 (a) – (d) where elastic forces of ENLSDOF systems are reduced with increased R-factors.

Table 3.1 Properties of the ENLSDOF Systems				
Fundamental Period, *T* (sec.)	**Mass kips-sec^2/in. (kN-sec^2/m)**	**Yield Strength, f_y ksi (MPa)**		
		R = 4.00	**R = 6.00**	**R = 8.00**
0.25	1.16 (203.14)	34.47 (237.662)	22.98 (158.44)	17.23 (118.79)
0.50	4.65 (814.29)	137.95 (951.13)	91.96 (634.04)	68.97 (475.53)
1.00	18.60 (3257.20)	305.01 (2102.96)	203.34 (1401.97)	152.28 (1049.93)
2.00	74.50 (13046.29)	610.83 (4211.52)	407.22 (2807.68)	305.42 (2105.79)

The straight-line 0-A shown on the figures represents the elastic force-deformation demands on ENLSDOF systems corresponding to their fundamental periods, (T), from the design spectrum and three bilinear plots represent the nonlinear force-deformation relationships.

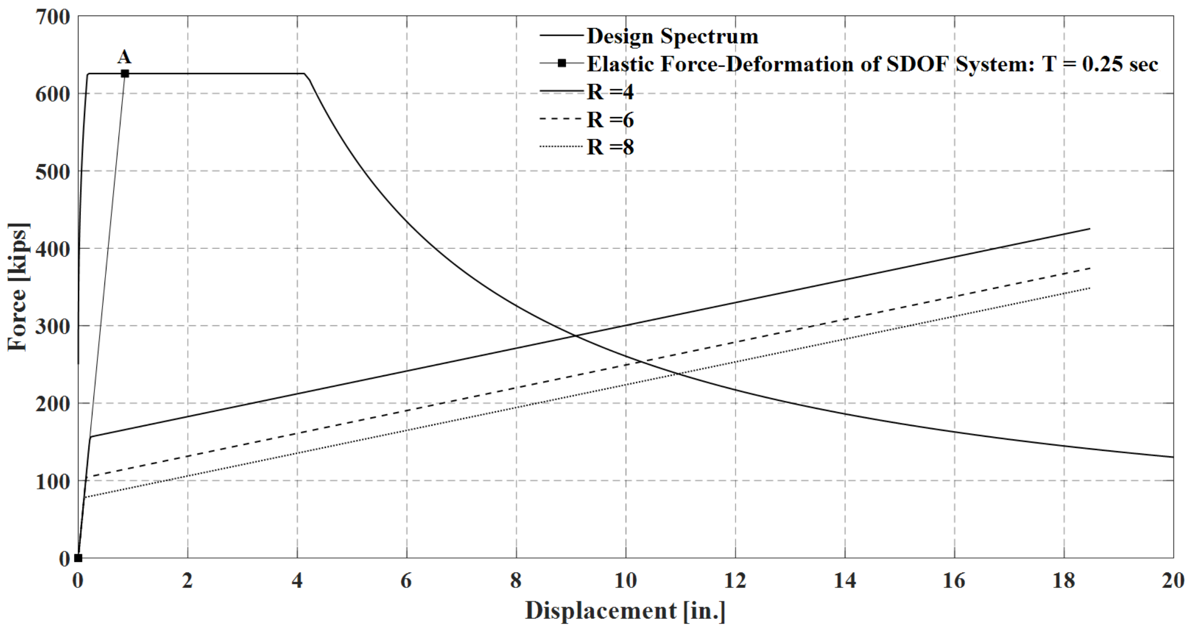

(a)

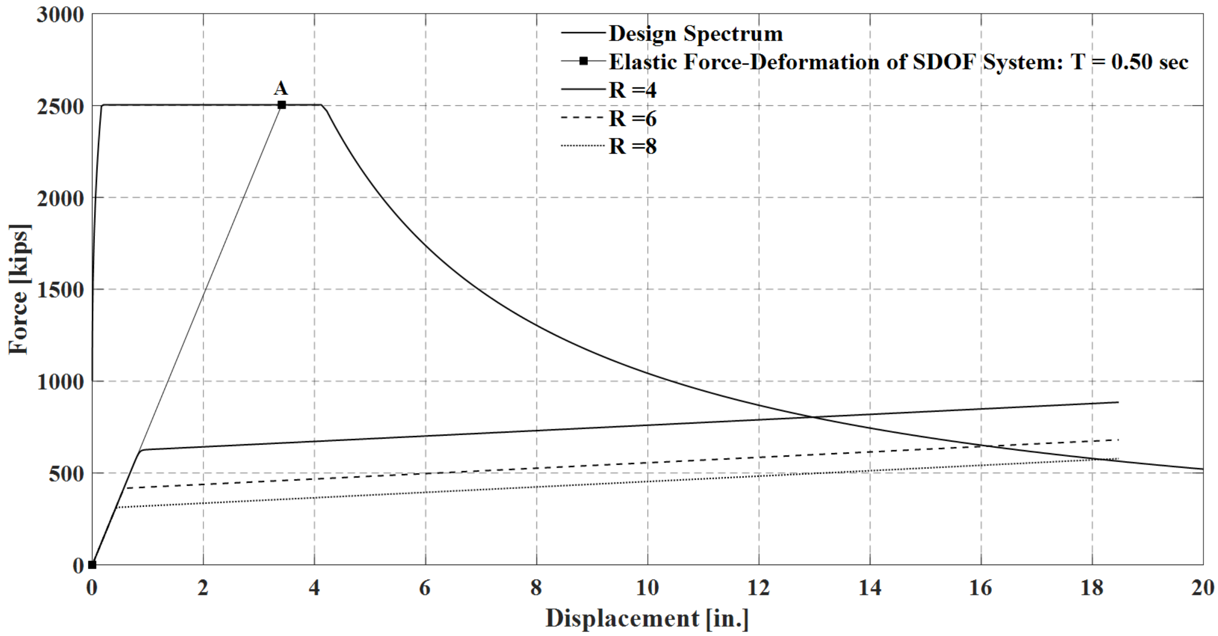

Design Spectrum
Elastic Force-Deformation of SDOF System: T = 0.50 sec
R =4
R =6
R =8
A
Force [kips]
Displacement [in.]

(b)

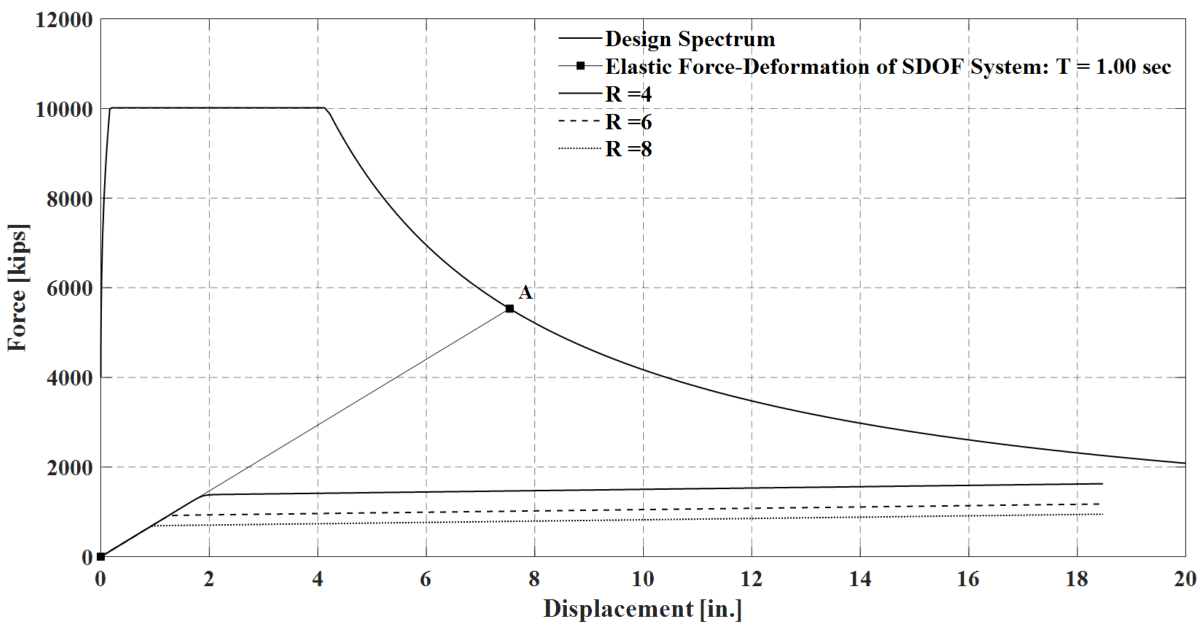

Design Spectrum
Elastic Force-Deformation of SDOF System: T = 1.00 sec
R =4
R =6
R =8
A
Force [kips]
Displacement [in.]

(c)

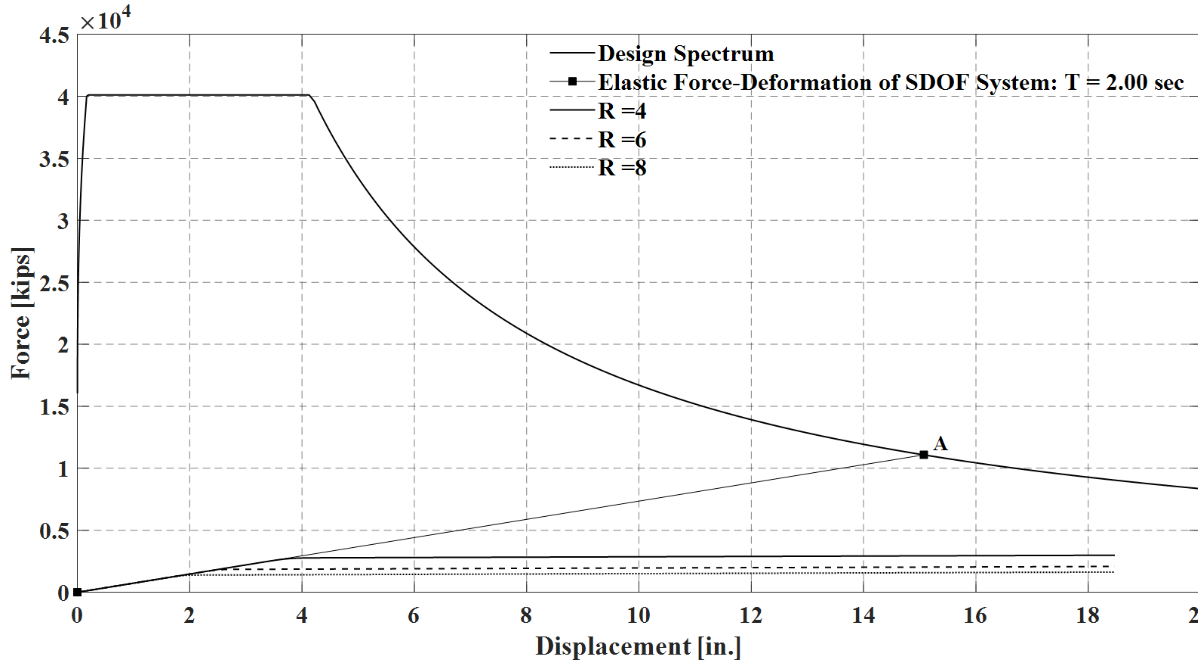

(d)

Figure 3.2 Comparison of static force-deformation relationships for SDOF systems with different T values: (a) 0.25 sec, (b) 0.50 sec, (c) 1.00 sec and (d) 2.00 sec

3.2.2 Selection and Scaling of Ground Motions

A suite of twenty ground motions was selected from the PEER strong motion database (2013) and summarized in Table B.1-B.4 of Appendix B.1. Since crustal earthquakes are frequent on the west coast of North America, the earthquake records were selected to be representative of crustal earthquakes whose moment magnitudes (M_w) were between 5.0 and 7.9 and closest site-fault distances were within 49.71 mi (80 km.). An average shear wave velocity in the top 100 ft (30 m) of soil within 600 ft/sec. (180 m/sec.) to 1,200 ft/sec. (360 m/sec.). The ground motions were scaled to the design spectrum (also termed as target spectrum in this study) representing site class D according to FEMA 302 (1997) and 10% probability of exceedance in 50 years hazard level adopted from Sabelli (2001). Those motions were amplitude scaled to the spectral acceleration corresponding to the fundamental period of each of the ENLSDOF systems. Moreover, the objective of scaling was to keep the mean values of the response spectra by 10% of the design spectrum within the range of 0.2 to 2.0 times the fundamental period (T), this is a requirement of ASCE/SEI 7-16 (2017) and NBCC (2015). The scaled acceleration response spectra of the ground motions are shown in Figure 3.3. The dashed vertical straight line shows where the spectral accelerations of the motions were scaled to the design spectrum. The vertical dotted line on the left represents 0.2 times of T and on the right represents 2.0 times of T. However, if the upper-limit (2.0T) of the range was less than 1.5 sec, the period range was set from 0.2T to 1.5 sec, as shown in Figure 3.3 (a) & 3.3 (b). Within this period range, scaling met the above requirement, except for scaling at 0.25 sec and 0.50 sec where the mean spectrum fell below the design spectrum by more than 10% close to the lower limit of the period range.

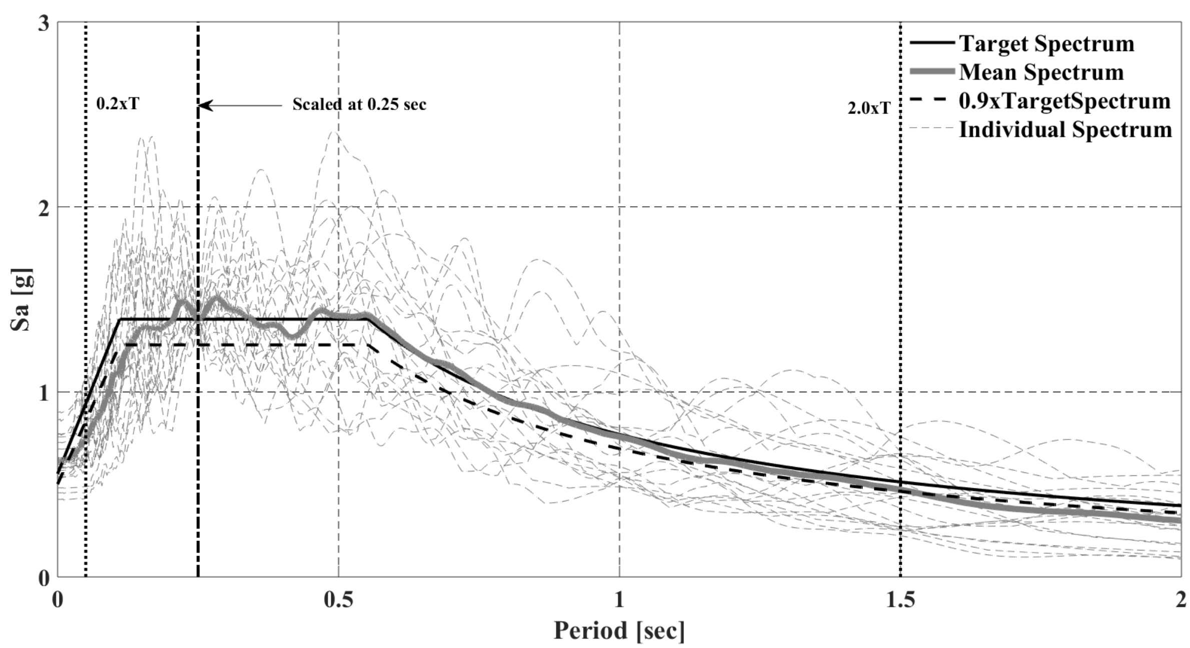

(a)

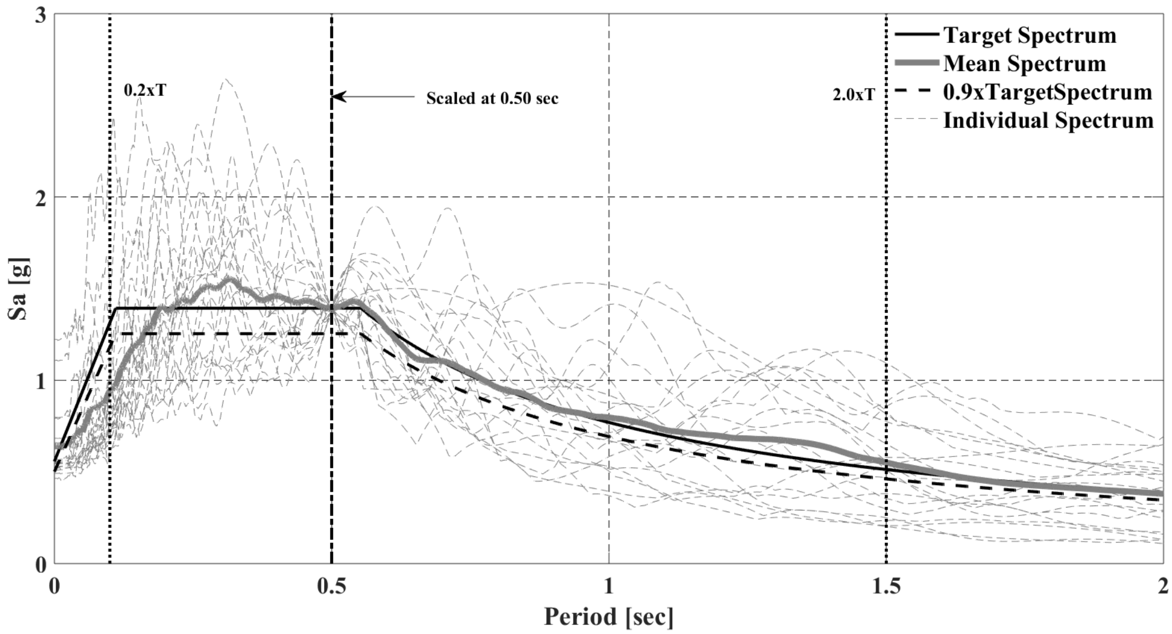
Target Spectrum
Mean Spectrum
0.9xTargetSpectrum
Individual Spectrum
0.2xT
Scaled at 0.50 sec
2.0xT
Sa [g]
Period [sec]
0
0.5
1
1.5
2
3

(b)

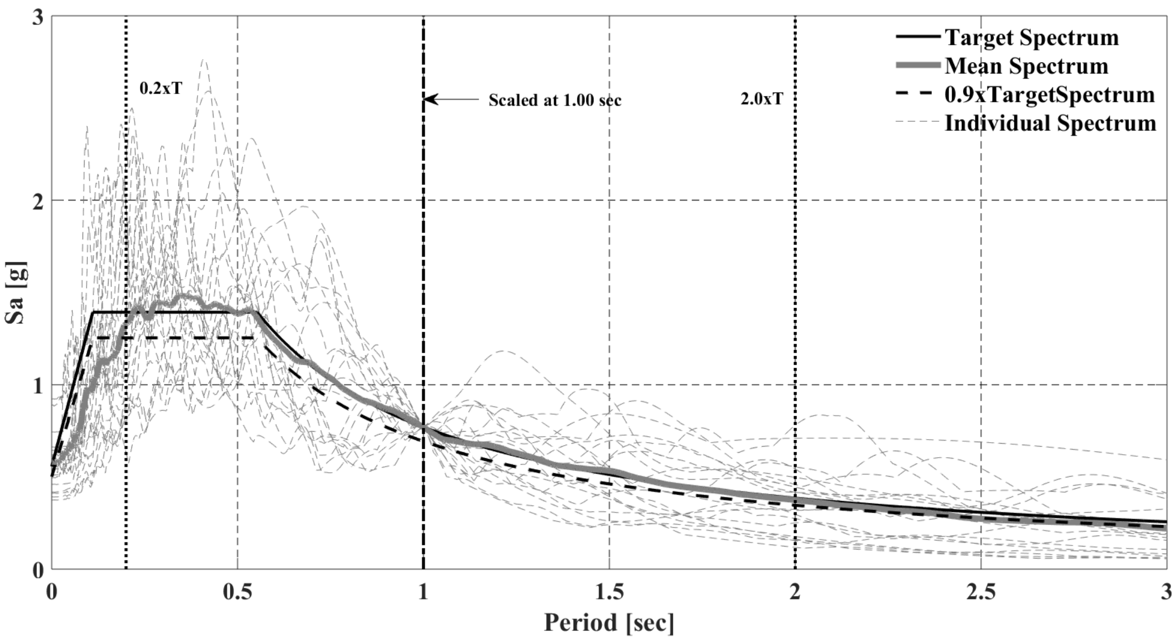
Target Spectrum
Mean Spectrum
0.9xTargetSpectrum
Individual Spectrum
0.2xT
Scaled at 1.00 sec
2.0xT
Sa [g]
Period [sec]
0
0.5
1
1.5
2
2.5
3

(c)

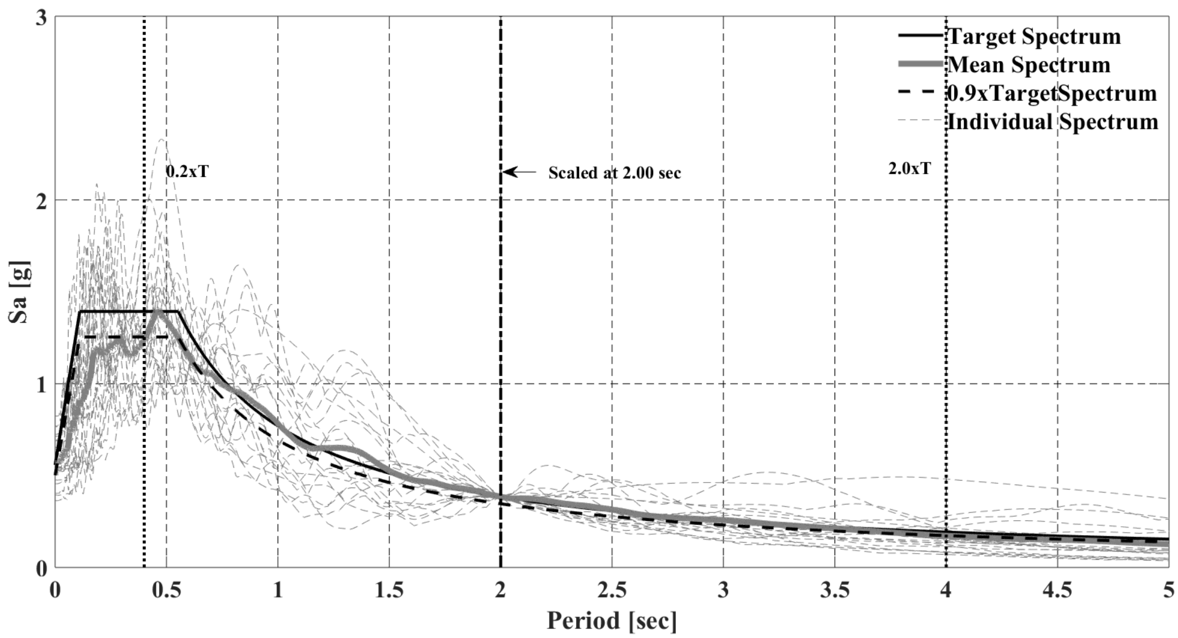

(d)

Figure 3.3 Acceleration response spectra of scaled ground motions used for the analysis of ENLSDOF systems: (a) at 0.25 sec, (b) at 0.50 sec, (c) at 1.00 sec and (d) 2.00 sec

3.3 Numerical Investigations for Quantification Parameters

In the development of equations for energy quantification factor and rise time, the dissipated energy was studied by subjecting the ENLSDOF systems to the scaled ground motions shown in Figure 3.3. The energy dissipation obtained by post-processing of force and deformation time histories was the basis for the development of the equations.

3.3.1 Energy Quantification Factor

The energy quantification factor, γ_{lp}, is a ratio of the input energy and dissipated energy in an ENLSDOF system as shown in Equation (3.1). Significance of the relationship as illustrated in Figure 3.5 lies in quantifying total energy to be dissipated, E_d, in an original building located at any site as a product of the input energy, E_i, and the factor, γ_{lp}, as in Equation (3.2):

$$\gamma_{lp} = \frac{E_d}{E_i} \tag{3.1}$$

E_d in Equation (3.2) is the energy dissipated by yielding in a steel structure and it can be expressed as follows (Chopra 2012):

$$E_d = \int_0^u f_s(u)du \tag{3.2}$$

where, $f_s(u)$ = resisting force of the inelastic SDOF system. E_d, the internal work done by the system, is a fraction of input energy exerted on the system by an earthquake. Input energy by the earthquake (E_i) to the system is the product of the mass of the system, m, and spectral acceleration, $S_a(T)$, and spectral displacement, $S_d(T)$ (= $\frac{4\pi^2 S_a(T)}{T^2}$), at the fundamental period of the system and can be expressed as follows:

$$E_i = \frac{1}{2} m S_a(T) S_d(T) \tag{3.3}$$

Figure 3.4 shows E_d and E_i relationship, where the grey trapezoidal area represents E_d and the black triangular area represents E_i. For the sake of simplicity, the total energy to be dissipated by an ENLSDOF system during an earthquake is shown by one trapezoidal area.

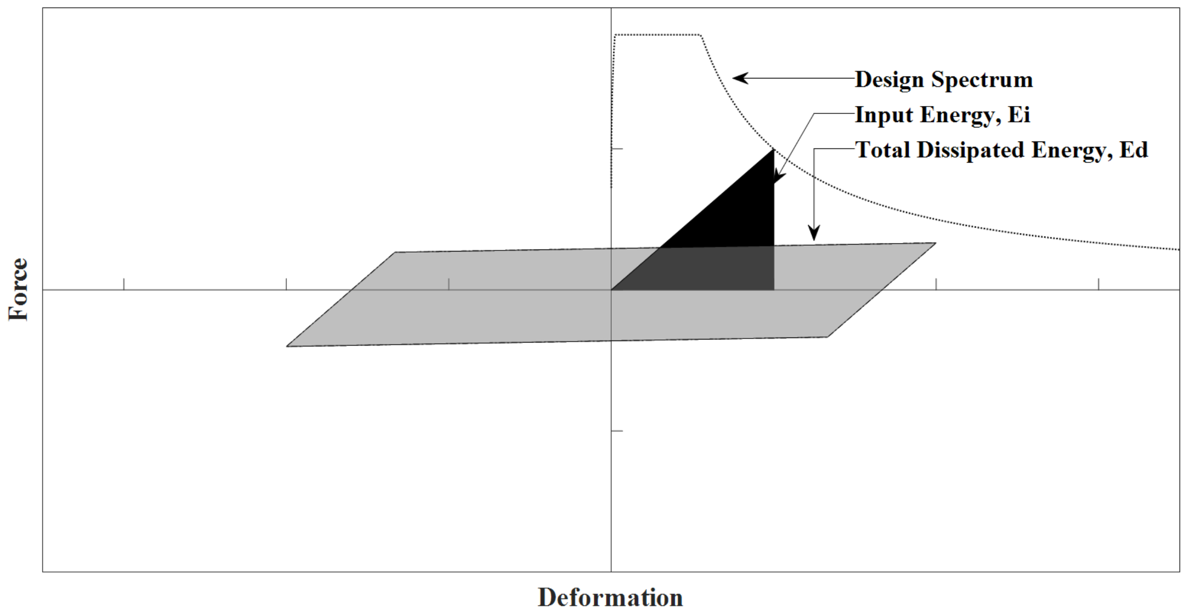

Figure 3.4 E_d-E_i relationship for determining Energy Quantification Factor, γ_{lp}

The energy quantification factor was determined during the post-processing of the results obtained from the nonlinear dynamic analysis of the ENLSDOF systems. Each ENLSDOF system was subjected to the ground motions scaled at the corresponding fundamental period to the design spectrum. The energy dissipated by an ENLSDOF system during an earthquake was calculated according to Equation (3.3). The total energy dissipated in the system during the earthquake normalized by input energy obtained from the target spectrum is the energy quantification factor, γ_{lp}. This procedure was repeated for four ENLSDOF systems whose yield strengths were modified by three response modification coefficients, R. For a specific ENLSDOF system and R-value, γ_{lp} was plotted against the fundamental period of the system. Hence, twenty γ_{lp} responses were plotted against the corresponding fundamental period. Those γ_{lp} responses were further categorized into three groups according to the R factors and the plots were shown in Figure B.2 of Appendix B.3. The development of the proposed equation as expressed in Equation (3.4) in this study was based on the median values of the energy quantification factors. For each group, a fit equation was proposed and the fit line corresponding to the equation was plotted as shown in Figure B.3 of Appendix B.3. It can be seen from the figure that the effect of R values is insignificant. Thus, the proposed Equation (3.4) is independent of R-value. The equation was fitted to the median γ_{lp} responses from ENLSDOF systems with R = 4.0, R = 6.0 and R = 8.0 respectively, as illustrated in Figure 3.5.

$$\gamma_{lp} = 0.09T^{-2.88} + 1.96 \tag{3.4}$$

Once the mass and stiffness of the building are known the designer can easily determine the energy quantification factor from Equation (3.4) and eventually quantify energy demand from the design spectrum.

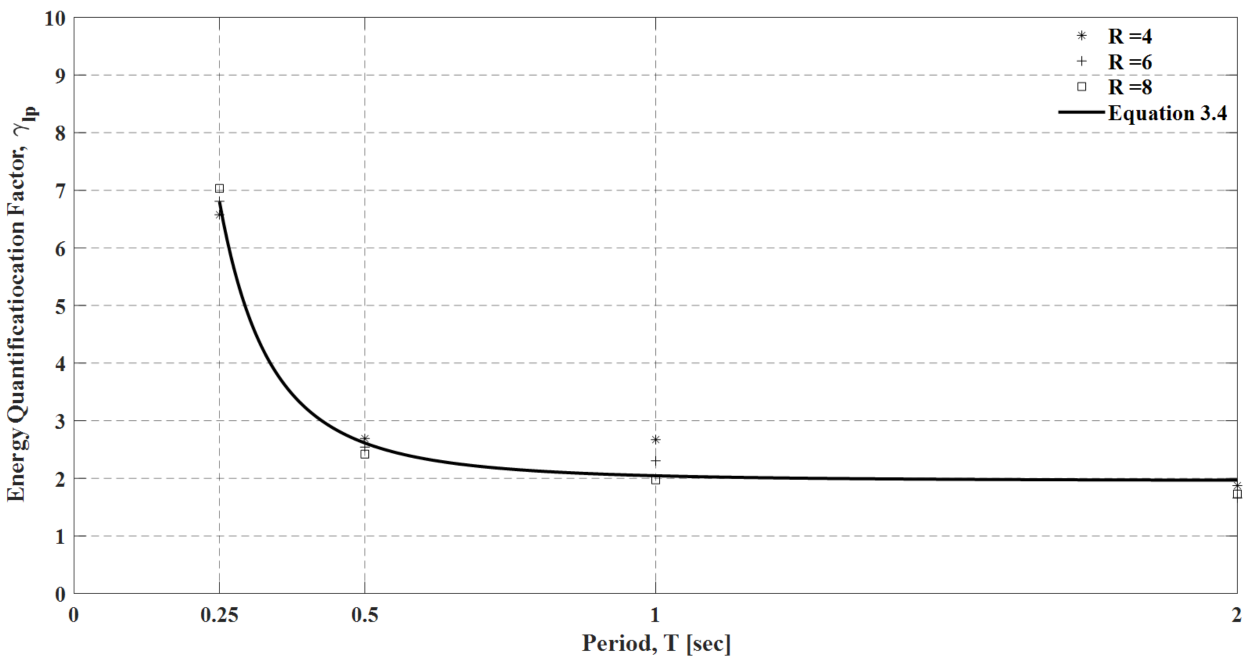

Figure 3.5 Fit line of proposed Equation (3.4) for Energy Quantification Factor, γ_{lp}

3.3.2 Rise Time

The concept of Rise Time, t_R, was inspired by the definition of effective duration of plastic work, which is obtained by normalizing dissipated energy by elastic work of BRB. The definition of the effective duration was provided by Dehghani and Tremblay (2012b). In this study, rise time, t_R, was defined as a rate at which energy was dissipated in the BRBs during an earthquake event. The time required to dissipate the total energy predicted from the design spectrum is called t_R. Hence, the energy dissipated during an earthquake is normalized by the product of E_i and γ_{lp}. The time required to accumulate 100% of this energy was further divided into 5%, 25%, 50%, 75% and 95% to provide load steps and accommodate cycles for the future possibility of development of loading protocols. The rise time is further illustrated in Figure 3.6. Note that, $t_{R5\%}$, $t_{R25\%}$, $t_{R50\%}$, $t_{R75\%}$, $t_{R95\%}$ and $t_{R100\%}$ are the rise times required to accumulate 5%, 25%, 50%, 75%, 95% and 100% of the total dissipated energy in the system.

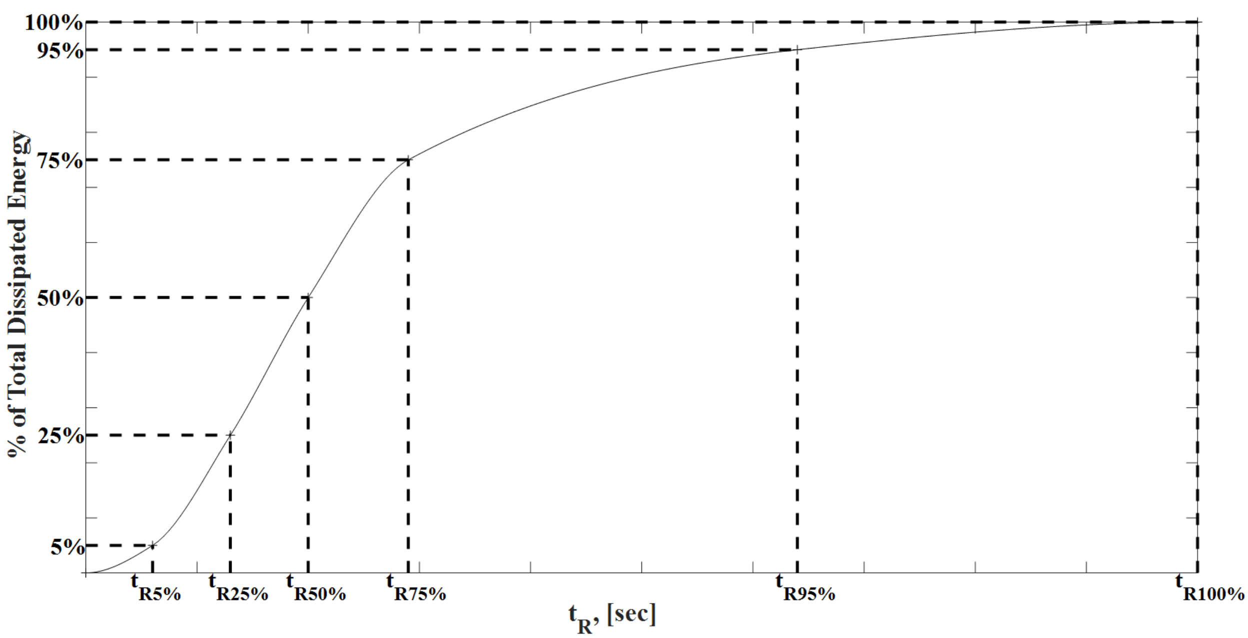

Figure 3.6 Schematic plot of Rise Time, t_R

Implementing the concept of rise time as defined above, equations as function of fundamental period for $t_{R5\%}$, $t_{R25\%}$, $t_{R50\%}$, $t_{R75\%}$, $t_{R95\%}$ and $t_{R100\%}$ were proposed. Nonlinear dynamic analyses on twelve ENLSDOF systems were performed using similar ground motions mentioned in Tables B.1 to B.4 of Appendix B.1 which were scaled at the corresponding fundamental period of the system to the design spectrum shown in Figure 3.3. The dissipated energy time history from an ENLSODF system for an earthquake was normalized to unity. The process was continued for all ENLSDOF systems subjected to the ground motions. Then, the median rise times were plotted against 5%, 25%, 50%, 75%, 95% and 100% of total dissipated energy in the system as shown in Figure B.4 of Appendix B.4. The figure shows t_R curves for each of the twelve ENLSDOF systems. The effect of the fundamental period (T) and response modification coefficient (R) was further investigated from two different points of view. In the first point of view, R-factors were kept constant and T of the systems were varied. The time to accumulate 100 percent of total dissipated energy (rise time) increased as fundamental periods of the systems were increased from 0.25 sec to 2.0 sec, as shown in Figure B.5 (a) – B.5 (c) of Appendix B.4. Then, the fundamental period T of the system was kept constant while R-factors were varied. It was observed that as R-factors were increased from 4.0 to 8.0, rise times increased as shown in Figure B.5 (d) – B.5 (g) of Appendix B.4. The increment in rise times was more prominent for systems with fundamental periods of 0.50 sec. and 1.00 sec. compared to systems with T of 0.25 sec and 2.00 sec.

The observations in Figure B.5 were useful for developing equations for rise time as a function of the fundamental period. The objective of such equations was similar to the energy quantification factor. The designers will be able to determine the rise time required to accumulate 5%, 25%, 50%, 75%, 95% and 100% of total dissipated energy respectively, once the mass and stiffness of a building are known. For that reason, rise times corresponding to 5%, 25%, 50%, 75%, 95% and

100% of total dissipated energy were obtained from an ENLSDOF system during an earthquake and plotted against the corresponding fundamental period. The process was continued for all ENLSDOF systems and ground motions. Based on the median values of the rise time responses, equations were proposed and fitted to the data as shown in Figure B.6 of Appendix B.4. The linear fit lines were shown separately in Figure B.7. Since there were no significant effects of R-factor values on the rise times, a set of equations for t_R were proposed irrespective of R-factors, see Equations (3.5a) – (3.5f).

$$t_{R5\%} = -0.09T + 1.67 \tag{3.5a}$$

$$t_{R25\%} = 0.86T + 3.19 \tag{3.5b}$$

$$t_{R50\%} = 1.95T + 4.94 \tag{3.5c}$$

$$t_{R75\%} = 4.83T + 6.23 \tag{3.5d}$$

$$t_{R95\%} = 8.74T + 9.39 \tag{3.5e}$$

$$t_{R100\%} = 2.36T + 31.11 \tag{3.5f}$$

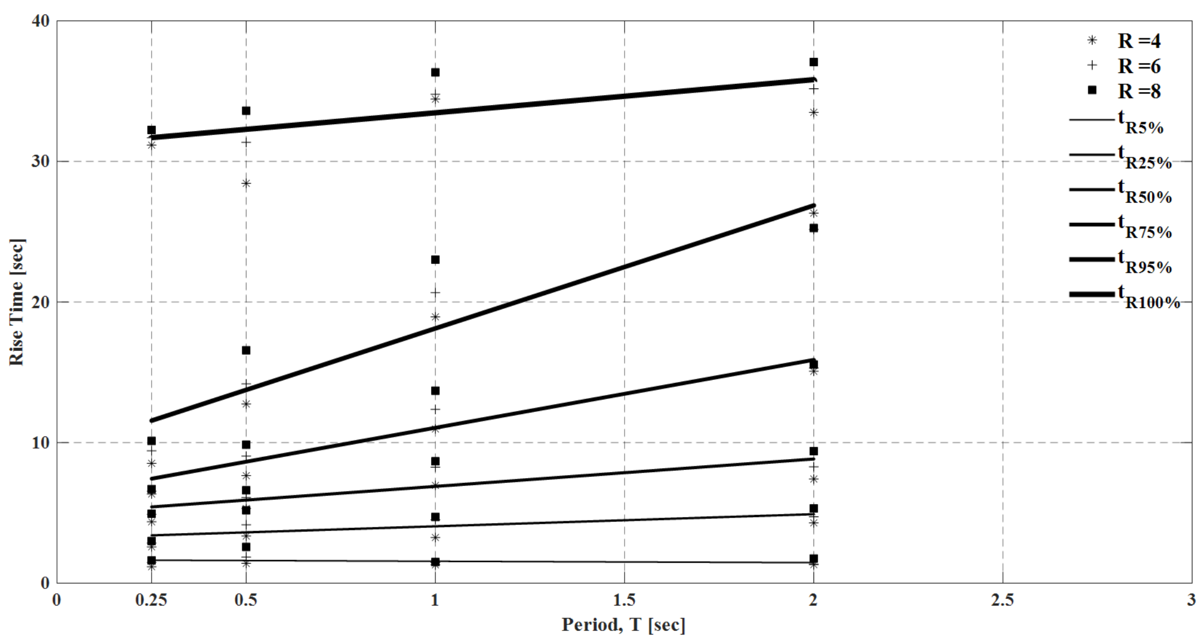

Figure 3.7 Fit line of proposed equations for Rise Time, t_R

The equations were fitted to the median responses obtained from the time history analyses as shown in Figure 3.7, where fit line of the equation for the time required to accumulate 5%, 25%, 50%, 75%, 95% and 100% of the total dissipated energy were shown from bottom to top respectively. Moreover, four rise time curves were obtained from the Equations (3.5a) – (3.5f) and compared with median rise time curves from time history analyses. For all the cases, the prediction fell within the cluster from time history analysis, as illustrated in Figure 3.8.

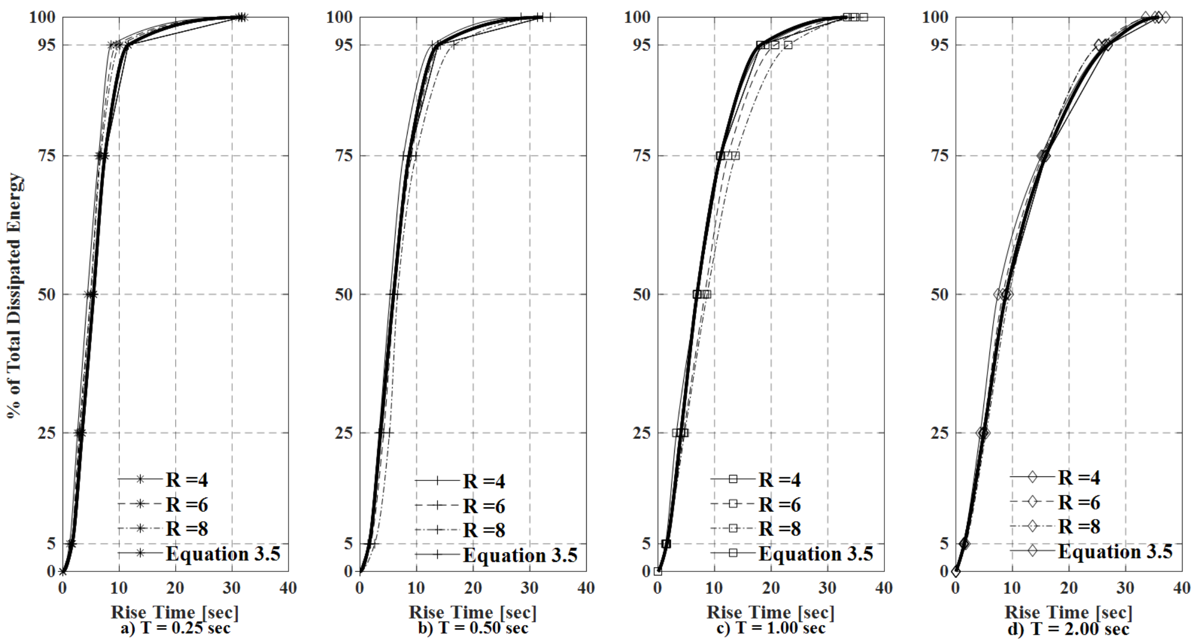

Figure 3.8 A comparison of the Rise Time curves from the proposed equations and time history analyses

3.4 Summary

The significance of the proposed approach lies in the simplicity of the application of the proposed equation for the Energy Quantification Factor (Equation (3.4)) and a series of equations for Rise Time (Equation (3.5)). Both parameters were proposed as a function of the fundamental period of a building. Moreover, the response modification factors did not have any significant effect on either the energy quantification factor or the rise time. Hence, once the mass and stiffness of a building are known, the engineers can easily quantify energy demand on BRB over time at different site locations.

Chapter 4: Distribution of Energy Dissipation Demand

4.1 Introduction

The chapter presents the development of an empirical equation for distributing dissipated energy demand for BRBs along the height of the building. The development and analysis of numerical models of prototype frames are discussed in Section 4.2. Based on the analysis results, the distribution procedure is developed and presented in Section 4.3.

4.2 Background on Numerical Procedure

The quantification approach has also been incorporated with a procedure to distribute energy demand over the floors. The objective is that once energy dissipation demand is determined from the design spectrum using Equation (3.5), the designers can easily approximate the distribution of dissipated energy over floors without conducting any nonlinear dynamic analysis. The proposed distribution procedure is based on distribution trends of dissipated energy observed in the numerical analysis of prototype frames.

4.2.1 Description of the Prototype Frames

A 3- and 6-storey prototype frame was adopted from Sabelli (2001) and modeled in this study. Moreover, numerical results of dissipated energy distribution over floors in an 8-storey frame were adopted from Choi and Kim (2006). The numerical results from these prototype buildings were the basis behind the development of the procedure to distribute dissipated energy.

The type of frame considered in this study was the moment-resisting frame (MRF) equipped with buckling-restrained braces (BRBs). MRFs equipped with conventional braces are effective lateral force resisting systems except the strength deteriorate significantly due to inelastic buckling during a strong earthquake shaking. BRBs are effective in overcoming this shortcoming of conventional braces. Different configurations of frames equipped with both conventional braces and BRBs studied by Sabelli (2001), laid a foundation and that worked for the development of recommended provisions for steel braced frames with BRBs by SEAOC-AISC Task Group in 2001 (Uang and Nakashima 2004). Three- and six-storey moment prototype frames equipped with BRBs of that study have been adopted to investigate the floor-wise distribution of dissipated energy. The 3-story prototype building has a rectangular plan with an overall dimension of $124' \times 184'$ $(37.8m \times 56.1m)$. Bay dimension and typical storey height are $30'(9.1m)$ and $13'(4m)$ respectively, as shown in Figure 4.1 (b). In each direction, there are four braced bays, as shown by thick black lines in Figure 4.1 (a). On the other hand, the 6-story prototype building has square plan with a total dimension of $154' \times 154'$ $(46.9m \times 46.9m)$. Typical storey height is $13'(4m)$, but, the height of the first story is $18'(5.5m)$ as shown in Figure 4.2 (b). Each direction contains six braced bays indicated by thick black lines as shown in Figure 4.2 (a). Only one braced bay was modeled for both 3- and 6-storey prototype frame.

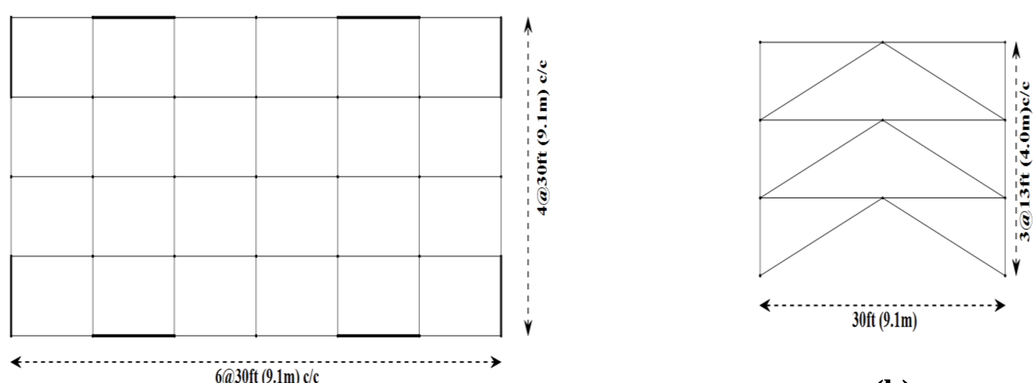

(a) **(b)**

Figure 4.1 3-Story prototype buildings: (a) plan view, and (b) elevation view of one of the bays equipped with BRBs

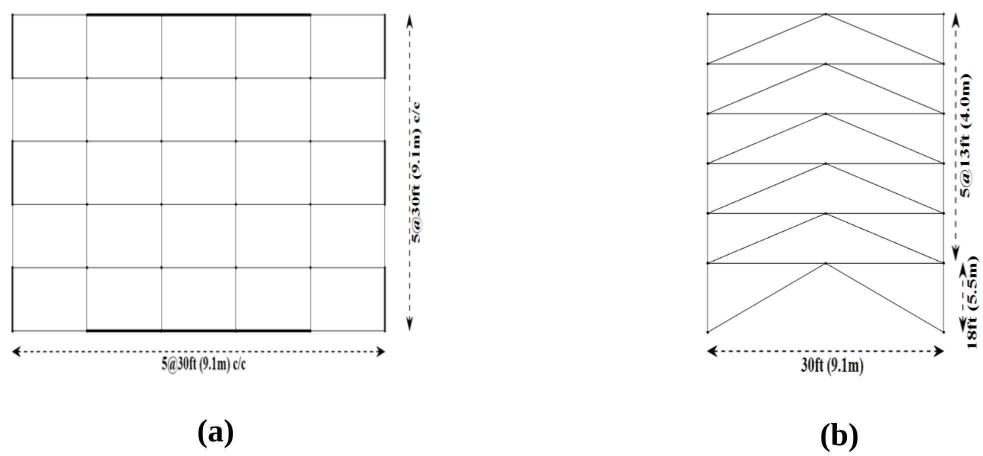

Figure 4.2 6-Story prototype building: (a) plan view and (b) elevation view of one of the bays equipped with BRBs

The 8-story building was selected from a study conducted by Choi and Kim (2006) where they proposed an energy-based design procedure using hysteretic energy spectra and accumulated ductility spectra for framed structures with BRBs. The building has three bays with bay width and typical story height of $24'(7.3m)$ and $12'(3.7m)$ respectively. However, the first story is $18'(5.5m)$ high as shown in Figure 4.3(b). Location of the braced frame is in mid-bays at the perimeter of the buildings as shown in Figure 4.3(a) with dark lines.

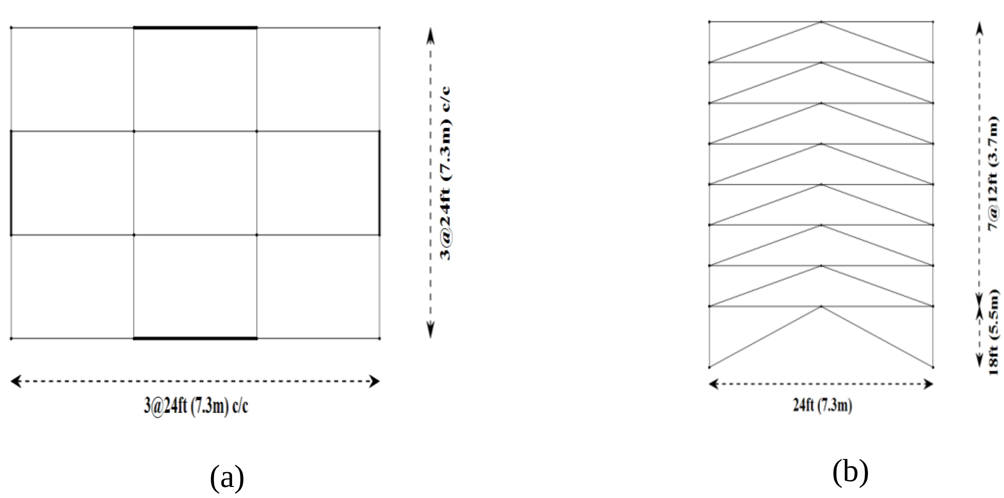

Figure 4.3 8-Story prototype building: (a) plan view and (b) elevation view of one of the bays equipped with BRBs

4.2.2 Design Information of the Prototype Buildings

In 3- and 6-storey frame design, similar criteria such as seismic weight of the building as in the SAC steel project research was incorporated (Sabelli et al. 2001). The seismic weight for the 3- and 6-storey building are 3,208 kips (14,270 kN) and 6,750 kips (30,025 kN) respectively. The buildings were designed according to FEMA 302/303 (1997) using the equivalent lateral force procedure to size the beams and columns and determine the brace axial capacity for braces. The design lateral force was based on a design spectrum corresponding to a hazard of 10% probability of exceedance in a 50-year period. Three response modification coefficient, (R) values namely 4.0, 6.0 and 8.0 were considered for this study. The occupancy type of the buildings was office-type, hence the importance factor of 1.0 was used in the design. The buildings belonged to seismic use group I and were designed considering seismic design category D. The buildings were located on a site in downtown, Los Angeles with site class D. While designing the buildings, the objective was to induce yielding in braces so that seismic force-resisting system remained elastic. The properties of beam and column sections and axial capacities of BRBs for 3- and 6-story buildings are shown in Table 4.1 and 4.2 respectively.

Table 4.1 Cross-sections of beams and columns and BRB axial capacities for 3-storey prototype building

Floor	Beam Section	Column Section	Axial Capacity of BRB kips (kN)		
			R = 4.00	R = 6.00	R = 8.00
3	W14X48	W12X96	234.00 (,1041.00)	156.00 (694.00)	117.00 (520.00)
2	W14X48	W12X96	392.00	261.00	196.00

			(1,744.00)	(1,161.00)	(872.00)
1	W14X48	W12X96	486.00 (2,162.00)	324.00 (1,441.00)	243.00 (1,081.00)

Table 4.2 Cross-sections of beams and columns and BRB axial capacities for 6-storey prototype building

Floor	**Beam Section**	**Column Section**	**Axial Capacity of BRB kips (kN)**		
			R = 4.00	**R = 6.00**	**R = 8.00**
6	W14X48	W14X132	176.00 (783.00)	117.00 (520.00)	88.00 (391.00)
5	W14X48	W14X132	320.00 (1423.00)	213.00 (947.00)	160.00 (712.00)
4	W14X48	W14X132	432.00 (1922.00)	288.00 (1281.00)	216.00 (961.00)
3	W14X48	W14X211	522.00 (2322.00)	348.00 (1548.00)	261.00 (1161.00)
2	W14X48	W14X211	584.00 (2598.00)	389.00 (1730.00)	292.00 (1299.00)
1	W14X48	W14X211	764.00 (3398.00)	509.00 (2264.00)	382.00 (1699.00)

In designing the 8-storey prototype frame equipped with BRBs, Choi and Kim (2006) adopted a modern design methodology based on the energy-balanced concept. Hysteretic energy demand was taken as the accumulated plastic energy in order to determine the required cross-sectional areas of the braces (Kim and Choi 2004). The hysteretic energy demand was obtained by constructing a hysteretic energy demand spectrum following a procedure proposed by Riddell and Garcia (2001). The accumulated plastic energy was the function of yield strength, yield deformation and accumulated ductility ratio which explained by Choi and Kim (2006). The total seismic weight of the building was 2,766 kips (12,304 kN). The member sizes and cross-sectional areas of BRBs are presented in Table 4.3.

Table 4.3 Cross-sectional dimension of beams and columns and areas of BRB for 8-storey prototype building

Floor	Beam Section	Column Section	BRB Area $in^2(cm^2)$
8	W18X40	W24X55	4.72 (30.46)
7	W18X40	W24X55	5.85 (37.71)
		W24X84	
6	W18X40	W24X84	6.37 (41.07)
5	W18X40	W24X84	7.09 (45.80)
		W24X94	
4	W18X40	W24X94	8.72 (56.29)
3	W18X40	W24X94	11.63 (75.06)
		W24X131	
2	W18X40	W24X131	15.07 (97.25)
1	W18X40	W24X131	28.71 (185.23)

4.2.3 Description of the Numerical Models

Two-dimensional finite element models were developed to simulate 3- and 6-storey prototype frames using OpenSees Navigator. The beams and columns were modeled using elastic beam-column elements with rigid beam-columns connections and pinned columns bases. The braces were modeled as Nonlinear truss elements with Steel02 material (Giuffré-Menegotto-Pinto material) to represent BRBs. The BRB force-deformation relationship was calibrated using the OpenSees platform against the experimental results obtained from the study conducted at UC Berkeley (Clark, et al. 1999) and shown in Figure 3.1. Masses were lumped at nodes based on the tributary area. The damping ratio of 2% was assigned in the analysis of 3- and 6-storey prototype frames, to be consistent with the analysis for the development of quantification parameters.

The 8-storey prototype frame was modelled in DRAIN-2D+ (Tsai and Li 1997) platform by Choi and Kim (2006). They modeled beam-column elements to remain elastic according to their design. An effective damping ratio of 2% was considered in their analysis. Nonlinear dynamic analysis was performed by subjecting the frame to 20 ground motion records which were developed for use in the FEMA/SAC project on steel moment-resisting frames located on soft rock sites.

4.2.4 Selection and Scaling of Ground Motions

In the selection of ground motions, similar criteria as discussed in Section 3.2 were followed. Then, the motions were scaled to the design spectrum consistent with the site where the prototype frames were located. The scaling was performed in accordance with the USA and Canadian codes (ASCE/SEI 7-16 2017, NBCC 2015) were followed. The fundamental periods of the 3- and 6-storey frame were 0.51 sec and 0.78 sec respectively. Hence, the ground motions were scaled to the different period range as shown in Figure 4.4, and scaling factors were different as well; this is shown in Table C.1 of Appendix C.1.

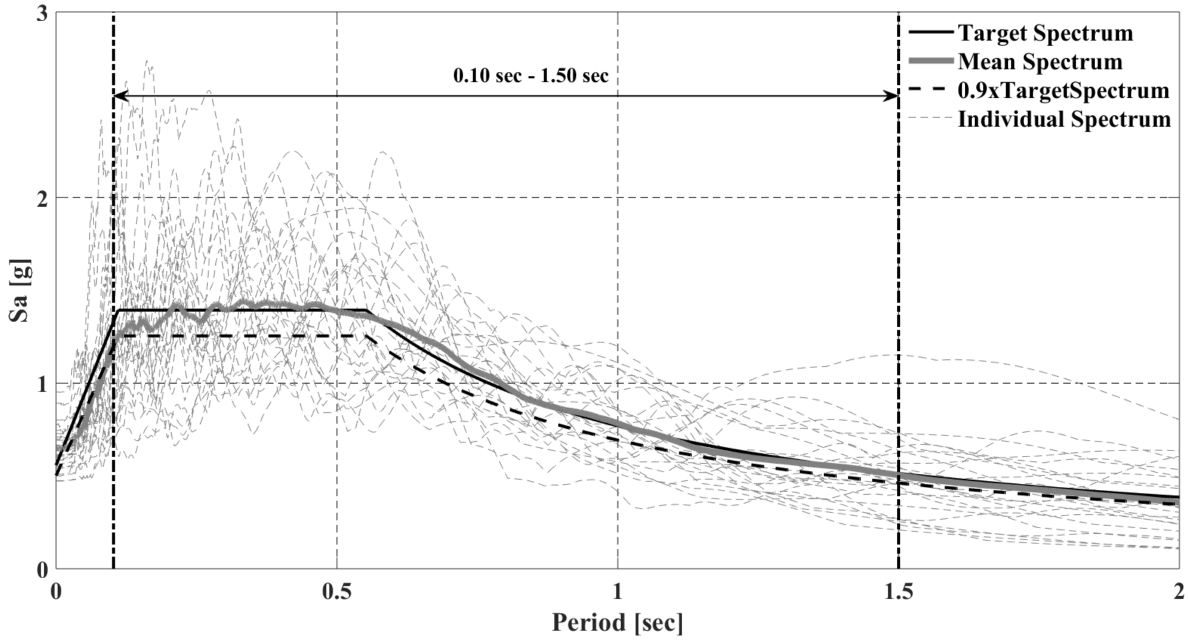

(a)

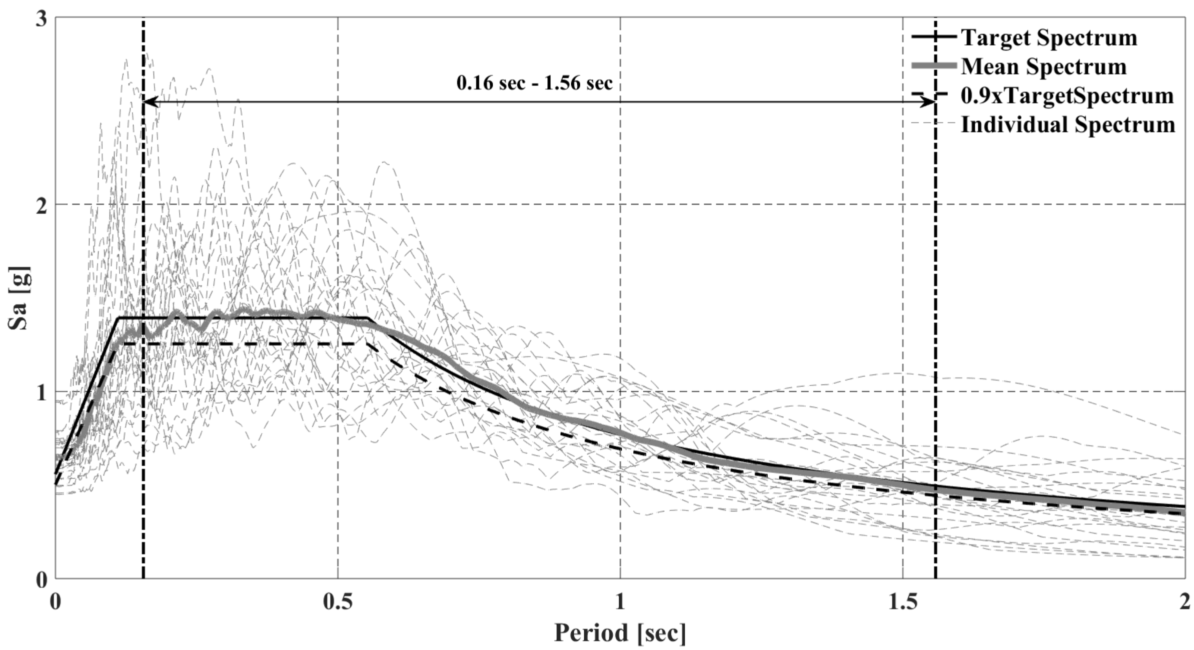

(b)

Figure 4.4 Acceleration response spectra of scaled ground motions used for the analysis of prototype frame: (a) 3-storey and (b) 6-storey

4.3 Floor-wise Distribution of Dissipated Energy

Empirical equations were proposed to distribute dissipated energy over the floors, where three coefficients govern the shape of the distribution. Equations as a function of the total number of storeys were also proposed to determine the coefficients. The development of the equations was based on distribution trends observed in the numerical results obtained from the nonlinear dynamic analysis of the above-mentioned prototype frames with BRBs.

4.3.1 Distribution from Numerical Analysis

Following the modeling approach, models of 3- and 6-storey prototype frames with three response modification coefficients, (R) were developed and subjected to 24 ground motions as presented in Table C.1. In the postprocessing, dissipated energy by BRB at each floor during an earthquake was obtained using Equation (3.2). Then, the dissipated energy at each floor was normalized by total dissipated energy which was the sum of the dissipated energy by BRB of all floors during that earthquake. For each floor, the normalized dissipated energy value at the end of the earthquake time history was the energy distribution for that floor. The procedure was applied for all earthquake time histories and all frames. The floor-wise dissipated energy distribution during each earthquake was plotted against the floor numbers in Figure C.1 of Appendix C.2. The median lines in that figure were corresponding to R values considered in this study. Figure 4.5 shows the results for R=8.0. The response modification coefficient (R) of 8.0 was relevant because ASCE 7-16 (2017) recommends the use of R=8.0 for the simplified seismic design of steel braced frames with BRBs.

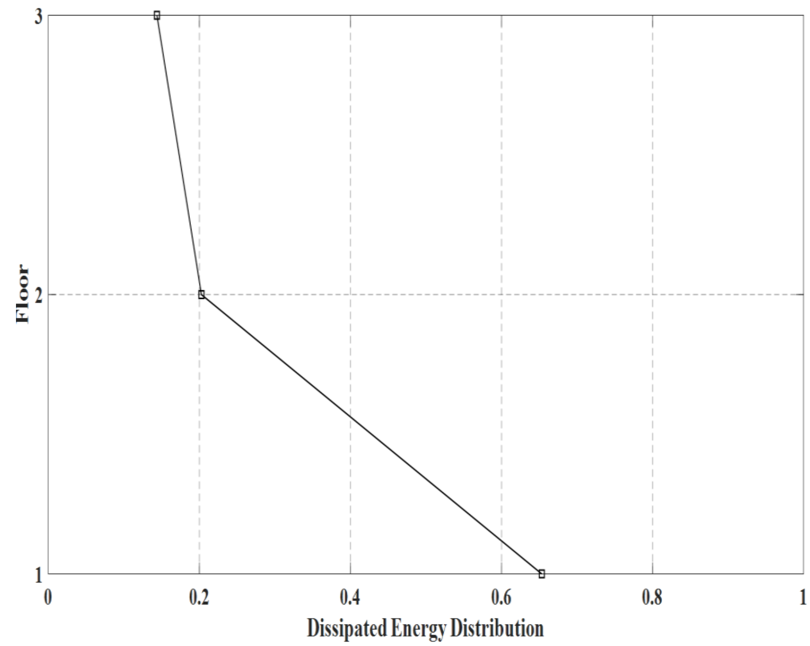

(a)

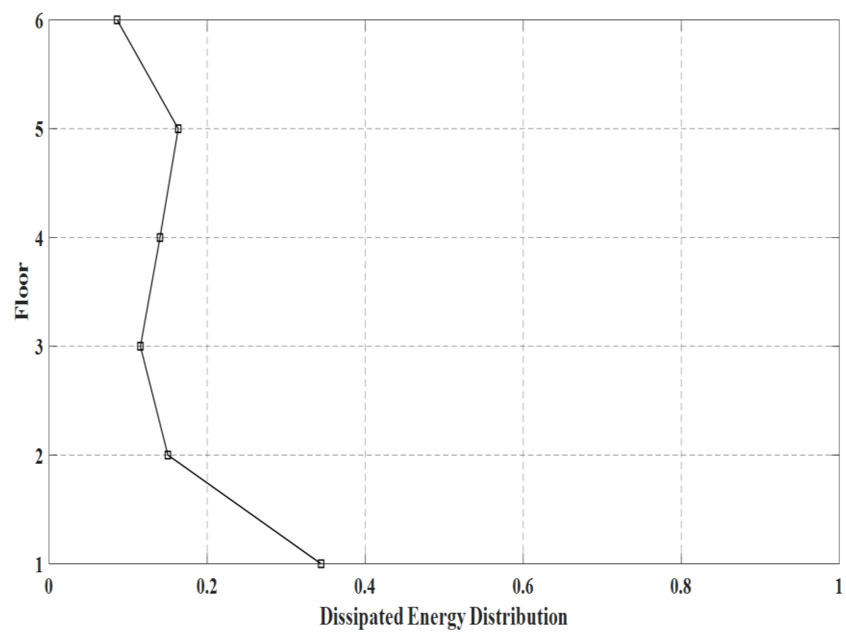

(b)

Figure 4.5 Median floor-wise dissipated energy distribution for prototype frames with R = 8.0: (a) 3-storey and (b) 6-storey

The floor-wise dissipated energy distribution for the 8-storey prototype frame was adopted here from the study conducted by Choi and Kim (2006) and as shown in Figure 4.6.

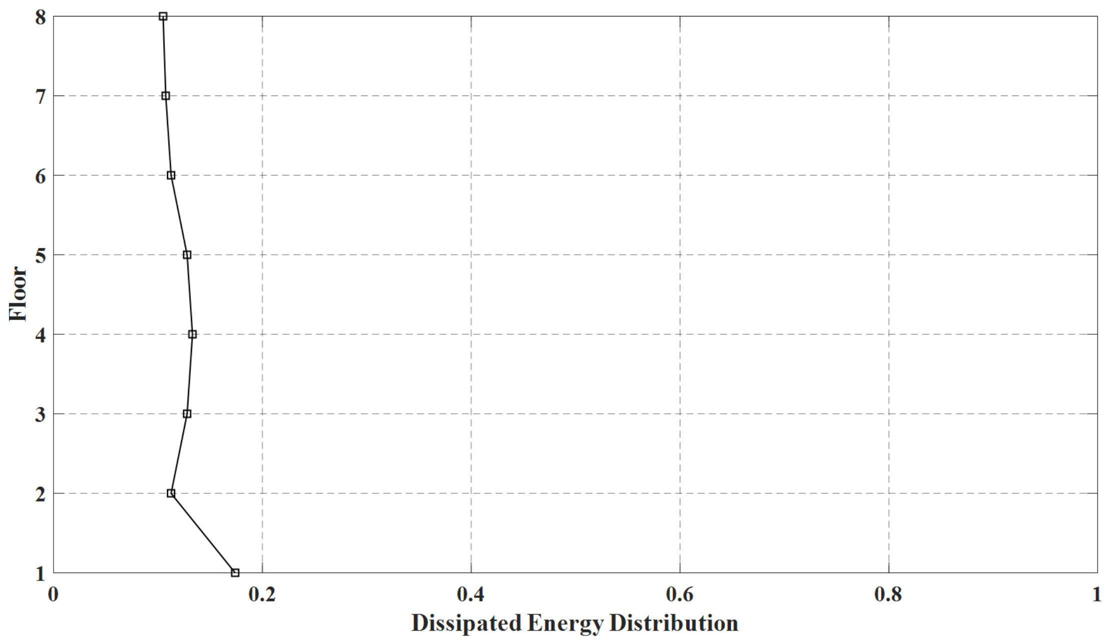

Figure 4.6 Median floor-wise dissipated energy distribution of 8-storey prototype frame

The floor-wise distribution for 3-storey frame is simple. From 1st floor to 2nd floor and then from 2nd floor to 3rd floor, the shape of the distribution is linear as shown in Figure 4.5 (a). Four transitions in the shape are observed in the floor-wise distribution for 6-storey frame as shown in Figure 4.5 (b). Similarly, five transitions are observed in the floor-wise dissipated energy distribution for 8-storey frame as shown in Figure 4.6 which are from 1st to 2nd, 2nd to 3rd, 3rd to 4th, 4th to 6th and 6th to 8th. In all those transitions, the transition from 1st to 2nd floor is significant in terms of relative difference from 2nd floor which are 222.14%, 128.86% and 54.55% for 3-, 6- and 8-storey prototype frames respectively. Transitions at other floor levels compared to 2nd floor range between 6% to 43% and 0% to 19% for 6-storey and 8-storey frames respectively. For 3-storey frame, the upper-floor transition is 29.09% relative to the 2nd floor. It should be noted that the absolute values of relative differences are reported here. It can also be observed that the number of transitions increases with the number of stories of the frame. The random nature of floor-wise distribution makes the approximation of the distribution difficult without some convenient and efficient assumptions.

4.3.2 Development of Proposed Distribution Procedure

Based on the previous observations, two assumptions were made to propose the procedure to distribute dissipated energy over the floors in a frame. The first assumption was that energy distribution for various floors is a function of energy distribution at the second-floor level. The second assumption was that the distribution shape is controlled by three transition zones. The transition zone 1 was defined as the relationship between 1st and 2nd floor energy distribution. The transition zone 2 was defined as the relationship between the floors from 2nd to (n-2)th floor with respect to 2nd floor. Finally, the transition zone 3 was defined as the relationship between the (n-2)th and nth floors. These transition zones are illustrated in Figure 4.7. For idealization purposes, the shape is shown as linear, however, actual shape is highly nonlinear as observed in postprocessing of dynamic analysis results.

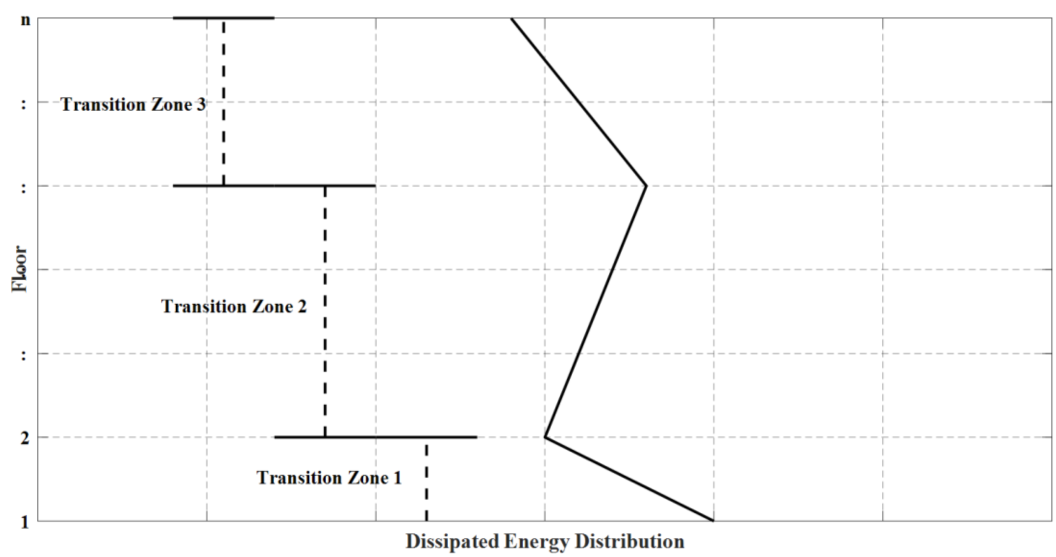

Figure 4.7 Idealized transition zones for floor-wise energy distribution

For the purpose of developing the energy distribution equation, a coefficient was proposed corresponding to each transition zone. For transition zone 1, a coefficient C_1 was proposed. If energy distribution in the second floor is E_2, then energy distribution of the first floor, E_1, is as follows:

$$E_1 = C_1 E_2 \tag{4.1}$$

For transition zone 2, a coefficient C_2 was proposed. Then, energy distributions from 3rd to (n-2)th floors are as follows:

$$E_i = (i-2) \times C_2 E_2 \tag{4.2}$$

where, i = 3, 4, ……., (n-2). The use of the Equation (4.2) can be illustrated for a n-storey prototype frame as follows:

$$E_3 = (3-2) \times C_2 E_2$$

$$E_4 = (4-2) \times C_2 E_2$$

$$\vdots \quad \vdots \quad \vdots$$

$$E_{n-2} = ((n-2)^{th} - 2) \times C_2 E_2$$

For transition zone 3, a coefficient C_3 was proposed. Energy distribution for (n-1)th and nth floor is determined relative to energy distribution in (n-2)th floor. As energy distribution in (n-2)th floor was related to E_2, so the energy distribution was expressed as follows:

$$E_{n-1} = 2(n-4) C_3 C_2 E_2 \tag{4.3}$$

$$E_n = (n-4) C_3 C_2 E_2 \tag{4.4}$$

The floor-wise energy distribution from the nonlinear dynamic analysis was obtained by normalizing energy dissipated at each floor by the sum of the energy dissipated during a specific earthquake and continuing for all the earthquake records, hence, the sum of the energy distributions is equal to 1. The total of the energy distributions can be expressed as follows:

$$\sum_{j=1}^{n} E_j = 1 \tag{4.5}$$

Equation (4.5) can be simplified by substituting E_1 to E_n from Equation (4.1) to (4.4) into Equation (4.5) as follows:

$$\left\{C_1 + 1 + \frac{(n-4)(n-3)}{2} C_2 + 3(n-4)C_3C_2\right\} E_2 = 1 \tag{4.6}$$

where, n = total number of stories. As Equation (4.6) was developed based on three transition zones, it could not be used for 3-storey prototype frame. Moreover, for n=3 and n=4, some parts of the equation became negative which was against the basic that total energy distribution is equal to 1, hence, the equation can only be used for n ≥ 5. Equations (4.7) and (4.8) for 3- and 4-storey prototype frames with BRBs respectively are as follows:

$$(C_1 + 1 + C_3C_2)E_2 = 1, \qquad for\ n = 3 \tag{4.7}$$

$$(C_1E_2 + 1 + C_2 + C_3C_2)E_2 = 1, \qquad for\ n = 4 \tag{4.8}$$

The following equations can be used to determine C_1, C_2 and C_3 values as a function of the number of storeys:

$$C_1 = 0.075n^2 - 1.035n + 5.43 \tag{4.9}$$

$$C_2 = 0.058n^2 - 0.9417n + 4.3 \tag{4.10}$$

$$C_3 = 0.005n^2 - 0.03n + 0.42 \tag{4.11}$$

In the development of the Equations (4.9) to (4.11), the floor-wise distribution of dissipated energy from the analysis of 3-, 6- and 8-storey prototype frames was compared with the predictions using the empirical equation. Equation (4.7) was used for the prediction of floor-wise distribution for 3-

storey frame. Values of C_1, C_2 and C_3 coefficients were varied using a ″trial-and-error″ approach until the shape of the distribution was close to the one obtained from nonlinear dynamic analysis. The comparison is shown in Figure 4.9. It was also observed from the comparison that the range of the relative difference between the prediction and the analysis was between 3% to10% as shown in Table 4.4.

Table 4.4 Comparison of the floor-wise energy distribution of 3-Story Frame

Floor (j)	**Nonlinear Dynamic Analysis**	**Predicted E_j**	**Relative Difference (%)**	**Remarks (overestimate↑ underestimate ↓)**
3	0.144	$E_3 = 0.158$	9.80	↑
2	0.203	$E_2 = 0.211$	3.81	↑
1	0.653	$E_1 = 0.632$	-3.32	↓
Total	1.00	1.00		

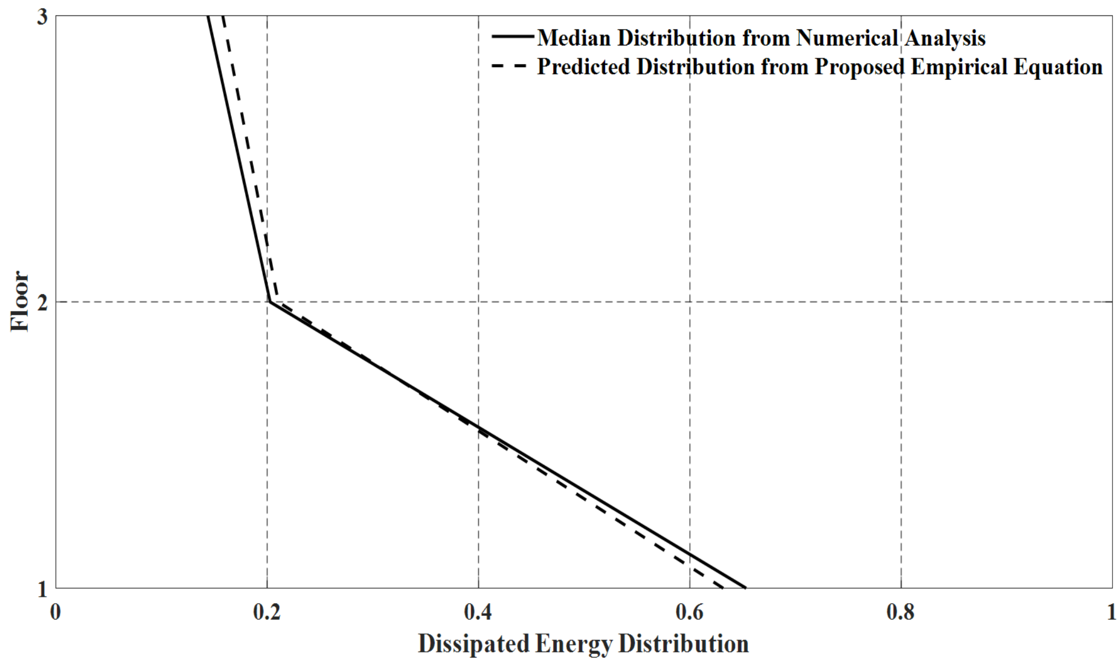

Figure 4.8 Comparison between floor-wise dissipated energy distribution from the prediction vs nonlinear dynamic analysis for 3-storey prototype frame

From Figure 4.8, it is evident that the prediction underestimated at 1st floor and overestimated at 2nd and 3rd floors. The difference between prediction and analysis is also presented in Table 4.4, where (↑) and (↓) are used to indicate overestimated and underestimated prediction. Similarly, the prediction of the floor-wise distribution of dissipated energy for 6- and 8-storey frames was obtained by implementing Equation 4.6. The comparisons for 6- and 8-storey frames are also shown in Figures 4.9 and 4.10 respectively. Numerical comparisons between the predicted floor-wise distribution of dissipated energy and distribution from the nonlinear dynamic analysis are shown in Tables 4.5 and 4.6.

Table 4.5 Comparison of the floor-wise energy distribution of 6-Story Frame				
Floor (j)	**Nonlinear Dynamic Analysis**	**Predicted E_j**	**Relative Difference (%)**	**Remarks (overestimate↑ underestimate ↓)**
6	0.086	$E_6 = 0.089$	3.64	↑
5	0.163	$E_5 = 0.178$	9.22	↑
4	0.140	$E_4 = 0.212$	51.44	↑
3	0.116	$E_3 = 0.106$	-8.02	↓
2	0.150	$E_2 = 0.142$	-5.82	↓
1	0.344	$E_1 = 0.272$	-20.99	↓
Total	1.00	1.00		

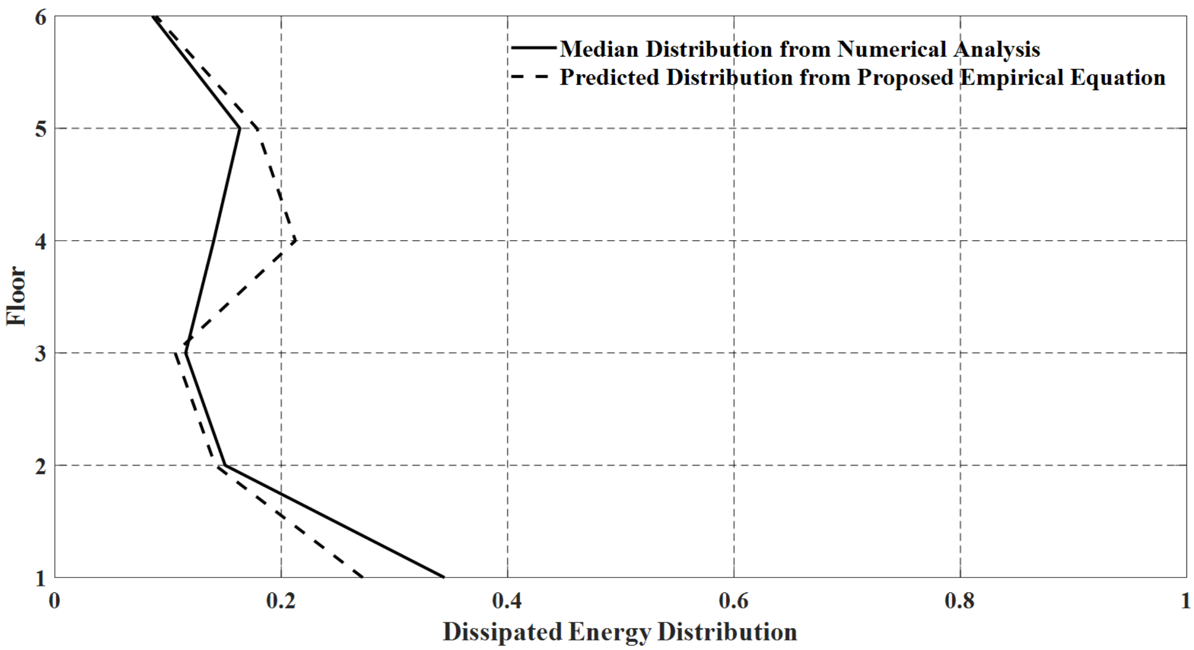

Figure 4.9 Comparison between floor-wise dissipated energy distribution from the prediction vs nonlinear dynamic analysis for 6-storey prototype frame

Table 4.6 Comparison of the floor-wise energy distribution of 8-Story Frame				
Floor (j)	**Nonlinear Dynamic Analysis**	**Predicted $\boldsymbol{E_j}$**	**Relative Difference (%)**	**Remarks (overestimate↑ underestimate ↓)**
8	0.105	$E_8 = 0.091$	-12.91	↓
7	0.107	$E_7 = 0.183$	70.04	↑
6	0.113	$E_6 = 0.183$	62.31	↑
5	0.128	$E_5 = 0.137$	7.12	↑
4	0.133	$E_4 = 0.091$	-31.33	↓
3	0.128	$E_3 = 0.046$	-64.29	↓
2	0.113	$E_2 = 0.091$	-18.85	↓
1	0.174	$E_1 = 0.178$	2.40	↑
Total	1.000	1.000		

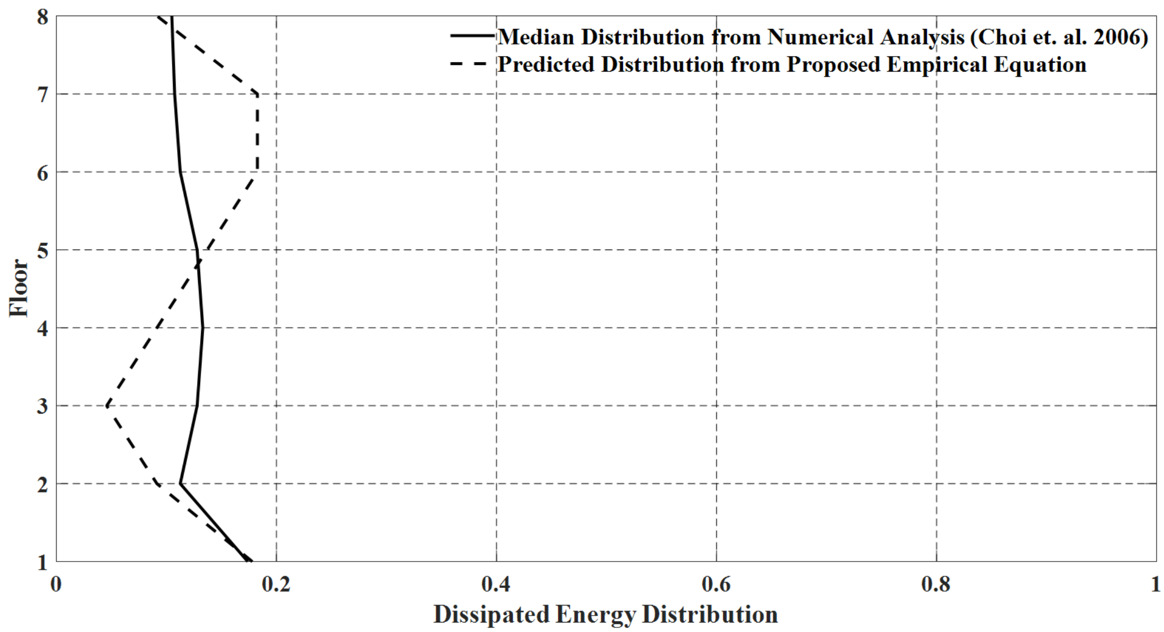

Figure 4.10 Comparison between floor-wise dissipated energy distribution from the prediction vs nonlinear dynamic analysis for 8-storey prototype frame

The relative differences in the prediction for 6- and 8-storey range between 3% to 52% and 2% to 71% respectively. The prediction for 6-storey frame underestimates from 1st to 3rd floor whereas overestimates from 4th to 6th floor, as shown in Table 4.5. The prediction for 8-storey frame underestimates from 2nd to 4th floor and at 8th floor whereas overestimates from 5th to 7th floor and at 1st floor. The values for C_1, C_2 and C_3 that resulted in the best prediction for floor-wise distribution as compared to nonlinear dynamic analysis are shown in Table 4.7. The empirical equation was developed to predict dissipated energy demand distribution at the floors with three coefficients assuming three transition zones. However, the distribution from nonlinear analysis for 8-storey frame has four transition zones. That is why it was difficult to obtain the best prediction of floor-wise distribution for 8-storey frame. However, the results were useful for developing equations to determine those coefficients without analysis.

The equations were proposed as a function of the total number of stories of the building. For that reason, a fit line for each coefficient against the total number of stories of their corresponding prototype frame was plotted in Figure 4.12. These fit lines were the basis for the equations for C_1, C_2 and C_3 presented in this chapter.

Table 4.7 Coefficients for the prediction of the floor-wise distribution of dissipated energy for 3-, 6- and 8-storey prototype frame

Prototype Frames	C_1	C_1 Relative to n = 8 (%)	C_2	C_2 Relative to n = 8 (%)	C_3	C_3 Relative to n = 8 (%)
3-Storey (n = 3)	3.000	154	2.000	400	0.375	75
6-Storey (n = 6)	1.920	99	0.750	150	0.420	84
8-storey (n = 8)	1.950	100	0.500	100	0.500	100

The values of C_1, C_2 and C_3 for the 3-, 6- and 8-storey frame was presented in Table 4.7. For C_1 and C_2 values, an increase of 154% and 400% was observed respectively, whereas for C_3 value a decrease of 75% was observed for 3-storey frame compared to 8-storey frame. For 6-storey, an increase of 150% was observed for C_2 values and a decrease of 99% and 84% was observed for C_1 and C_3 values. For C_2 values, an increasing trend was observed with decreasing height of the building. For C_3 values, a decreasing trend was observed with decreasing height of the building. However, C_1 trend was not as uniform as other two. The trends were further illustrated in Figure 4.11.

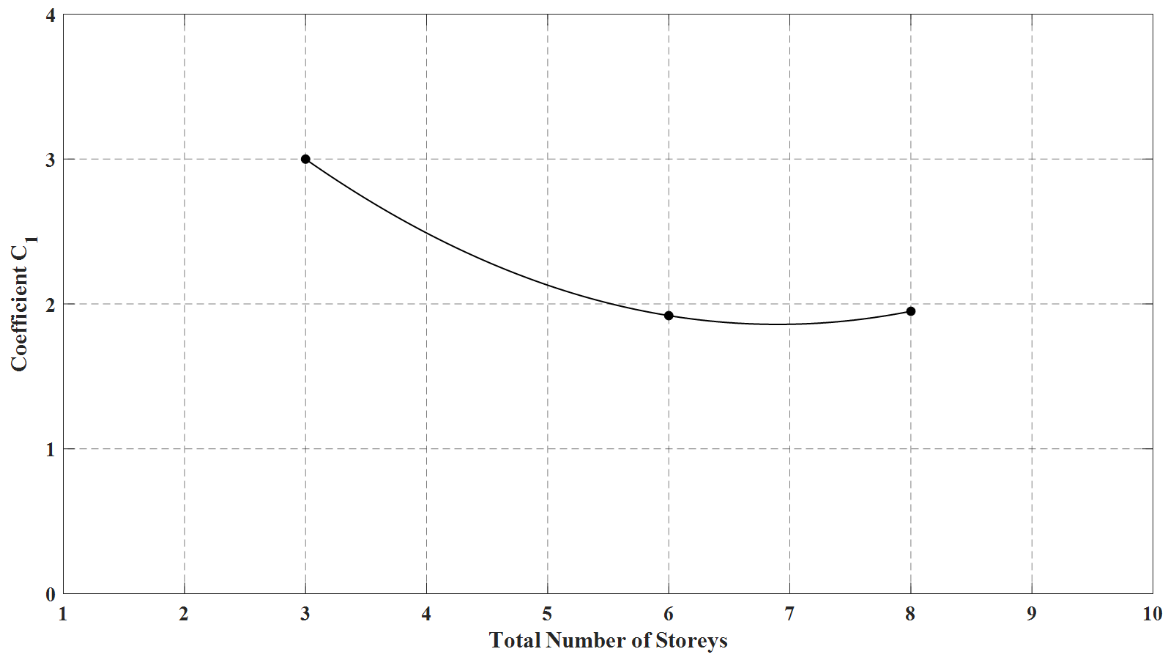

Coefficient C_1
Total Number of Storeys

(a)

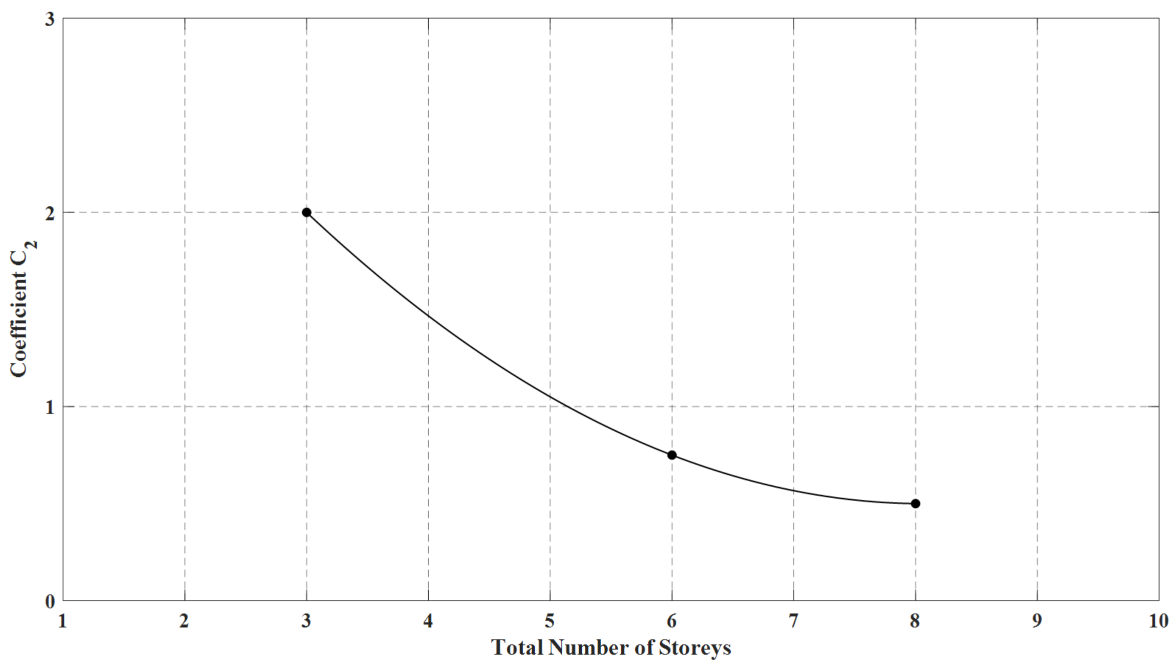

Coefficient C_2
Total Number of Storeys

(b)

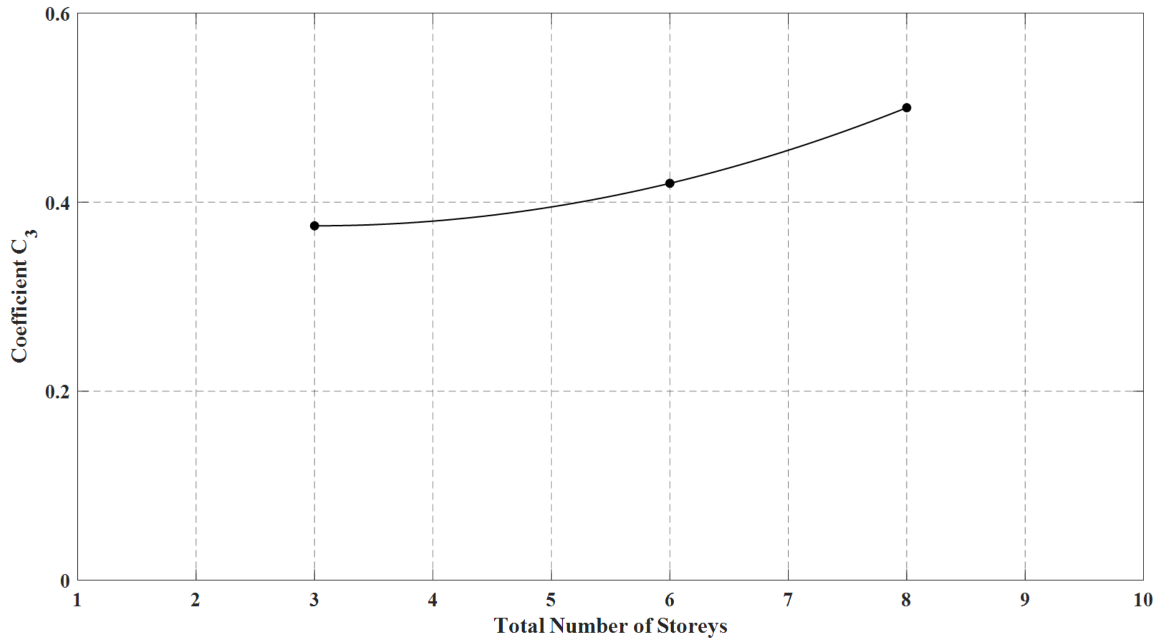

(c)

Figure 4.11 Fit Lines for coefficients (a) C_1 (b) C_2 and (c) C_3

4.4 Summary

A procedure was developed to obtain an estimate of floor-wise energy distribution for a frame equipped with BRBs without conducting a nonlinear dynamic analysis. An empirical equation for floor-wise energy distribution was developed using three coefficients based on numerical analysis results. Equations to determine the coefficients based on the number of storeys in buildings were also developed. The proposed empirical equation was applied to 3-, 6- and 8-storey prototype frame buildings. This application was useful for comparing the shape of the energy distribution to median distribution from numerical analysis. It was observed that the prediction obtained from the empirical equations was relatively close to the analysis values. The equations were proposed to determine the coefficients as a function of the number of storeys in a building. The significance of the proposed floor-wise procedure lies in the distribution of dissipated energy for BRBs located at different floors once the energy demand was predicted using equations developed in Chapter 3.

Chapter 5: Validation of the Proposed Quantification Approach

5.1 Introduction

The proposed quantification approach is applied to a 5-storey frame configuration in this chapter. The description and development of numerical models of the prototype frame are discussed in Section 5.2. The procedure has been validated in Section 5.3 by comparing energy distribution and energy demand over time to the demand obtained from numerical analysis.

5.2 Prototype Building for Application of the Approach

The effectiveness and efficiency of the proposed approach were investigated by applying it to a 5-storey prototype frame. The configuration of the BRBs was diagonal. The seismic hazard intensity parameters used in the seismic design of 5-storey configuration were S_{ds} = 0.733g and S_{d1} = 0.60g whereas, in the development of the approach, it was S_{ds} = 1.393g and S_{d1} = 0.77g. The differences in site seismicity of the location were crucial for the validation of the proposed approach as the energy demand was quantified from the design spectrum. The BRB force-deformation relationship was adopted from a test on BRB by Merritt (2003), hence the validation was performed proved for a different BRB than the one that used for the development of the approach.

5.2.1 Description of the Prototype Building

The prototype building was designed considering that site location was in an area of moderate to high seismicity according to ASCE 7-10 (Bruneau, et al. 2011). The floor plan of the building has a dimension of 150′ (45.72m) x 150′ (45.72m) with a bay dimension of 30′ (9.1m) as shown in Figure 5.1 (a). The typical storey height of the building is 13′ (4m), except for the first story which is 18′ (5.5m) high. The braced frames are located along the building perimeters. The braced frames are further subdivided into three bays with the bay dimension of 20′ (6.1m) as shown in Figure 5.1 (b).

The design was performed according to ASCE 7-10 (2010) and AISC 341 (2010). A global yield mechanism was expected in which the braces yield in both tension and compression, and plastic hinges form at the column bases and the frame elements (Bruneau, et al. 2011). The building was designed for force modification coefficient, R, of 8.0 and the importance factor, I, of 1.0. The design spectrum representing the building site class D was developed in accordance with ASCE 7-10 (2010). The seismic weight of the building was 11,550 kip (51,377 kN). The detailed design of frame members and BRBs was conducted by Bruneau (2011). The member sizes for beams, columns and axial capacities of BRBs are shown in Table 5.1.

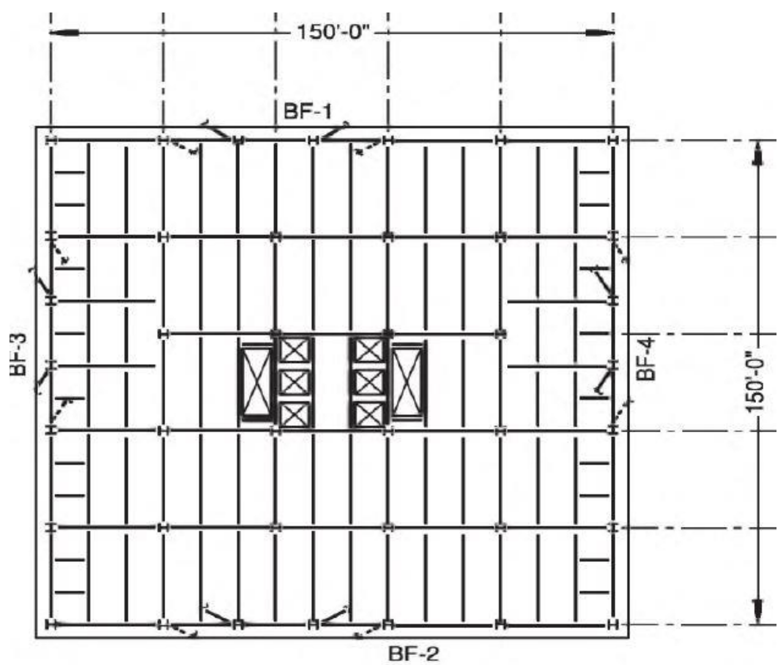

(a)

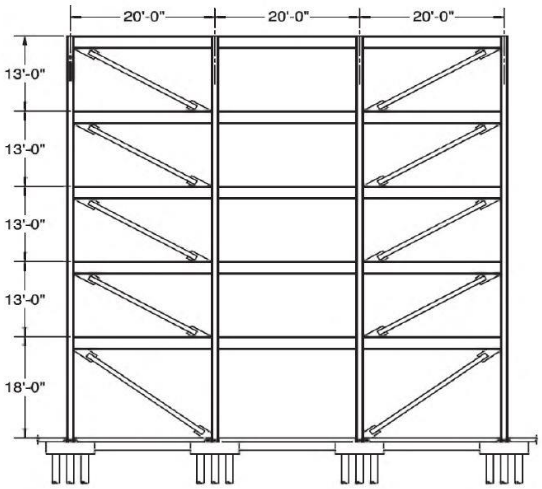

(b)

Figure 5.1 5-storey prototype building: (a) floor plan, and (b) elevation of perimeter frame equipped with BRBs (Bruneau et. al. 2011)

Table 5.1 Beam and column member specifications and axial capacities of BRBs

Floor	**Beam Section**	**Column Section**		**Axial Capacities of BRB (kip (kN))**
		Exterior	**Interior**	
5	W18X50	W14X74	W14X68	92 (409.00)
4	W18X60	W14X74	W14X68	166 (738.00)
3	W21X73	W14X74	W14X68	219 (974.00)
2	W21X73	W14X145	W14X132	253 (1125.00)
1	W21X83	W14X145	W14X132	305 (1357.00)

5.2.2 Development of Numerical Model

A two-dimensional finite element model was developed to represent the 5-story frame using the OpenSees software platform. Since the design assumed that plastic hinge would develop at the column bases, the frame was modeled as fixed-base. The beams and columns were modeled using the fiber force beam-column elements with rigid connections. Braces were designed to yield in both tension and compression. Hence, a BRB was modeled as a nonlinear truss element with Steel02 material (Giuffré-Menegotto-Pinto material). The BRB force-deformation relation was calibrated using the OpenSees platform against the experimental results from the study conducted at the UCSD (Merritt, et al. 2003) as shown in Figure 5.2. Seismic masses were lumped at each node. The damping of 2% was assigned in the analysis to be consistent with the analysis performed in Chapters 3 and 4.

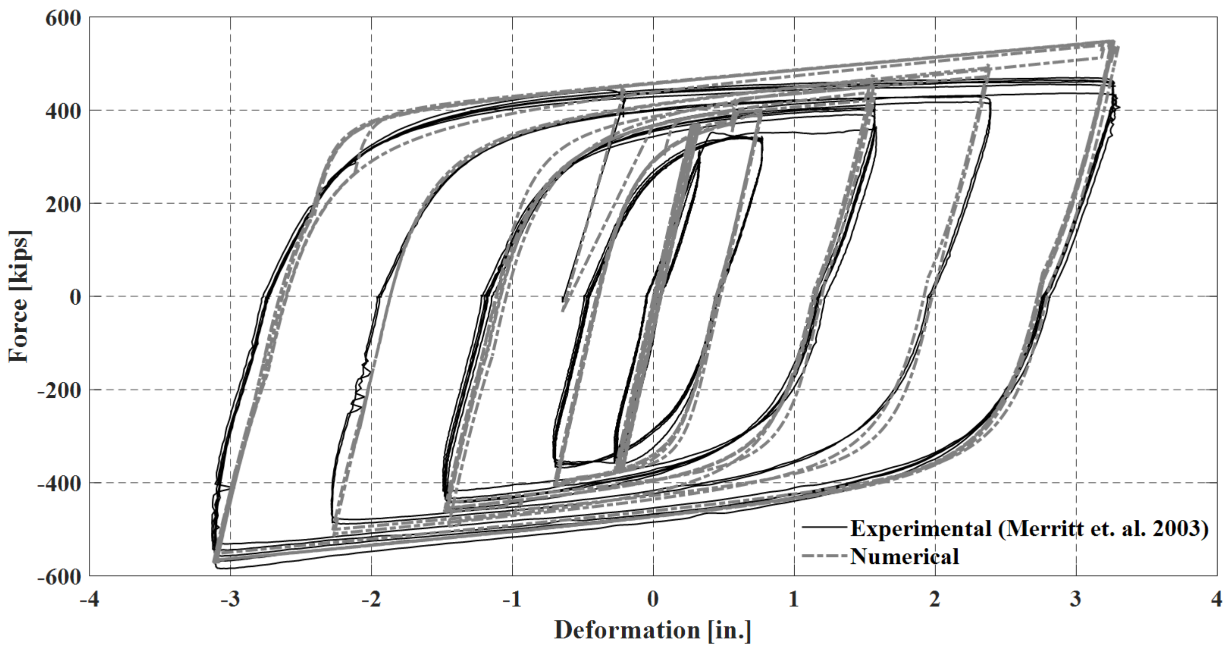

Figure 5.2 Comparison of experimental force-deformation relationship for BRB and OpenSees numerical simulation

5.2.3 Selection and Scaling of Ground Motions

A set of twenty-four ground motion records was selected from the PEER (2013) database following similar criteria discussed in Section 3.2.2. The records were scaled within the range of 0.2T (0.29 sec.) to 2.0T (2.85 sec.) where, T is the fundamental period of the frame equal to 1.427 sec, based on the modal analysis conducted in OpenSees platform. The scaling criterion was to ensure that the mean spectrum does not fall below the target spectrum by 10% as shown in Figure 5.3. The scaling factors presented in Table D.1 of Appendix D.1.

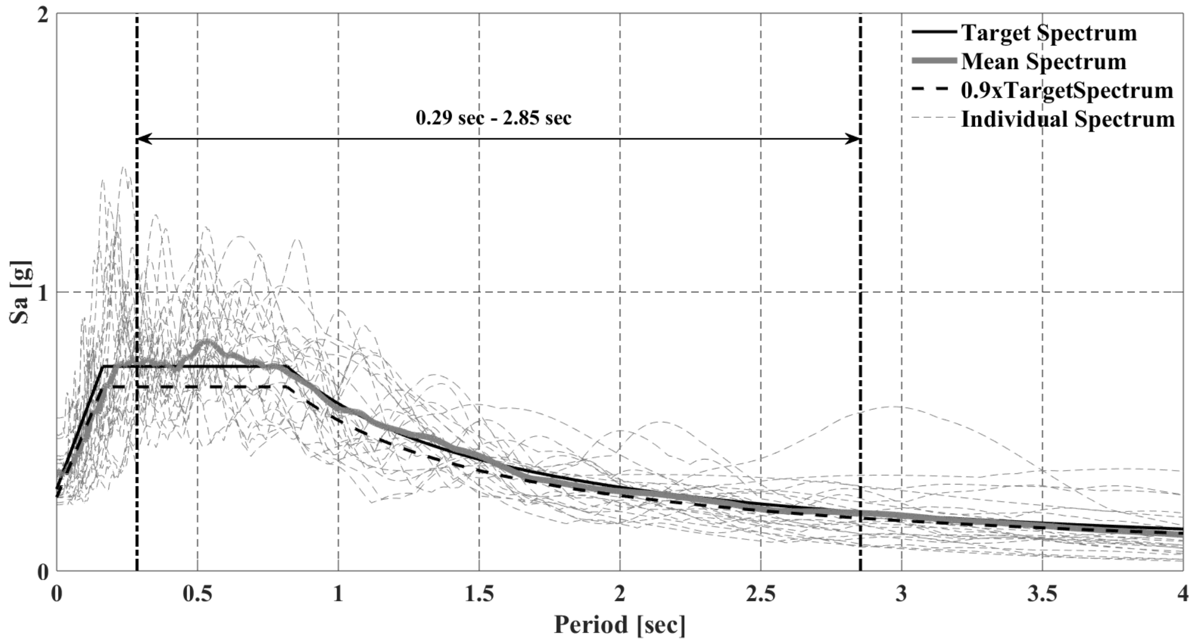

Figure 5.3 Acceleration response spectra of scaled ground motions used for the analysis of 5-storey prototype frame

5.3 Application and Validation of the Proposed Approach

The validation is presented in the form of a comparison between the approximated floor-wise distributions of dissipated energy from prediction and dynamic analysis performed using scaled ground motion records. Also, predicted dissipated energy demand time history was compared with dissipated energy time history from nonlinear dynamic analysis. For predicted energy demand, the quantification approach discussed in the Chapter 3 was applied to the prototype frame. Energy demands from real earthquakes were obtained by subjecting the numerical model to the scaled ground motions using the OpenSees platform.

5.3.1 Comparison of Floor-wise Distribution of Dissipated Energy

In the postprocessing, energy dissipated by the BRBs was calculated from the axial force-deformation response using Equation (3.2). The dissipated energy at each floor of the frame was normalized by total dissipated energy for a specific earthquake record. The total dissipated energy in the building for that specific earthquake record was equal to the sum of dissipated energies of all floors. The dissipated energy distribution at each floor was the normalized value at the end of the duration of that specific earthquake record. The procedure was continued for all earthquake records and all floors. The dissipated energy distribution was plotted against their corresponding floors as shown in Figure D.1 of Appendix D.2. The median trend of the distribution was also plotted for each floor. Then, the distribution of dissipated energy was predicted using the procedure proposed in Section 4.2.2, as follows:

1) Coefficients, C_1, C_2 and C_3 were calculated using Equation 4.9-4.11 as shown in Table 5.2.

2) The calculated values and the total number of storeys were substituted in Equation 4.6 to obtain the energy distribution in the second floor.

3) the predicted energy distribution ratio for the remaining floors was determined as shown in Table 5.3.

Table 5.2 Energy distribution coefficients for 5-storey prototype frame

Coefficients	Expressions for Fit Equations	Values for n = 5
C_1	$0.075 \times n^2 - 1.035 \times n + 5.43$	2.13
C_2	$= 0.058 \times n^2 - 0.942 \times n + 4.30$	1.04
C_3	$= 0.005 \times n^2 - 0.03 \times n + 0.42$	0.40

Table 5.3 Comparison of the floor-wise energy distribution of 5-storey frame			
Floor (j)	**Nonlinear Dynamic Analysis**	**Predicted E_j**	**Relative Difference (%)**
5	0.0772	$E_5 = C_3 C_2 E_2 = 0.40 \times 1.04 \times 0.18 = 0.0768$	-0.54 (↓)
4	0.183	$E_4 = 2C_3 C_2 E_2 = 2 \times 0.40 \times 1.04 \times 0.18 = 0.154$	-16.04 (↓)
3	0.220	$E_3 = C_2 E_2 = 1.04 \times 0.18 = 0.192$	-12.75 (↓)
2	0.180	$E_2 = 0.185$	2.54 (↑)
1	0.340	$E_1 = C_1 E_2 = 2.13 \times 0.18 = 0.393$	15.63 (↑)

Note:

(↓) is used when prediction underestimates;

(↑) is used when prediction overestimates;

As expected, the prediction overestimated the actual energy distribution at some floors and underestimated at others. The floor-wise distribution of dissipated energy was overestimated by 15.63% and 2.54% in 1st and 2nd floor respectively, and underestimated by 12.75%, 16.04% and 0.54% in 3rd, 4th and 5th floor. The differences between prediction and analytical results were illustrated in Figure 5.4.

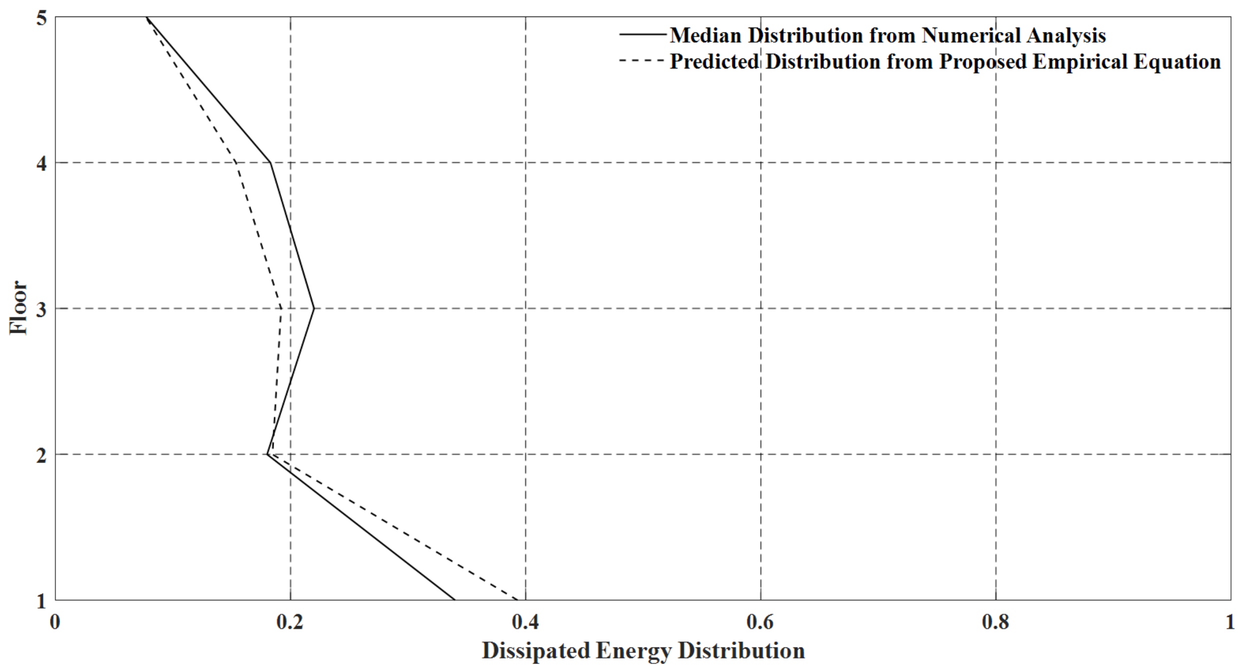

Figure 5.4 Comparison of the floor-wise dissipated energy distribution

5.3.2 Comparison of Dissipated Energy over Time

The proposed quantification approach was validated by comparing the predicted dissipated energy demand over time at each floor with dissipated energy time history demand from nonlinear dynamic analysis. For comparison purposes, the duration for each earthquake was selected such that plateau at the end of dissipated energy time history was attained. The duration was set at 60 sec for this study. The analysis was conducted for all earthquake records and plotted against time for each floor, as shown in Figure D.2 of Appendix D.3.

The predicted dissipated energy demand over time was obtained by implementing the energy quantification factor and rise time. At first, dissipated energy demand was obtained as a product of input energy and energy quantification factor. The input energy into the system, E_i was determined as follows:

$$E_i = \frac{1}{2} m S_a(T) S_d(T)$$

$$= \frac{1}{2} * 14.95 * 162.47 * 8.38$$

$$E_i = 10177.20 \text{ kip} - \text{in} \; (1150.69 \text{ kN} - \text{m})$$

$m = \frac{11550}{2*32.2*12} = 14.945 \approx 14.95\ kip - \frac{sec^2}{in}\ (2618.02\ kN - \frac{sec^2}{m})$

$S_a(T) = 0.42046\text{g} = 0.42046 * 32.2 * 12 = 162.47\ \frac{in}{sec^2}\ (4.127\ \frac{m}{sec^2})$

$S_d(T) = \frac{S_a(T)*T^2}{4\pi^2} = \frac{162.47*1.427^2}{4\pi^2} = 8.38\ in\ (0.213\ m)$

and T = 1.427 sec.

where, m = mass of the frame equal to $1/2$ of total seismic mass of the building since there are two braced frames in each principal direction;

$S_a(T)$ = spectral acceleration from design spectrum at fundamental period T of the frame;

$S_d(T)$ = spectral displacement from design spectrum at fundamental period T of the frame;

T = fundamental period of the frame.

The energy quantification factor, γ_{lp}, was determined from Equation (3.4) as follows:

$$\gamma_{lp} = 0.09T^{-2.88} + 1.96 \approx 1.992$$

Dissipated energy demand, where $\gamma_{lp} = \frac{E_d}{E_i}$ from Equation (3.1), on the prototype frame can be calculated as

$$E_d = \gamma_{lp} * E_i = 1.992 * 10177.20 = 20272.98\ kip - in\ (2292.17\ kN - m)$$

Subsequently, the floor-wise dissipated energy demand was obtained as a product of E_d and floor-wise predicted distribution of dissipated energy demand as presented in Table 5.4. For example, dissipated energy demand on first storey was obtained as $E_d \times E_j = E_d \times E_1 = $ 20272.98*0.393 = 7967.28 kip-in (900.82 kN-m).

Table 5.4 Floor-wise dissipated energy demand		
Floor (n)	**Predicted Energy Distribution, E_n**	**Dissipated Energy Demand, kip-in (kN-m)**
5	0.077	1561.02 (176.50)
4	0.154	3122.04 (352.99)
3	0.192	3892.41 (440.09)
2	0.185	3750.50 (424.05)
1	0.393	7967.28 (900.82)

The quantification approach incorporated a parameter called Rise Time, t_R to investigate the rate at which energy will be dissipated in a system. Rise Time was used to plot the predicted dissipated energy demand over time for each floor (see Section 3.3.2). The Rise Time was further discretized in six-time steps required to accumulate 5%, 25%, 50%, 75%, 95% and 100% of the dissipated energy demand for each floor. The frame was designed for force modification coefficient, R = 8.0. Hence, for the fundamental period of the frame, T = $1.427\ sec.$, rise times were calculated from Equation 3.5(a-f), as tabulated in Table 5.5.

Table 5.5 Rise Times for 5-storey prototype frame		
% of Dissipated Energy Demand	**Equations**	**Rise Time (sec.)**
5	$t_{R5\%} = -0.09 \times T + 1.67$	1.54
25	$t_{R25\%} = 0.86 \times T + 3.19$	4.42
50	$t_{R50\%} = 1.95 \times T + 4.94$	7.72
75	$t_{R75\%} = 4.83 \times T + 6.23$	13.12
95	$t_{R95\%} = 8.74 \times T + 9.39$	21.86
100	$t_{R100\%} = 2.36 \times T + 31.11$	34.48

Now, the dissipated energy demand over time was developed by distributing dissipated energy demand for each floor from Table 5.4 corresponding to rise times in Table 5.5. For example, dissipated energy demand corresponding to $t_{R5\%}$ (time required to accumulate 5% of total dissipated energy demand) for the 1st floor is equal to the product of the value from Table 5.4 (7967.28 kip-in) and 0.05 (5%). The resulting value is 398.36 kip-in. Similarly, dissipated energy demand corresponding remaining rise times are shown below:

Energy dissipated demand corresponding to $t_{R25\%}$ = 7967.28*0.25 = 1991.82 kip-in;

Energy dissipated demand corresponding to $t_{R50\%}$ = 7967.28*0.5 = 3983.64 kip-in;

Energy dissipated demand corresponding to $t_{R75\%}$ = 7967.28*0.75 = 5975.46 kip-in;

Energy dissipated demand corresponding to $t_{R95\%}$ = 7967.28*0.95 = 7568.92 kip-in;

Energy dissipated demand corresponding to $t_{R100\%}$ = 7967.28*1.00 = 7967.28 kip-in;

Dissipated energy demands corresponding to the rise times for remaining floors are presented in Table 5.6. The dissipated energy demand values for each floor were plotted corresponding to the rise times and a smooth curve was fitted. For comparison with nonlinear time history analysis, the demand corresponding to $t_{R100\%}$ was continued to 60.00 sec for each floor as shown in the last row of Table 5.6. The plots of the predicted dissipated energy demand over time were compared to median plots of the dissipated energy demand time histories from real earthquakes as shown in Figure 5.5.

Table 5.6 Floor-wise dissipated energy demand distributed over Rise Times

% E_d	t_R, (sec.)	1^{st} Floor (kip-in)	2^{nd} Floor (kip-in)	3^{rd} Floor (kip-in)	4^{th} Floor (kip-in)	5^{th} Floor (kip-in)
5	1.54	398.36	187.53	194.62	156.10	78.05
25	4.42	1991.82	937.63	973.10	780.51	390.26
50	7.72	3983.64	1875.25	1946.21	1561.02	780.51
75	13.12	5975.46	2812.88	2919.31	2341.53	1170.77
95	21.86	7568.92	3562.98	3697.79	2965.94	1482.97
100[1]	34.48	7967.28	3750.50	3892.41	3122.04	1561.02
100[2]	60.00	7967.28	3750.50	3892.41	3122.04	1561.02

Note:

1. 100% of E_d for earthquake record duration of 34.48 sec

2. 100% of E_d for earthquake record duration of 60.00 sec

A comparison between the median and predicted demand is presented in Figure 5.5. It was observed that the prediction overestimated the analysis at 1st floor and underestimated at 3^{rd} and 4^{th} floors by large margin, as shown in Figure 5.4. Similarly, for 2^{nd} and 5^{th} floors, the difference between the prediction and analysis values are not significantly different. The dissipated energy demand over time was compared with dissipated time history demand from earthquakes and their median as illustrated in Figure D.2 of Appendix D.

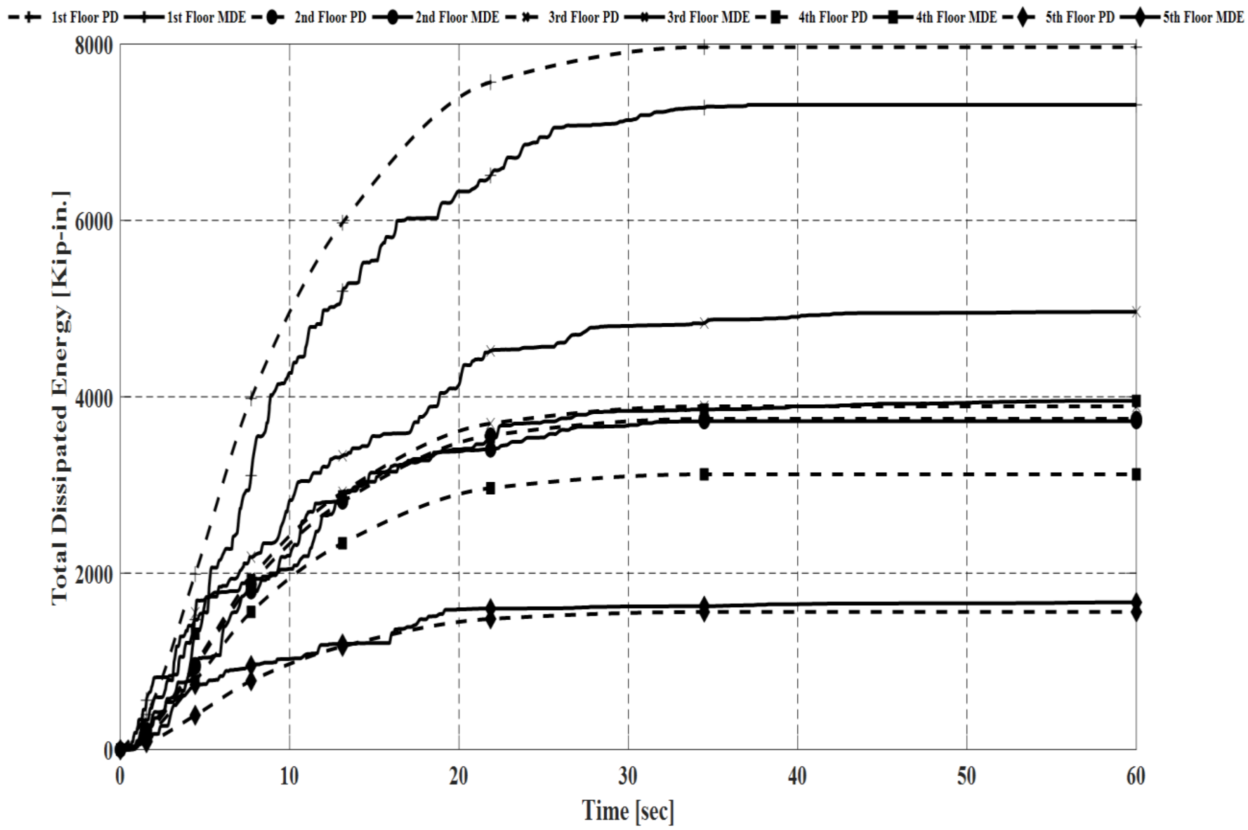

Note: PD = Predicted Demand; MDE = Median Demand from Earthquakes

Figure 5.5 Comparison of dissipated energy demand over time for different floors

5.4 Summary

The quantification approach was validated on a 5-storey frame in a building. BRBs in the building were designed in a diagonal configuration whereas in Chapter 4 the bracing members were in the form of inverted V. Moreover, the seismic hazard parameters were different from the one that was used in the development of the proposed quantification approach. These differences were selected intentionally to comprehensively investigate the application of the proposed approach. The prediction of floor-wise distribution was close to the one obtained from numerical analysis. The comparisons of dissipated energy demand over time with the median dissipated energy demand obtained from the nonlinear time history analysis were also close. The trends both in floor-wise distribution and dissipated energy demand over time complimented each other very well. Hence, it can be depicted from the validation that the approach is efficient and effective.

Chapter 6: Conclusion

Experimental investigation of a component traditionally relies on a conservative approach to evaluate its performance. Moreover, an experimental validation requires to sustain a large amount of deformation-related demand parameters without a rational basis. Contrary to this approach, a novel procedure was developed where demand can be quantified without conducting time history analyses. The demand parameter was energy which was not considered explicitly in the previous development of experimental investigations. In the limited range of this study, the approach was found to be effective and efficient. This chapter summarizes the development of the approach. Section 6.1 outlines a framework for design engineers to quantify energy demand for buildings with Buckling-Restrained Braces (BRBs). The development of the framework is summarized in Section 6.2. Section 6.3 identifies possible future research studies related to the scope of this work.

6.1 Framework for Quantification Approach

BRB is a novel energy dissipation device. Quantification of dissipated energy demand on such a novel device has not been investigated explicitly. Based on this study, a framework for the quantification approach of BRBs can be narrowed down to the following steps:

1) Obtain design criteria for the building in which the device will be used and seismic hazard parameters for the building site;
2) Determine the fundamental period of the building, and total energy from design spectrum based on the seismic hazard parameters from Equation 3.3;
3) Determine the energy quantification factor, (γ_{lp}), from Equation 3.4 and quantify total dissipated energy from Equation 3.1;
4) Determine energy distribution along the height of the building from Equation 4.6, where the coefficients can be determined from Equation 4.9-4.11. Dissipated energy demand for each

floor can be obtained as a product of the total dissipated energy and energy distribution for that floor;

5) Finally, Rise Time, (t_R), will be determined from Equation 3.5. Dissipated energy demand is to be distributed over those rise times.

6.2 Summary of the Approach

The development of the novel methodology to obtain dissipated energy demand from the design spectrum was based on analysis conducted on BRBs. For the purpose of this study, a range of equivalent nonlinear single degree of freedom (ENLSDOF) systems and a series of prototype frames were investigated. The development and application of the proposed quantification approach can be summarized as followings:

- The equation for estimating energy quantification factor, γ_{lp}, was the outcome of the analysis conducted on ENLSODF systems (see Chapter 3),
- Based on the analysis of ENLSDOF systems set of equations were also proposed to quantify the rate at which energy dissipates in a building. The Rise Time parameter, t_R, defines the time required to dissipate the total energy from an earthquake event fed into a structural system equipped with BRBs. The rise time was sub-divided into six time-steps to obtain 5%, 25%, 50%, 75%, 95% and 100% of the total energy dissipation demand. The equations were proposed as a function of the fundamental period of the structure to determine the time corresponding to those steps.
- The approach incorporated a procedure to predict the distribution pattern of the seismic energy demand along the building height using an empirical equation which contains three controlling parameters, (C_1 to C_3), that can be calculated using equations as a function of the number of storeys in the structure. The approach for determining energy distribution was an

outcome of the analyses conducted on the series of prototype frames with variable heights (3-, 6- and 8-storey).

- A prototype 5-storey structure was selected to demonstrate and verify the applicability of the proposed approach.

6.3 Recommendation for Future Studies

With the growing application and development of performance-based design, there is a need for quantifying performance standards based on the hazard intensity of a site. Following the path laid by the pioneers in the development of such methods, the proposed approach is believed to be useful for comparing the experimental findings to expected demand. As the study is still in its early stage of development, future studies need to consider the following:

- The range of the fundamental periods was from 0.25 sec. to 2.00 sec. Fundamental periods above 2.00 sec. should be investigated to address the application to tall buildings.
- A series of prototype frames with different configurations and locations with different seismic hazard parameters should be investigated to further validate empirical equations for floor-wise distribution of energy demand.
- Since in this study buildings were designed following the conventional design method such as equivalent lateral force procedure (ELFP), future studies should include buildings designed following novel design procedures such as performance-based plastic design (PBPD) and equivalent energy design procedure (EEDP) to investigate the applicability of the proposed methodology.
- The BRBs in this study were considered as the only energy dissipation device in the building. Recently, they have become popular as either primary or secondary structural fuses where they dissipate energy in conjunction with other devices. Floor-wise energy distribution of the

system where BRBs are used as fuses should be further investigated. Moreover, other dampers such as Welded Wide Flange Fuse (WWFF), Honeycomb Structural Fuse (HSF), etc. should also be included.

- Ground motions selected in this study were crustal earthquake records from the PEER database. The investigation should be further extended for sub-crustal or sub-duction earthquake records.
- The study should be extended to develop loading protocols using the proposed energy quantification procedure.
- Finally, experimental studies should be employed to validate the analytical study.

Bibliography

Aguaguina, M., Ying Zhou, and Yun. Zhou. 2019. "Loading Protocols for Qualification Testing of BRBs Considering Global Performance Requirements." *Engineering Structures* (Elsevier) 189: 440-457. doi:10.1016/j.engstruct.2019.03.094.

Aiken, Ian D, and Isao Kimura. 2001. *The Use of Buckling-Restrained Braces in United States.* Proceedings of Japan Passive Control Symposium, Yokohama, Japan: Tokyo Institute of Technology.

ANSI/AISC 341-16. 2016. *Seismic Provisions for Structural Steel Buildings.* Chicago, Illinois: AISC.

ASCE/SEI 7-10. 2010. *Minimum Design Loads and Associated Criteria for Builidngs and Other Structures.* Reston: ASCE.

ASCE/SEI 7-16. 2017. *Minimum Design Loads and Associated Criteria for Builidngs and Other Structures.* Reston, Virginia: ASCE.

ATC-24. 1992. *"Guidelines for Cyclic Seismic Testing of Components of Steel Structures for Buildings," Report No. ATC-24.* Redwood City, California: Applied Technology Council.

Bayat, M Reza, Subhash C Goel, and Shih-Ho Chao. 2010. *Performance-Based Plastic Design of Earthquake Resistant Concentrically Braced Steel Frames.* Research Report UMCEE 10-02 September, Ann Arbor, MI: The University of Michigan.

Black, Cameron J., N. Makris, and Ian D. Aiken. 2004. "Component Testing, Seismic Evaluation and Characterization of Buckling-Restrained Braces." *Jounal of Structural Engineering* (ASCE) 880-894.

Black, R. Gary, W. A. Bill Wenger, and Egor P. Popov. 1980. *Inelastic Buckling of Steel Struts under Cyclic Load Reversals.* Report to Sponsors NSF and AISI, Department of Civil Engineering, University California, Berkeley: Earthquake Engineering Research Center.

Bruneau, M., C.-M. Uang, and R. Sabelli. 2011. *Ductile Design of Steel Structures.* 2nd. New York: McGraw-Hill Companies, Inc.

Carden, L., A. Itani, I. Buckle, and I. Aiken. 2004. "Buckling Restrained Braces for Ductile End Cross Frames in Steel Plate Girder Bridges." *Proceedings of 13th World Conference on Earthquake Engineering.* Vancouver, BC, Canada: WCEE.

Chang, K.-C., and G. C. Lee. 1987. "Strain Rate Effect on Structural Steel Under Cyclic Loading." *Journal of Engineering Mechanics* (ASCE) 113 (9): 1292-1301. doi:10.1061/(ASCE)0733-9399(1987)113:9(1292).

Chang, KyongHo, GabChul Jang, Siegfried F. Stiemer, and N. Loewen. 2013. "Dynamic Hysteretic Characteristics of High-Strength Steels (POSTEN60, POSTEN80) and Application of a Dynamic Hysteresis Model to FE Analysis." *Journal of Materials in Civil Engineering* (ASCE) 25 (10): 1549-1557. doi:10.1061/(ASCE)MT.1943-5533.0000629.

Choi, Hyunhoon, and Jinkoo Kim. 2006. "Energy-based seismic design of buckling-restrained braced frames using hysteretic energy spectrum." *Engineering Structures* 28: 304-311. doi:10.1016/j.engstruct.2005.08.008.

Chopra, Anil K. 2012. *Dynamics of Structures: Theory and Application to Earthquake Engineering.* California, Berkeley: Prentice Hall.

Clark, P, K Frank, H Krawinkler, and R Shaw. 1997. *Protocol for Fabrication, Inspection, Testing and Documentation of Beam-Column Connection Tests and Other Experimental*

Specimens. Redwood City, California: SAC Steel Project Background Document. October, Report No. SAC/BD-97/02.

Clark, P., I. Aiken, K. Kasai, E. Ko, and I. Kimura. 1999. "Design Procedures for Buildings Incorporating Hysteretic Dmaping Devices." *Proceedings of 68th Annual Convention of the Strucutral Engineers Association of California.* Santa Barbara, California.

Clark, Peter W, Kazuhiko Kasai, Ian D. Aiken, and Isao Kimura. 2000. "Evaluation of Design Methodologies for Structures Incorporating Steel Unbonded Braces for Energy Dissipation." *12th World Conference on Earthquake Engineering. Proceedings, Paper No. 2240.* New Zealand Society for Earthquake Engineering.

Comerio, Mary C., S. Tobriner, and Fehrenkamp Ariane. 2006. *Bracing Berkeley-A guide to Seismic Safety on the UC Berkeley Campus.* Department of Architecture, University of California, Berkeley: Pacific Earthquake Engineering Research Center.

CUREE-Caltech. 2001. *"Development of a Testing Protocol for Woodframe Structures," CUREE Publication No. W-02.* Richmond, California: CUREE-Caltech: Krawinkler, H.; Parisi, F.; Ibarra, L.; Ayoub, A.; Medina, R.

Dehghani, M. 2016. *Seismic Design and Qualification of All-Steel Buckling-Restrained Braced Frames for Canadian Applications.* PhD Thesis, Département des génies Civil, Géologique et des Mines , École Polytechnique de Montréal , Ann Arbor: ProQuest.

Dehghani, M, and R Tremblay. 2012b. "Standard Dynamic Loading Protocols for Seismic Qualification of BRBFs in Eastern and Western Canada." *Proceedings of the15th World Conference on Earthquake Engineering.* Lisbon, Portugal: 15th World Conference on Earthquake Engineering.

Dehghani, Morteza, and Robert Tremblay. 2012a. "Development of Standard Dynamic Loading Protocol for Buckling-Restrained Braced Frames." In *STESSA 2012: Behaviour of Steel Structures in Sesmic Areas*, by Federico M. Mazzolani and Ricardo Herrera, 61-67. Santiago, Chile: CRC Press.

Dolan, J. D., and C. P. Heine. 1997. *Sequential Phased Displacement Cyclic Tests of Wood-Frame Shear Walls with Various Openings and Base Restraint Configurations.* Blacksburg, Virginia: Report No. TE-1997-002, Virginia Polytechnic Institute and State University.

El-Bahey, S., and M. Bruneau. 2010. "Structural Fuse Concept for Bridges." *The 9th U.S. National and 10th Canadian Conference on Earhtquake Engineering.* Toronto, Canada.

Erochko, J., C. Christopher, R. Tremblay, and H. Kim. 2013. "Shake Table Testing and Numerical Simulation of a Self-centering Energy Dissipative Braced Frame." *Earthquake Engineering and Structural Dynamics* 42 (11): 1617-1635.

Fell, B. V., A. M. Kanvinde, G. G. Deierlein, and A. T. Myers. 2009. "Experimental Investigation of Inelastic Cyclic Buckling and Fracture of Steel Braces." *Journal of Structural Engineering* 135 (1): 19-35.

FEMA 302. 1997. *NEHRP Recommended Provisions for Seismic Regulations for New Buildings and Other Structures.* Vol. Part 1: Provisions. Washington, D.C.: Building Seismic Safety Council.

FEMA. 2007. *Interim Protocols for Determining Seismic Performance Characteristics of Structural and Nonstructural Components Through Laboratory Testing.* FEMA 461 Draft, Washington, DC: Federal Emergency Management Agency.

Filiatrault, A., D. Perrone, E. Brunesi, C. Beiter, and R. Piccinin. 2018. "Effects of Cyclic Loading Protocols on Experimental Seismic Performance Evaluation of Suspended Piping Restraint Installations." *International Journal of Pressure Vessels and Piping* 61-71.

Filippou, F. C., E. P. Popov, and V. V. Bertero. 1983. *Effects of Bond Deterioration on Hysteretic Behavior of Reinforced Concrete Joints.* Technical Report UCB/EERC-83/19, College of Engineering, Earthquake Engineering Research Center, Berkeley, California: University of California.

FM Approvals LLC. 2013. *Approval Standard for Seismic Sway Braces for Pipe, Tubing and Conduit.* FM Approvals Certification, Norwood, MA, USA: FM Global Group.

Fujimoto, Morihisa, Akira Wada, Eiichiro Saeki, Toru Takeuchi, and Atsushi Watanabe. 1990. "Development of Unbonded Braces." *Quarterly Column* 115: 91-96.

Gray, M. G., C. Christopoulos, and J. A. Packer. 2014. "Cast Steel Yielding Brace System for Concentrically Braced Frames: Concept Development and Experimental Validations." *Journal of Structural Engineering* 140 (4): 04013095.

Housner, G. W. 1956. "Limit Design of Structures to Resist Earthquakes." *Proceeding of the 1st World Conference on Earthquake Engineering.* California, U.S.A.

ISO. 2003. "Timber Structures – Joints Made with Mechanical Fasteners – Quasi-Static Reversed-Cyclic Test Method." In *International standard; ISO 16670*, by ISO, 0-24. Genève, Switzerland: International Organization for Standardization.

Iwata, M. 2004. "Applications-Design of Buckling Restrained Braces in Japan; ." *Proceedings of 13th World Conference on Earthquake Engineering.* Vancouver.

Iwata, M., T. Kato, and A. Wada. 2000. "Buckling-Restrained braces as Hysteretic Dampers." Edited by Federico M. Mazzolani and R. Tremblay. *Proceedings of The Third International Conference STESSA.* Montreal, Canada: A.A.Balkema. 33-38.

Iwata, Mamoru, and M. Murai. 2006. "Buckling-restrained Brace using Steel Mortar Planks; Perfromance Evaluation as a Hysteretic Damper." *Earthquake Engineering and Structural Dynamics* 35: 1807-1826. doi:10.1002/eqe.608.

Kim, Jinkoo, and Hyunhoon Choi. 2004. "Energy-based seismic design of buckling-restrained braces." *13th World Conference on Earthquake Engineering.* Vancouver, Canada.

Ko, Eric, and Caroline Field. n.d. *The Unbonded BraceTM: From Research to Californian Practice.* San Francisco: Arup.

Koetaka, Y., P. Chusilp, Z. Zhang, M. Ando, K. Suita, K. Inoue, and N. Uno. 2005. "Mechanical Property of Beam-to-Column Moment Connection With Hysteretic Dampers for Column Weak Axis." *Engineering Structures* 27 (1): 109-117.

Krawinkler, H, A Gupta, R Medina, and N Luco. 2000. *Development of Loading Histories for Testing of Steel Beam-to-Column Assemblies.* Redwood City, California: SAC Background Report SAC/BD-00/10.

Krawinkler, H, M Zohrei, B Lashkari-Irvani, N Cofie, and H Hadidi-Tamjed. 1983. *Recommendations for Experimental Studies on the Seismic Behavior of Steel Components and Materials.* A Research Project Sponsored By the National Science Foundation, Stanford, California: The John A. Blume Earthquake Engineering Center, Department of Civil and Environmental Engneering, Stanford University.

Krawinkler, H., A. Gupta, R. Medina, and N. Luco. 2000. *Loading Histories for Seismic Performance Testing of SMRF Components and Assemblies.* Stanford, California: SAC Steel Project Background Document. August, Report No. SAC/BD-00/10.

Krawinkler, H., F. Parisi, L. Ibarra, A. Ayoub, and R. Medina. 2001. *"Development of a Testing Protocol for Woodframe Structures," CUREE Publication No. W-02.* Richmond, California: CUREE-Caltech.

Krawinkler, Helmut. 2009. "Loading Histories for Cyclic Tests in Support of Performance Assessment of Structural Components." *3rd International Conference on Advances in Experimental Structural Engineering.* San Francisco, California: University of California, Berkeley, CA.

Kurama, Y. C. 2000. "Seismic Design of Unbonded Post-Tensioned Precast Concrete Walls with Supplemental Viscous Damping." *ACI Structural Journal* 97 (4): 648-658.

Lanning, Joel T. 2014. *Using Buckling-Restrained Braces on Long-Span Bridges Near Seismic Faults.* PhD Thesis, UC San Diego, San Diego: eScholarship.org Powered by California Digital Library. https://escholarship.org/uc/item/9d77k2sc.

Lanning, Joel, G. Benzoni, and C.-M. Uang. 2016. "Using Buckling-Restrained Braces on Laong-Span Bridges. II: Feasibility and Development of a Near-Fault Laoding Protocol." *Jounral of Bridge Engineering* (ASCE) 21 (5): 04016002-1:12. doi:10.1061/(ASCE)BE.1943-5592.0000804.

Lopes, A. P., P. Dusicka, and J. W. Berman. 2012. "Design of the Linked Column Frame Structural System." *The 7th International Conference on Behaviour of Steel Structures in Seismic Areas.* Sattiago, Chile.

Lu, Lyan-Ywan, Tzu-Kang Lin, Rong-Jie Jheng, and Hsin-Hsien Wu. 2018. "Theoretical and Expreimental Investigation of Position-Controlled Semi-Active Friction Damper for Seismic Structures." *Journal of Sound and Vibration* 412: 184-206. doi:https://doi.org/10.1016/j.jsv.2017.09.029.

Ma, X., H. Krawinkler, and G. G. Deierlein. 2013. *Seismic Design and Behavior of Self-Centering Braced Frame with Controlled Rocking and Energy Dissipating Fuses.* Report No. 174, John A. Blume Earthquake Engineering Center, Stanford Digital Repository.

Makris, N, and M.C. Constantinou. 1990. *Viscous Dampers: Testing, Modeling and Application in Vibration and Seismic Isolation.* Technical Report NCEER-90-0028, Department of Civil Engineering, State University of New York at Buffalo, Springfield, VA: U.S. Department of Commerce.

Malakoutian, M. 2012. "Seismic Response Evaluation of the Linked Column Frame System." Dissertations and Theses, University of Washington.

Mergos, Panagiotis E., and Katrin Beyer. 2014. "Loaidng Protocols for European Regions of Low to Moderate Seismicity." *Bulletin of Earthquake Engineering (Official Publication of the European Association for Earthquake Engineering)* 12 (6): 2507-2530. doi:10.1007/s10518-014-9603-3.

Mergos, Panagiotis, and Katrin Beyer. 2015. "Loading Protocols for Structures Designed for Different Behaviour Factors." *SECED 2015 Conference: Earthquake Risk and Engineering towards a Resilient World.* Cambridge, UK: EPFL. doi:record/217006.

Merritt, S., C.-M. Uang, and G. Benzoni. 2003. *Subassemblage Testing of Star Sesimic Buckling-Restrained Braces (Report No. TR-2003/04).* Structural Systems Research Projects: A

Final Report to Star Seismic, LLC, Department of Structural Engineering, University of California, San Diego, La Jolla, California: University of California.

NBCC. 2015. *National Building Code of Canada.* Vol. 1. Ottawa, Ontario: National Research Council Canada.

OpenSees Navigator 2.5. 2013. "Open System for Earthquake Engineering Simulation (OpenSees) Framework." Pacific Earthquake Engineering Research Center (PEER) Center. Accessed 09 01, 2017. https://openseesnavigator.berkeley.edu/.

PEER. 2013. *PEER Ground Motion Database - Pacific Earthquake Engineering Research Center.* University of California, Berkeley, CA. Accessed 2019. https://ngawest2.berkeley.edu/.

Porter, M. L. 1987. "Sequential Phased Displacement (SPD) Procedure for TCCMAR Testing." *3rd Meeting of the Joint Technical Coordinating Committee on Masonry Research.* Tomamu, Hokkaido: US-Japan Coordinated Research Program.

Qian, Hui, Hongnan Li, and Gangbing Song. 2016. "Expreimentla Investigations of Building Structure with a Superelastic Shape Memory Alloy Friction Damper Subject to Seismic Loads." *Smart Materials and Structures* 25 125026. doi:doi:10.1088/0964-1726/25/12/125026.

Richards, Paul, and Chia-Ming Uang. 2003. *Development of Testing Protocol for Short Links in Eccentrically Braced Frames.* Report No. SSRP-2003/08; Structural Systems Research Project; Finla Report Submitted to AISC, La Jolla, California: University of California, San Diego.

Riddell, R., and J. E. Garcia. 2001. "Hysteretic Energy Spectrum and Damage Control." *Earthquake Engineering and Structural Dynamics* 30 (12): 1791-1816. doi:10.1002/eqe.93.

Sabelli, R, and Ian Aiken. 2003. *Development of Building Code Provisions for Buckling-Restrained Braced Frames.* Proceedings of 72nd Annual Conventiion, Sacramento, California: Structural Engineers Association of California.

Sabelli, R., S. Mahin, and C. Chang. 2003. "Seismic Demands on Steel braced Frame Buildings with Buckling-Restrained Braces." *Engineering Structures* 25: 655-666. doi:10.1016/S0141-0296(02)00175-X.

Sabelli, Rafael. 2001. *Research on Improving the Design and Analysis of Earthquake-Resistant Steel-Braced Frames.* The 2000 NEHRP Professional Fellowship Report, Department of Civil and Environmental Engineering, University of California, Berkeley, California: Earthquake Engineering Research Institute.

SEAOSC. 2001. *Report of A Testing Program of Light-Framed Walls with Wood-Sheathed Shear Walls.* Los Angeles, California: City of Los Angeles Department of Building and Safety.

Shafei, Behrouz, and Farzin Zareian. 2008. "Development of a Quasi-Static Loading Protocol for Displacement-Sensitive Nonstructural Building Components." *Proceedings of the 14th World Conference on Earthquake Engineering.* Beijing, China: 14th World Conference on Earthquake Engineering.

Shen, Y., C. Christopoulos, N. Mansour, and R. Tremblay. 2011. "Seismic Design and Performance of Steel Moment-Resisting Frames with Nonlinear Replaceable Links." *Journal of Strucutral Engineering* 137 (10): 1107-1117.

SPD. 1987. "Porter, M. L;Sequential Phased Displacement (SPD) Procedure for TCCMAR Testing." *3rd Meeting of the Joint Technical Coordinating Committee on Masonry Research.* Tomamu, Hokkaido: US-Japan Coordinated Research Program.

Symans, Michael D., William F. Cofer, Y. Du, and Kenneth J. Fridley. 2002. *Evaluation of Fluid Dampers for Seimic Energy Dissipation of Woodframe Structures.* The CUREE-Caltech Woodframe Project, California Institute of Technology, Richmond, California: Consortium of Universities for Research in Earthquake Engineering (CUREE).

Takeuchi, T., and A. Wada. 2018. "Review of Buckling-Restrained Brace Design and Application to Tall Building." *International Journal of High-Rise Buildings* 7 (3): 187-195. https://doi.org/10.21022/IJHRB.2018.7.3.187.

Takeuchi, T., H. Ozaki, R. Matsui, and F. Sutcu. 2014. "Out-of-plane Stability of Buckling-restrained Braces Including Moment Transfer Capacity." *Earthquake Engineering & Structural Dynamics* 43: 851-869. doi:10.1002/eqe.2376.

Takeuchi, T., J.F. Hajjar, R. Matsui, K. Nishimoto, and I.D. Aiken. 2012. "Effect of Local Buckling Core Plate Restraint in Buckling Restrained Braces." *Engineering Structures* 44: 304-311. doi:10.1016/j.engstruct.2012.05.026.

Takeuchi, T., J.F. Hajjar, R. Matsui, K. Nishimoto, and I.D. Aiken. 2010. "Local Buckling Restraint Condition for Core Plates in Buckling Restrained Braces." *Journal of Constructional Steel Research* 66 (2): 139-149. doi:10.1016/j.jcsr.2009.09.002.

Takeuchi, T., K. Yasuda, and M. Iwata. 2009. "Seismic Retrofitting using Energy Dissipation Façades." *ATC & SEI 2009 Conference on Improving the Seismic Performance of Existing Buildings and Other Structures.* San Francisco, California: ASCE. 1000-1008. doi:10.1061/41084(364)91.

Takeuchi, T., R. Matsui, and S. Mihara. 2016. "Out-of-plane Stability Assessment of Buckling-Restrained Braces Including Connections with Chevron Configuration." *Earthquake ENgineering & Structural Dynamics* 45: 1895-1917. doi:10.1002/eqe.2724.

Takeuchi, Toru. 2018. "Buckling-Restrained Brace: History, Design and Applications." *Key Engineering Materials* 50-60. doi:10.4028/www.scientific.net/KEM.763.50.

Technical Committee CEN/TC 250. 2004. *Eurocode 8: Design of Structures for Earthquake Resistance - Part 1: General Rules, Seismic Actions and Rules for Buildings.* Brussels, Belgium: European Standard EN 1998-1.

Tena-Colunga, A., and H. Hernández-Ramirez. 2017. "Code-oriented Global Design Parameters for Moment-Resisting Steel Frames with Metallic Structural Fuses." *Frontiers in Built Environment* 3 (19): 1-16.

Tremblay, R., E. St-Onge, C. A. Rogers, T. Morrison, F. Légeron, E. Desjardins, L. Tirca, M. G. Gray, C. Christopoulos, and J. A Packer. 2011. "Overview of Ductile Seismic Brace Fuse Systems in Canada." *Proceedings of the 6th European Conference on Steel and Composite Structures.* Budapest, Hungary.

Tremblay, R., P. Bolduc, R. Neville, and R. DeVall. 2006. "Sesimics Testing and Performance of Buckling-Restrained Bracing Systems." *Canadian Journal of Civil Engineering* (NRC Canada) 33 (2): 183-198. doi:10.1139/L05-103.

Tsai, K. C., and J. W. Li. 1997. "DRAIN2D+, A General Purpose Computer Program for Static and Dynamic Analyses of Inelastic 2D Structures Supplemented with a Graphic Processor." National Taiwan University, Taipei.

Tsai, K.-C., H.-W. Chen, C.-P. Hong, and Y.-F. Su. 1993. "Design of Steel Triangular Plate Energy Absorbers for Sesimic-Restraint Construction." *Earthquake Spectra* 9 (3): 505-528.

Uang, Chia-Ming, and Masayoshi Nakashima. 2004. "Chapter 16: Steel Buckling-Restrained Braced Frames." In *Earthquake Engineering from Engineering Seismology to Performance-Based Engineering*. CRC Press LLC.

Vargas, R., and M. Bruneau. 2009a. "Analytical Response and Design of Buildings with Metallic Structural Fuses I." *Journal of Structural Engineering* 135 (4): 386-393.

Wada, Akira, Mamoru Iwata, Atsushi Watanabe, and H. Kuribayashi. 1990. "Properties of Brace Encased in Concrete-Filled Steel Tube." *IABSE Symposium* 60: 493-494. doi:http://doi.org/10.5169/seals-46530.

Wang, Shiang-Jung, I-Chen Chiu, Chung-Han Yu, and Kuo-Chun Chang. 2018. "Experimental and Analytical Study on Design Performance of Full-Scale Viscoelastic Dampers." *Earthquake Engineering and Engineering Vibration* 17 (4): 693-706. doi:https://doi.org/10.1007/s11803-018-0469-2.

Wijanto, Stefan. 2012. *Behaviour and Design of Generic Buckling Restrained Brace Systems.* Master's Thesis, Department of Civil and Environmental Engineering, The University of Auckland, Auckland: Earthquake Commission [NZ]. https://www.eqc.govt.nz.

Yang, T. Y., D. P. Tung, and Y. Li. 2015. "Performance-based Plastic Design and Evaluation of Linked Column Frames." *Progress in Steel Building Structures* 17 (1).

Yang, T. Y., P.T. Tung, and Yuanjie Li. 2018. "Equivalent Energy Design Procedure for Earhtquake Resilient Fused Strucutres." *Earthquake Spectra* (Earthquake Engineering Research Institute) 34 (2): 1-21.

Yang, T. Y., Y. Li, and S. Leelataviwat. 2014. "Performance-based Design and Optimization of Buckling Restrained Knee Braced Truss Moment Frame." *Journal of Perfromance of Constructed Facilities* 28 (6): A4014007-1:11.

Zayas, V. A., S. A. Mahin, and E. P. Popov. 1980. *Cyclic Inelastic Behavior of Steel Offshore Structures.* Report to Sponsors NSF and AISI, Department of Civil Engineering, University of California, Berkeley: Earthquake Engineering Research Center.

Zhou, X. Q., L. Wang, D.Y. Yu, and C.Y. Zhang. 2019. "Experimental Investigiation of the Dissipation Characteristic of Snadwich Structures with Periodically Perforated Viscoelastic Damping Material Core." *Journal of Vibration and Control* 25 (14): 2008-2024. doi:10.1177/1077546319844545.

Appendices

Appendix A Loading Protocols Developed by Codes and Researchers

A.1 Loading Protocol Developed for BRB Qualification

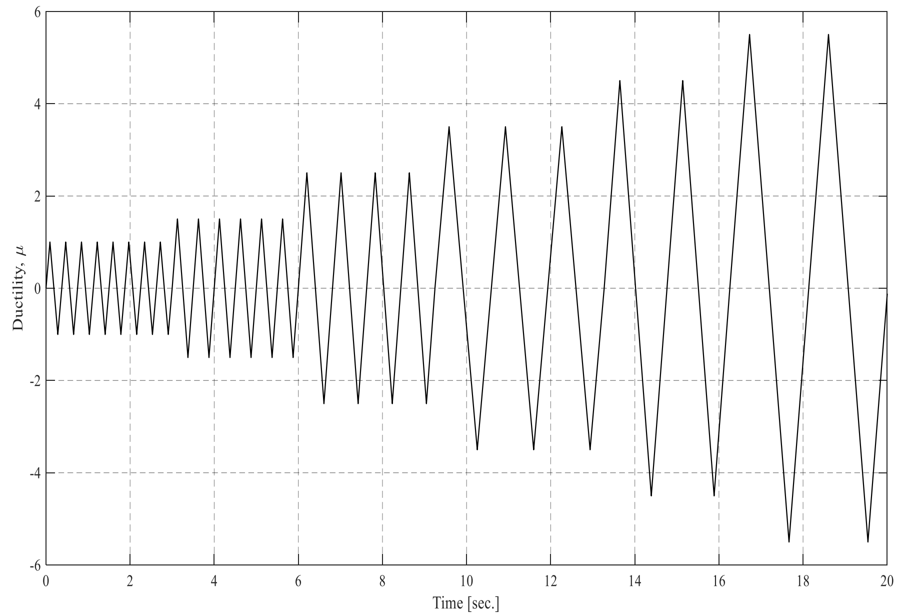

Figure A.1 Loading protocol developed by Dehghani (2012a)

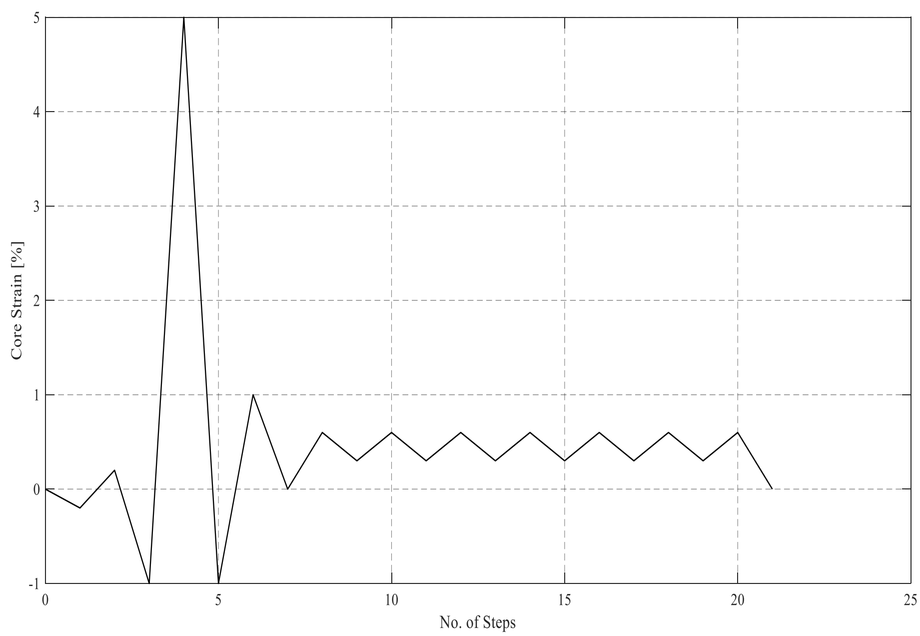

(a)

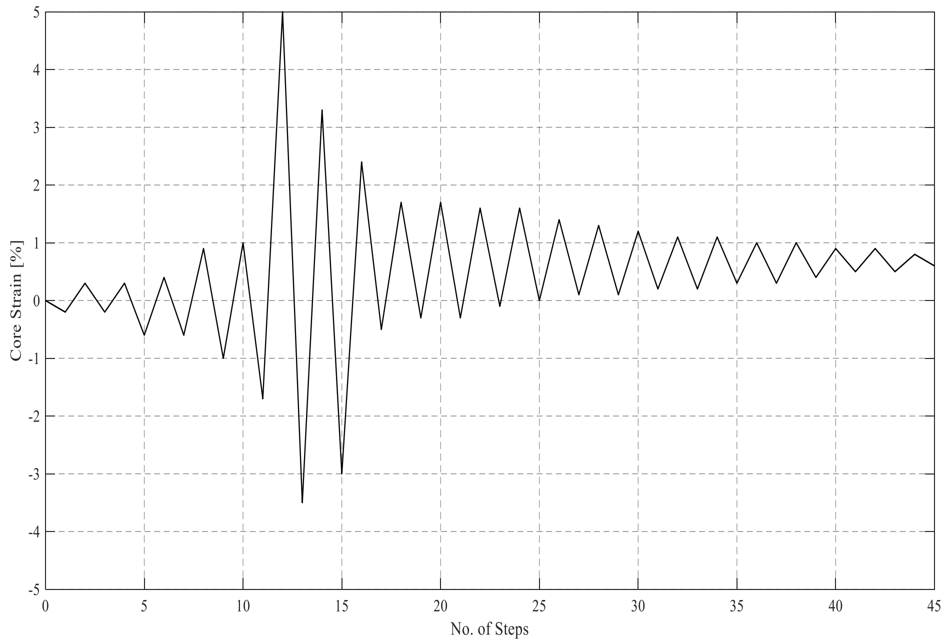

(b)

Figure A.2 Loading protocol developed by Lanning (2016): (a) VTB Proof Protocol and (b) VTB Near-Fault Protocol

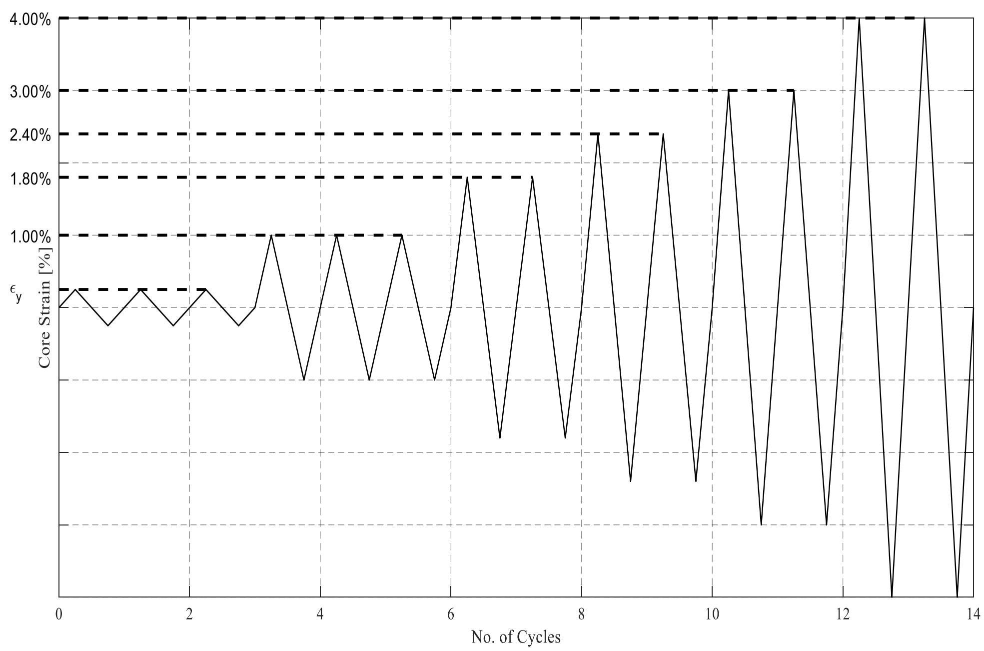

Figure A.3 Loading protocol developed by Aguaguiña (2019)

A.2 Testing Protocols for Components other than BRB

<table>
<tr><th colspan="2">Table A.1 Testing Protocols of Different Components</th></tr>
<tr><th>Protocol Designation</th><th>Protocol Feature</th></tr>
<tr><td>SPD (1987)</td><td>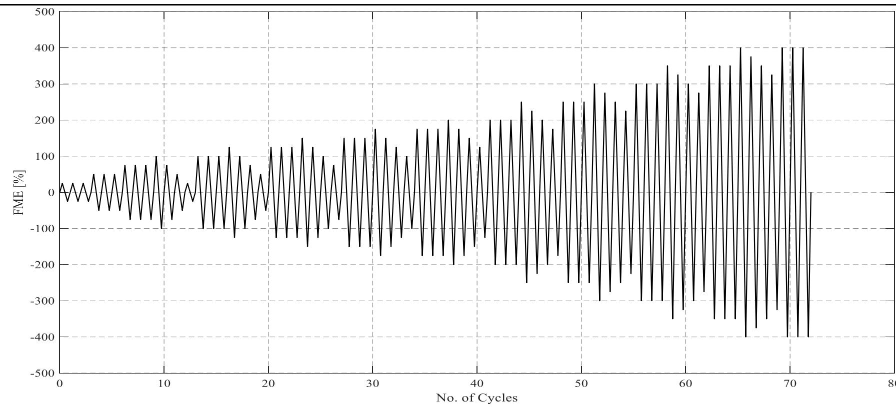

FME = First Major Event = Anticipated Yield Displacement</td></tr>
<tr><td>ATC-24 (ATC-24 1992)</td><td>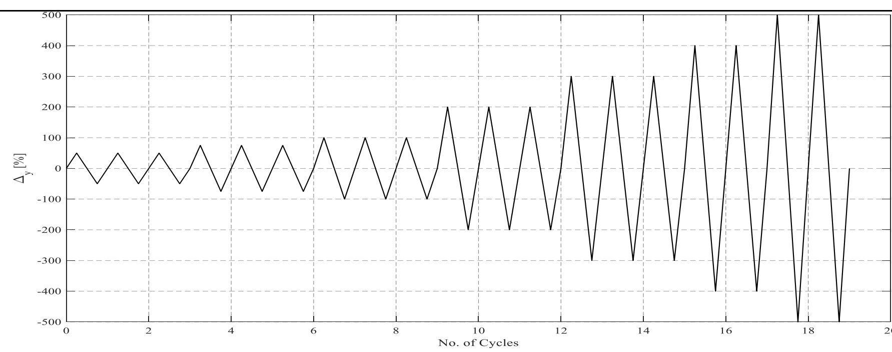

Δ_y = Yield Deformation obtained from a Monotonic Test</td></tr>
<tr><td>SAC Basic Loading Protocol – SAC (1997)</td><td>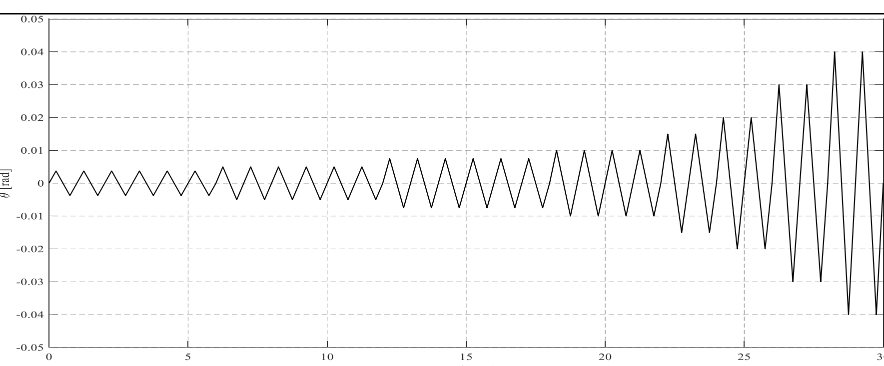

θ = Story Drift</td></tr>
</table>

SAC Near-Fault Loading Protocol – SAC (2000)	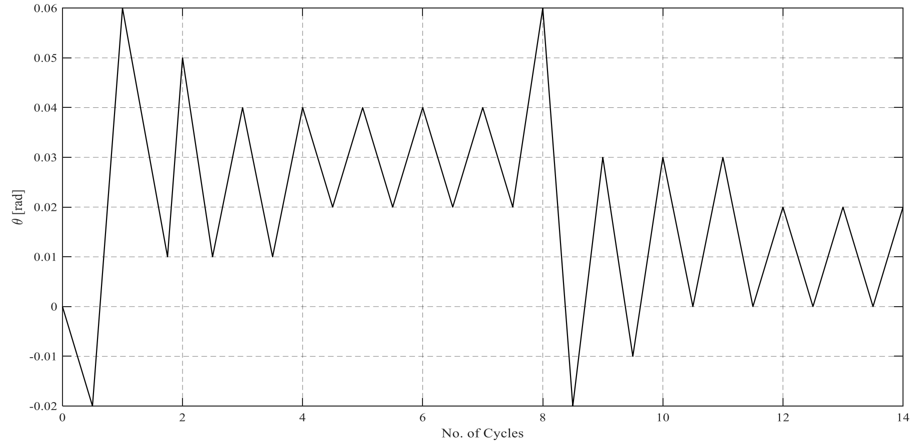 θ = Story Drift
CUREE-Caltech Basic (Krawinkler, Parisi, et al. 2001)	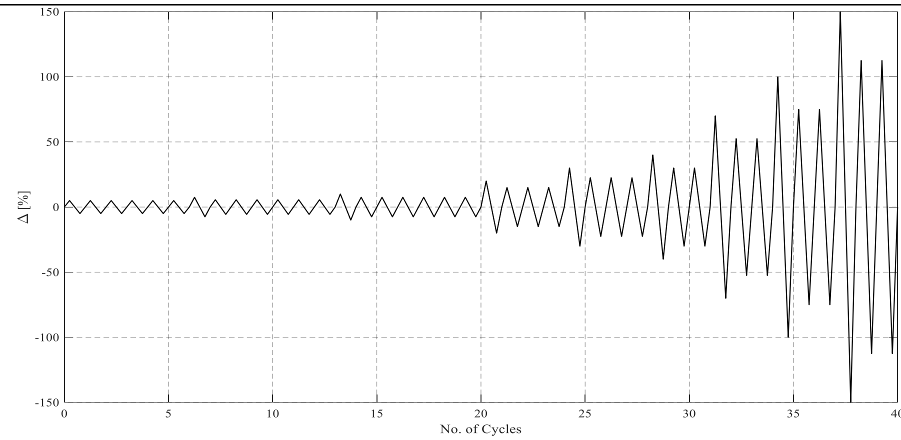 Δ = 60% of Δ_{mon}
CUREE-Caltech Near-Fault (Krawinkler, Parisi, et al. 2001)	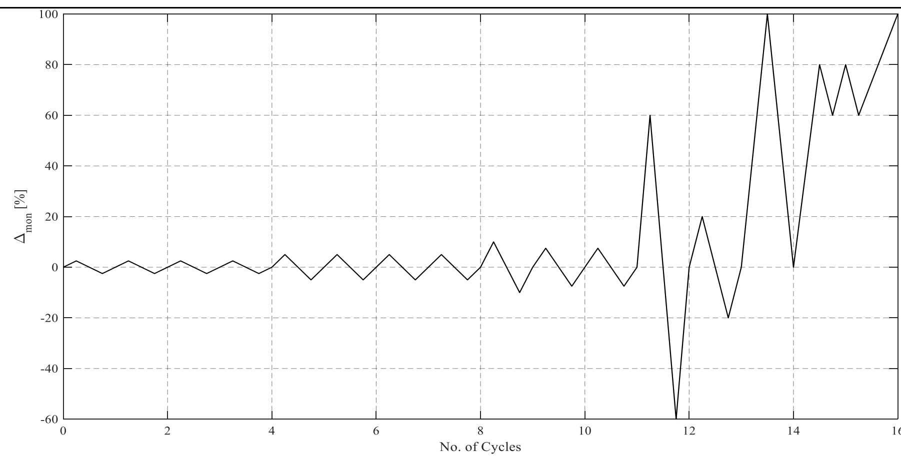

<table>
<tr><td>ISO (ISO 2003)</td><td>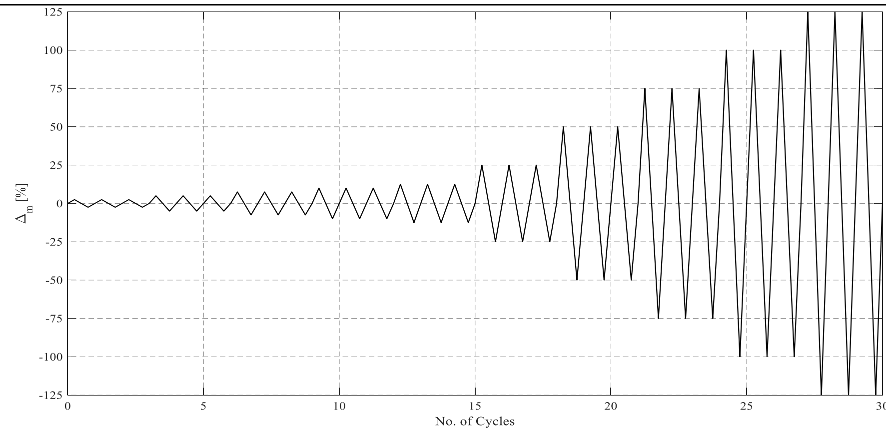

Δ_m = Maximum Displacement at Ultimate Load</td></tr>
<tr><td>EBF Short Link (Richards and Uang 2003)</td><td>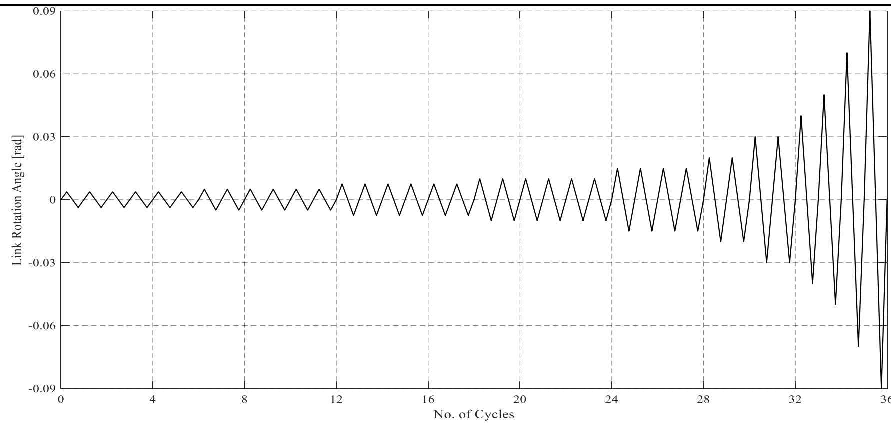

Link rotation angle is vertical displacement of link over length of the link.</td></tr>
<tr><td>FEMA-461 (FEMA 2007)</td><td>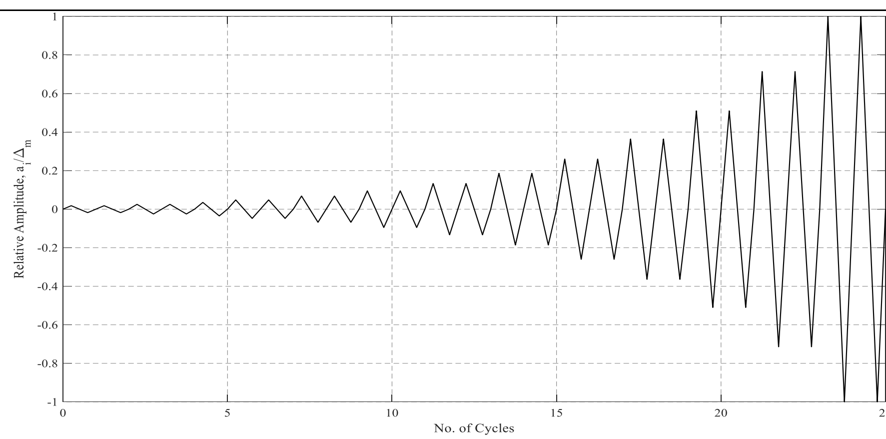
</td></tr>
</table>

	a_i = Amplitude of The Protocol at ith step; Δ_m = Targeted Displacement from Monotonic Test or as Recommended by FEMA
Displacement-Sensitive Nonstructural Component (Shafei and Zareian 2008)	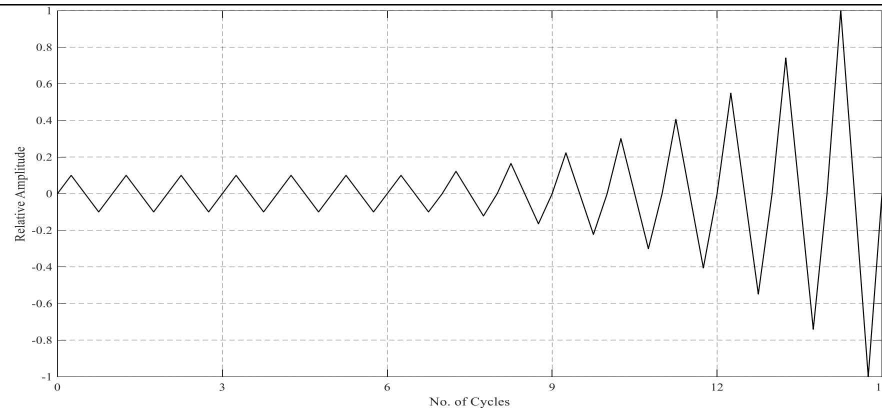
FM-1950 (FM Approvals LLC 2013)	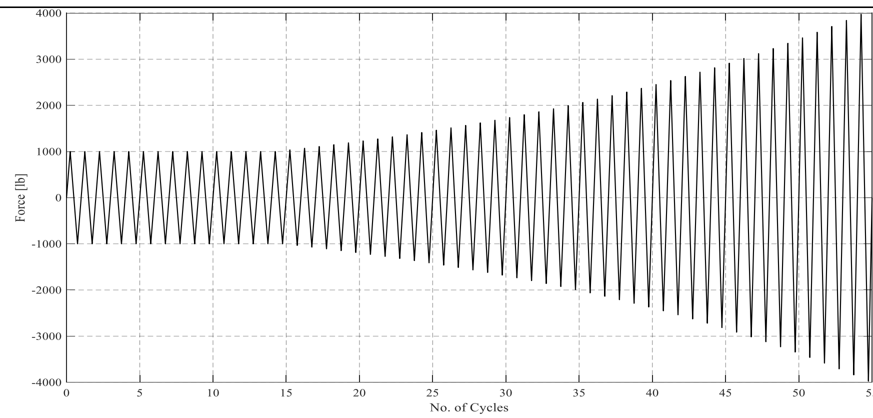
Loading Protocols for European Regions (Mergos and Beyer 2014)	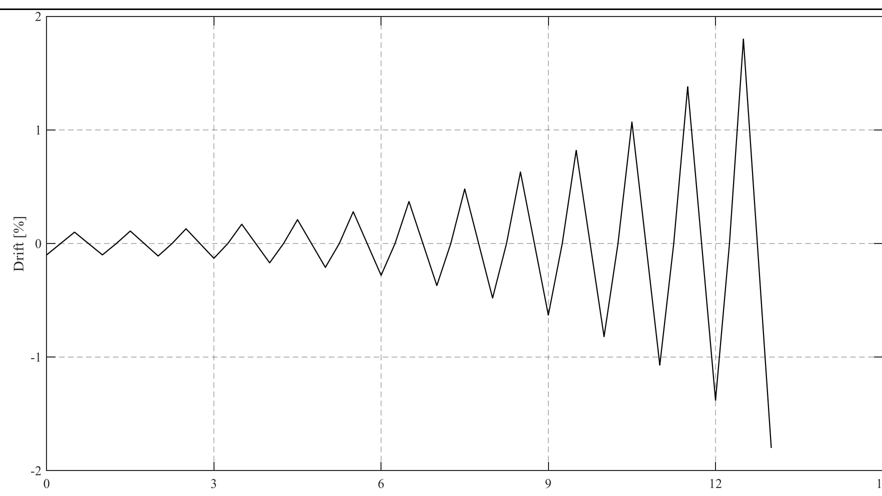

Appendix B SDOF Systems

B.1 Ground Motions for SDOF Systems

Table B.1 Ground Motions Scaled @ T = 0.25 sec						
Event	**Year**	**Station**	**M_w**	**R_{jb} (km)**	**V_{s30} (m/sec.)**	**SF**
N. Palm Springs	1986	North Palm Springs	6.06	0.00	344.67	1.29
Northridge-01	1994	Canyon Country - W Lost Cany	6.69	11.39	325.6	1.47
Chalfant Valley-02	1986	Zack Brothers Ranch	6.19	6.44	316.19	1.21
Coalinga-01	1983	Pleasant Valley P.P. - yard	6.36	7.69	257.38	1.15
Coalinga-05	1983	Burnett Construction	5.77	8.30	352.20	2.38
Managua_ Nicaragua-01	1972	Managua_ ESSO	6.24	3.51	288.77	1.65
Christchurch_ New Zealand	2011	Christchurch Botanical Gardens	6.20	5.52	187.00	1.00
Chalfant Valley-01	1986	Zack Brothers Ranch	5.77	6.07	316.19	2.85
Whittier Narrows-01	1987	Lakewood - Del Amo Blvd	5.99	22.40	267.35	1.99

Parkfield-02_ CA	2004	PARKFIELD - VINEYARD CANYON	6.00	4.36	340.45	3.24
Morgan Hill	1984	Halls Valley	6.19	3.45	281.61	3.45
Westmorland	1981	Parachute Test Site	5.90	16.54	348.69	2.48
Taiwan SMART1(45)	1986	SMART1 M04	7.30	55.55	306.38	3.53
40204628	2007	San Jose; CHP Field Office Junction Ave; 1-story; ground level	5.45	12.55	266.31	3.66
Manjil_ Iran	1990	Abhar	7.37	75.58	302.64	3.18
Imperial Valley-02	1940	El Centro Array #9	6.95	6.09	213.44	1.71
Chi-Chi_ Taiwan	1999	CHY101	7.62	9.94	258.89	2.50
Chi-Chi_ Taiwan-06	1999	CHY002	6.30	49.27	235.13	3.62
Superstition Hills-02	1987	El Centro Imp. Co. Cent	6.54	18.20	192.05	2.16
El Mayor-Cucapah_ Mexico	2010	Chihuahua	7.20	18.21	242.05	2.93

Table B.2 Ground Motions Scaled @ T = 0.50 sec						
Event	**Year**	**Station**	**M_w**	**R_{jb} (km)**	**V_{s30} (m/sec.)**	**SF**
Imperial Valley-06	1979	El Centro Array #8	6.53	3.86	206.08	1.82
Parkfield-02_ CA	2004	Parkfield - Cholame 1E	6.00	1.66	326.64	2.78
Coalinga-05	1983	Burnett Construction	5.77	8.30	352.20	2.68
Whittier Narrows-01	1987	Burbank - N Buena Vista	5.99	20.37	320.57	3.78
Landers	1992	Coolwater	7.28	19.74	352.98	1.86
Coyote Lake	1979	Gilroy Array #4	5.74	4.79	221.78	2.28
Christchurch_ New Zealand	2011	Christchurch Cathedral College	6.20	3.22	198.00	1.44
Kocaeli_ Turkey	1999	Duzce	7.51	13.60	281.86	2.11
Loma Prieta	1989	APEEL 2E Hayward Muir Sch	6.93	52.53	271.06	3.28
Westmorland	1981	Parachute Test Site	5.90	16.54	348.69	2.20
Darfield_ New Zealand	2010	Christchurch Cashmere High School	7.00	17.64	204.00	2.32

Taiwan SMART1(45)	1986	SMART1 M04	7.30	55.55	306.38	3.83
Manjil_ Iran	1990	Abhar	7.37	75.58	302.64	3.95
Iwate_ Japan	2008	Nakashinden Town	6.90	29.37	276.30	2.35
Montenegro_ Yugoslavia	1979	Ulcinj - Hotel Olimpic	7.10	3.97	318.74	2.16
Umbria Marche_ Italy	1997	Castelnuovo-Assisi	6.00	17.28	293.00	3.30
Chi-Chi_ Taiwan-06	1999	CHY002	6.30	49.27	235.13	2.60
Superstition Hills-02	1987	El Centro Imp. Co. Cent	6.54	18.2	192.05	2.22
Chi-Chi_ Taiwan	1999	CHY015	7.62	38.13	228.66	3.59
El Mayor-Cucapah_ Mexico	2010	Chihuahua	7.20	18.21	242.05	2.21

Table B.3 Ground Motions Scaled @ T = 1.00 sec						
Event	**Year**	**Station**	**M_w**	**R_{jb} (km)**	**V_{s30} (ft/sec.)**	**SF**
Whittier Narrows-01	1987	LA - Fletcher Dr	5.99	11.07	329.06	3.10
Managua_ Nicaragua-02	1972	Managua_ ESSO	5.20	4.33	288.77	3.51
Imperial Valley-06	1979	Aeropuerto Mexicali	6.53	0.00	259.86	1.85
Coyote Lake	1979	Gilroy Array #4	5.74	4.79	221.78	2.33
Duzce_ Turkey	1999	Duzce	7.14	0.00	281.86	1.45
Northridge-01	1994	LA - Fletcher Dr	6.69	25.66	329.06	3.53
Coalinga-01	1983	Pleasant Valley P.P. - bldg	6.36	7.69	257.38	1.30
Loma Prieta	1989	APEEL 2E Hayward Muir Sch	6.93	52.53	271.06	3.00
Parkfield-02_ CA	2004	Parkfield - Fault Zone 4	6.00	0.73	220.75	3.75
Dinar_ Turkey	1995	Dinar	6.40	0.00	219.75	1.28
Westmorland	1981	Parachute Test Site	5.90	16.54	348.69	3.21

40204628	2007	San Jose; CHP Field Office Junction Ave; 1-story; ground level	5.45	12.55	266.31	3.97
Taiwan SMART1(45)	1986	SMART1 C00	7.30	56.01	309.41	3.07
Imperial Valley-02	1940	El Centro Array #9	6.95	6.09	213.44	1.64
Taiwan SMART1(45)	1986	SMART1 I02	7.30	56.10	309.41	2.73
Chuetsu-oki_ Japan	2007	Kubikiku Hyakken Joetsu City	6.80	20.71	342.74	2.62
Chi-Chi_ Taiwan	1999	TCU055	7.62	6.34	359.13	2.60
Landers	1992	Desert Hot Springs	7.28	21.78	359.00	3.35
Superstition Hills-02	1987	El Centro Imp. Co. Cent	6.54	18.20	192.05	2.49
Kobe_ Japan	1995	Sakai	6.90	28.08	256.00	4.06

Table B.4 Ground Motions Scaled @ T = 2.00 sec						
Event	**Year**	**Station**	**M_w**	**R_{jb} (km)**	**V_{s30} (ft/sec.)**	**SF**
Imperial Valley-06	1979	El Centro Array #8	6.53	3.86	206.08	1.35
Managua_ Nicaragua-02	1972	Managua_ ESSO	5.20	4.33	288.77	2.72
Christchurch_ New Zealand	2011	Christchurch Botanical Gardens	6.20	5.52	187.00	1.25
Parkfield-02_ CA	2004	Parkfield - Fault Zone 15	6.00	0.80	307.59	4.15
Northridge-01	1994	Canoga Park - Topanga Can	6.69	0.00	267.49	1.51
Taiwan SMART1(40)	1986	SMART1 I02	6.32	58.85	309.41	2.62
Cape Mendocino	1992	Fortuna Fire Station	7.01	16.54	355.18	1.61
Kocaeli_ Turkey	1999	Yarimca	7.51	1.38	297.00	1.60
Loma Prieta	1989	Hollister City Hall	6.93	27.33	198.77	2.21
Westmorland	1981	Parachute Test Site	5.90	16.54	348.69	1.74
Landers	1992	Yermo Fire Station	7.28	23.62	353.63	2.15

Darfield_ New Zealand	2010	Kaiapoi North School	7.00	30.53	255.00	1.82
Taiwan SMART1(45)	1986	SMART1 O07	7.30	54.17	314.33	3.09
Imperial Valley-02	1940	El Centro Array #9	6.95	6.09	213.44	1.95
Chi-Chi_ Taiwan-06	1999	CHY036	6.30	45.10	233.14	4.05
Chi-Chi_ Taiwan	1999	CHY088	7.62	37.48	318.52	3.01
Superstition Hills-02	1987	El Centro Imp. Co. Cent	6.54	18.20	192.05	2.15
El Mayor-Cucapah_ Mexico	2010	Chihuahua	7.20	18.21	242.05	2.92
Chuetsu-oki_ Japan	2007	Niigata Nishi Kaba District	6.80	27.83	254.68	2.95
Kobe_ Japan	1995	Sakai	6.90	28.08	256.00	3.41

B.2 Dissipated Energy Plots

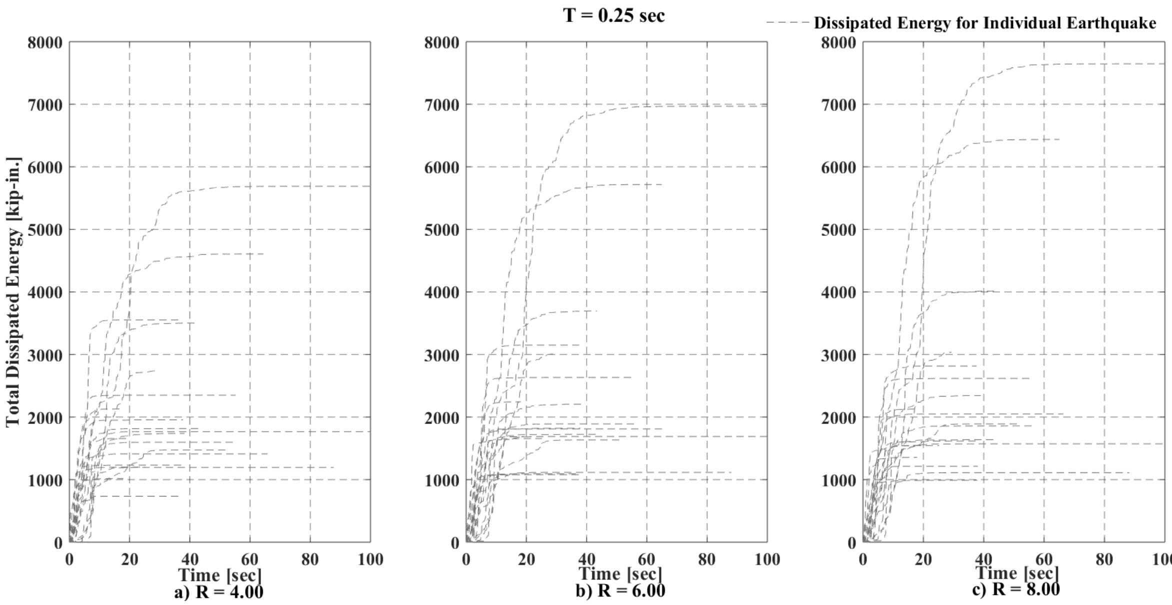

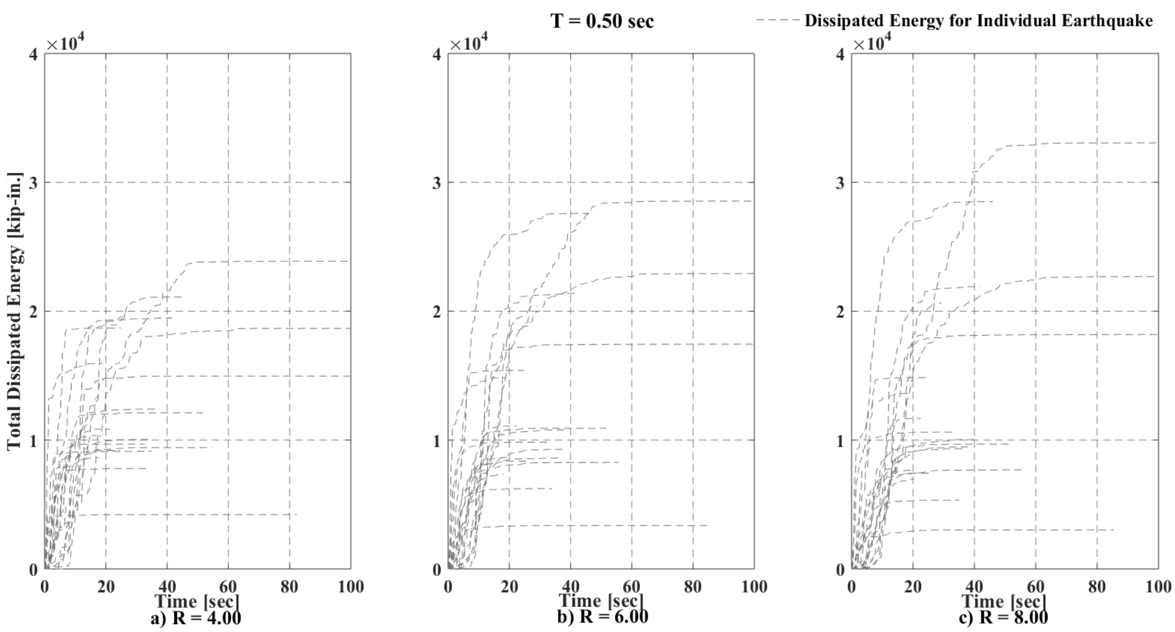

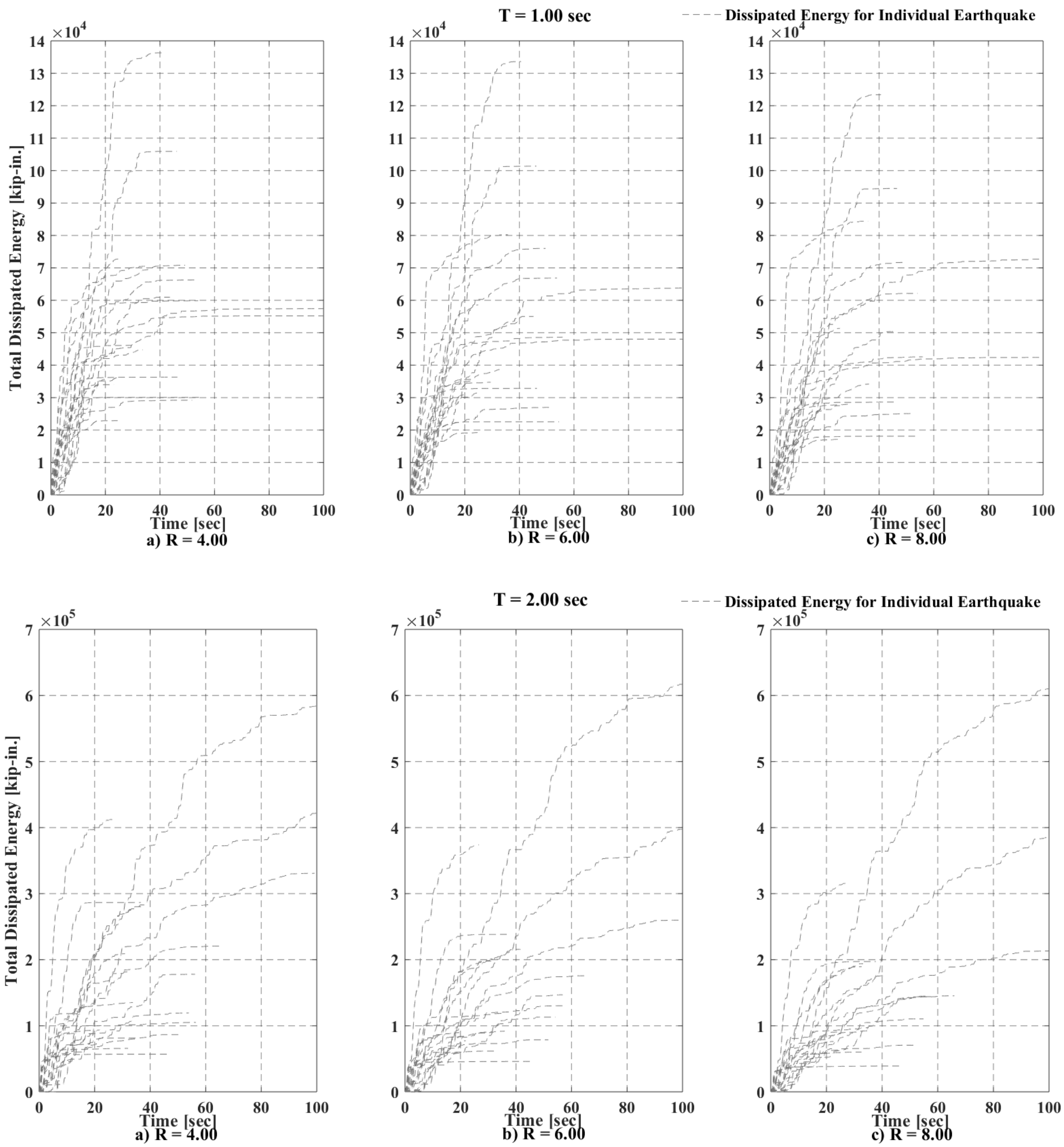

Figure B.1 Dissipated energy in equivalent nonlinear single-degree-of-freedom systems

B.3 Energy Quantification Factor Plots

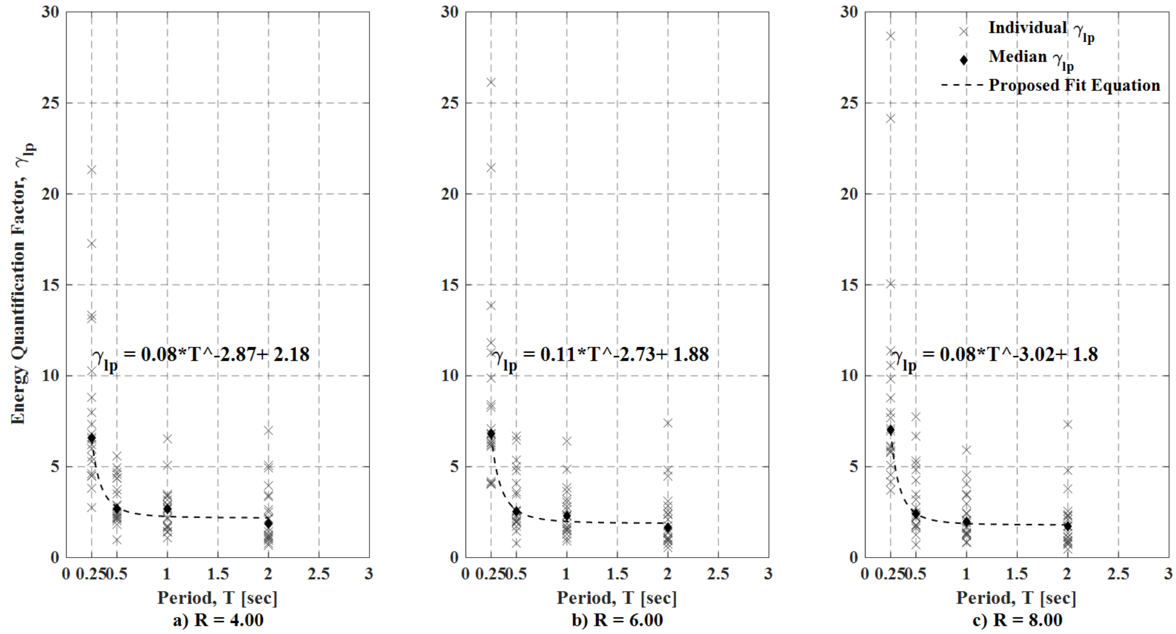

Figure B.2 Medians of energy quantification factor, (γ_{lp})s for a) R = 4.00, b) R = 6.00 and c) R = 8.00

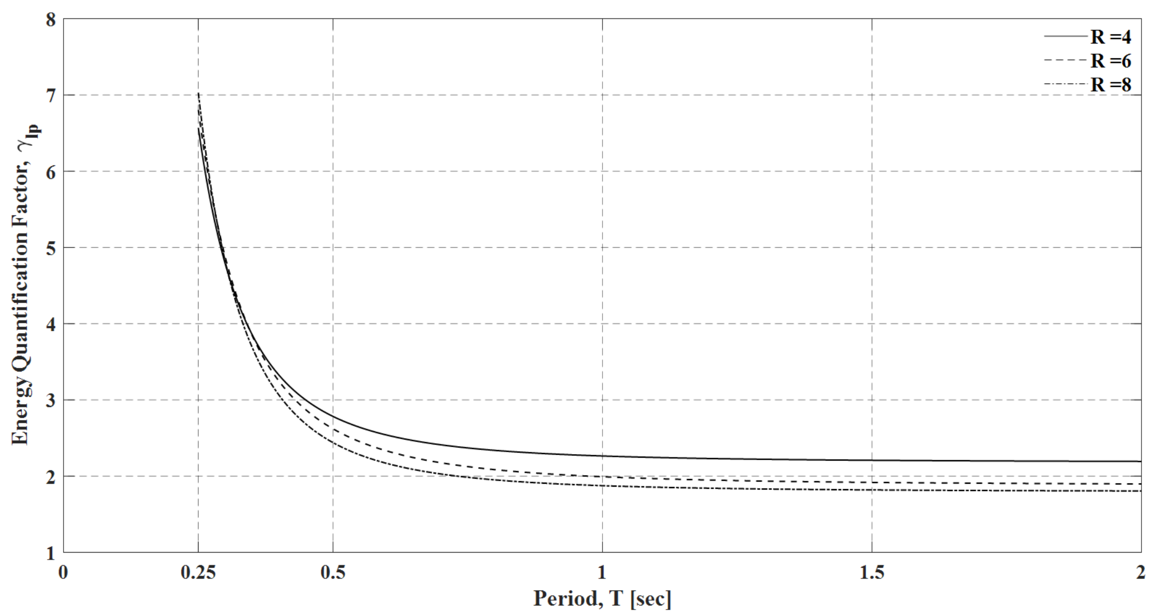

Figure B.3 Fit line for proposed equations of γ_{lp} for different R-factors

B.4 Rise Time Plots

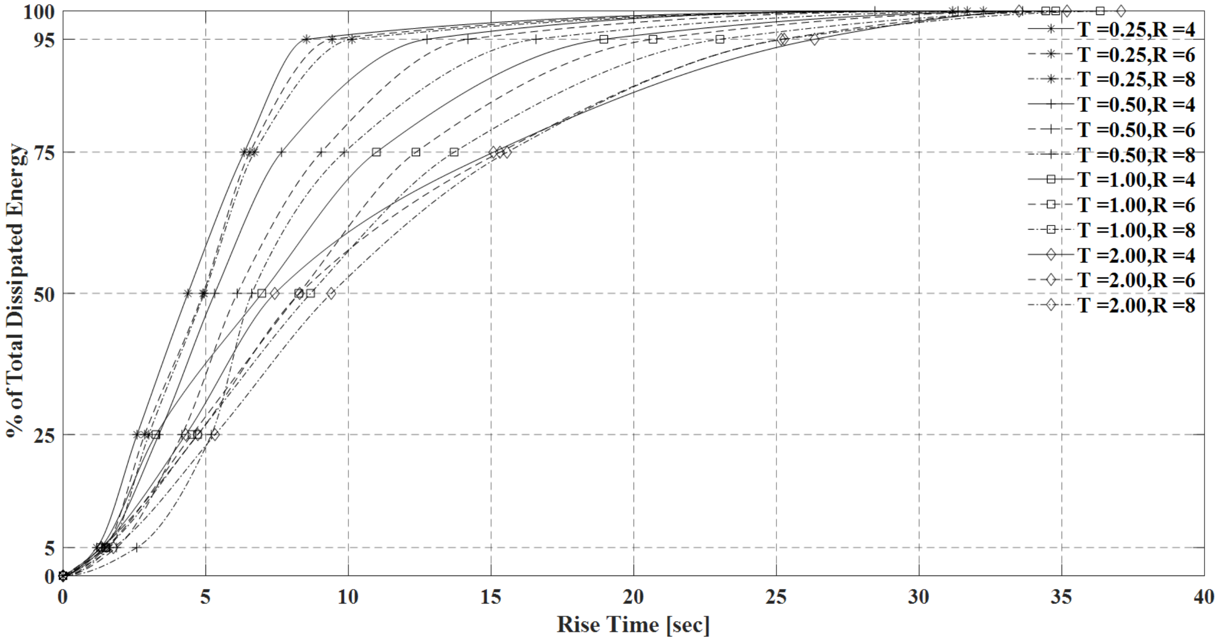

Figure B.4 Medians of Rise Time

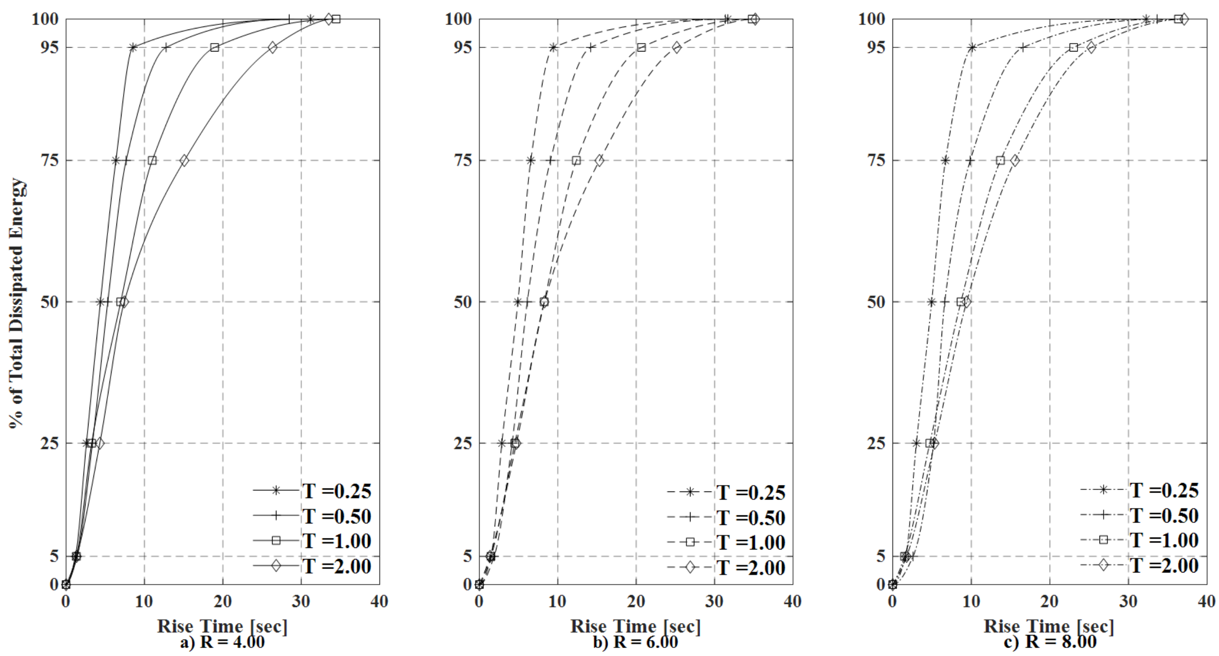

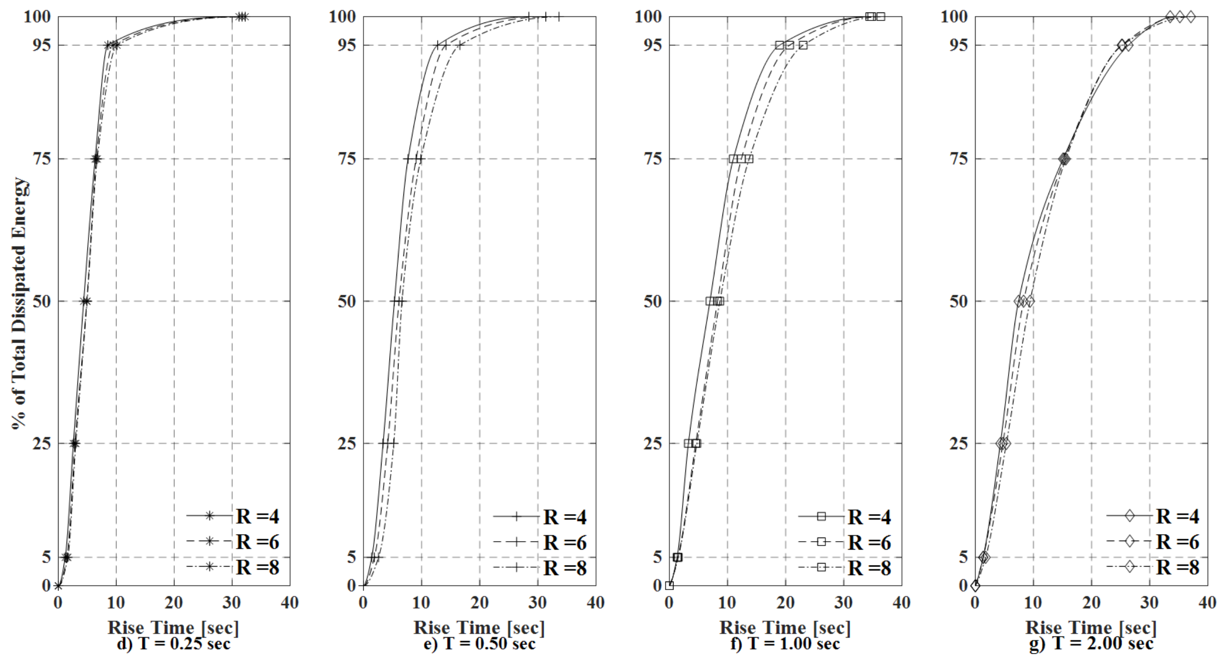

Figure B.5 Medians of rise time for (a) R = 4.0 with different Ts; (b) R = 6.0 with different Ts; (c) R = 8.0 with different Ts; (d) T = 0.25 sec with different R values; (e) T = 0.50 sec with different R values; (f) T = 1.00 sec with different R values; (g) T = 2.00 sec with different R values

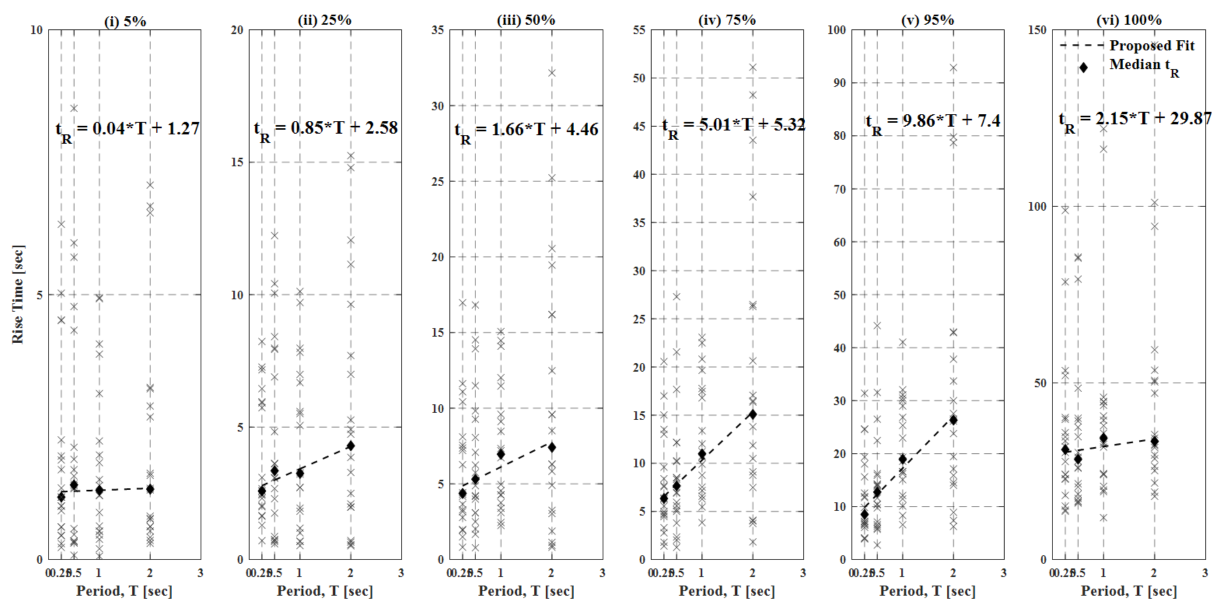

a) R = 4.00

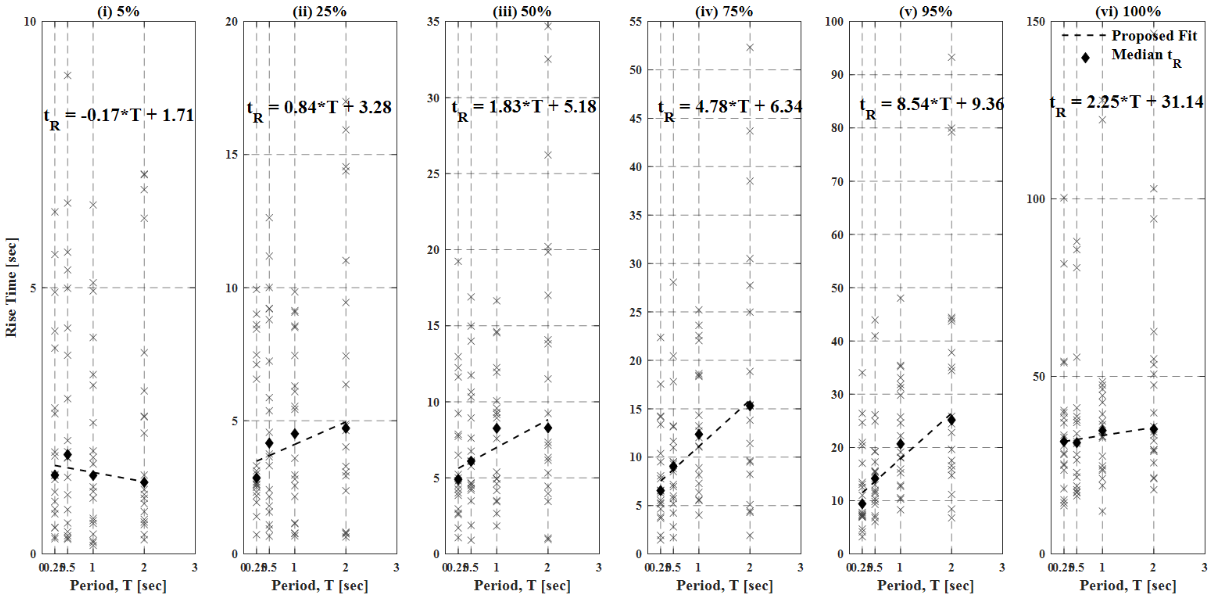

b) R = 6.00

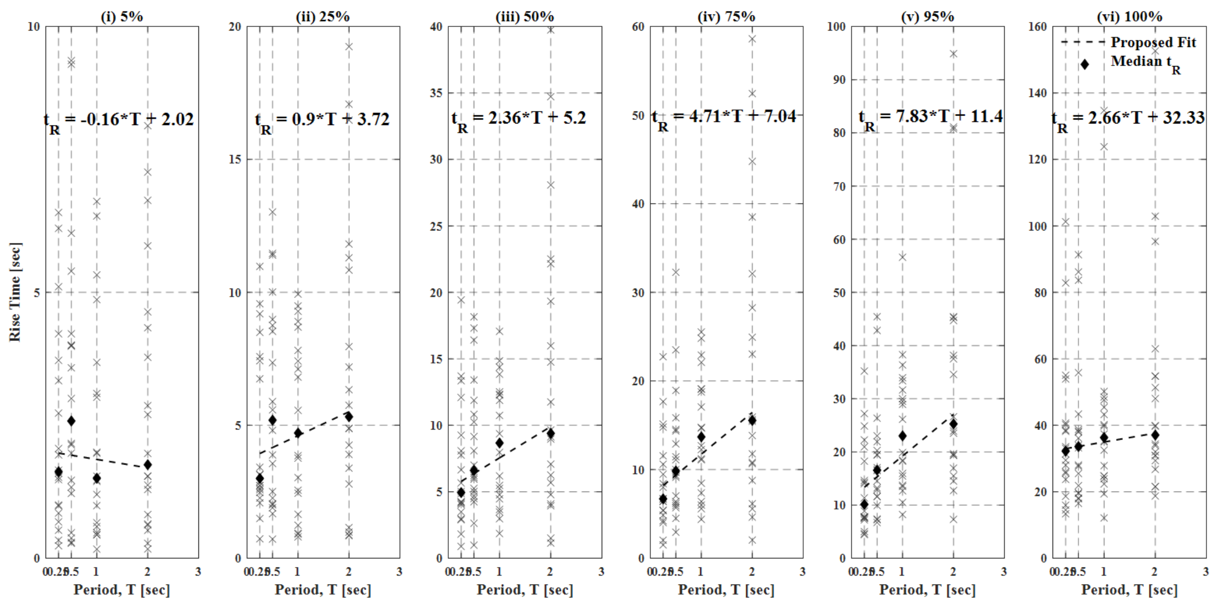

c) R = 8.00

Figure B.6 Medians of rise time, (t_R)s for a) R = 4.00, b) R = 6.00 and c) R = 8.00

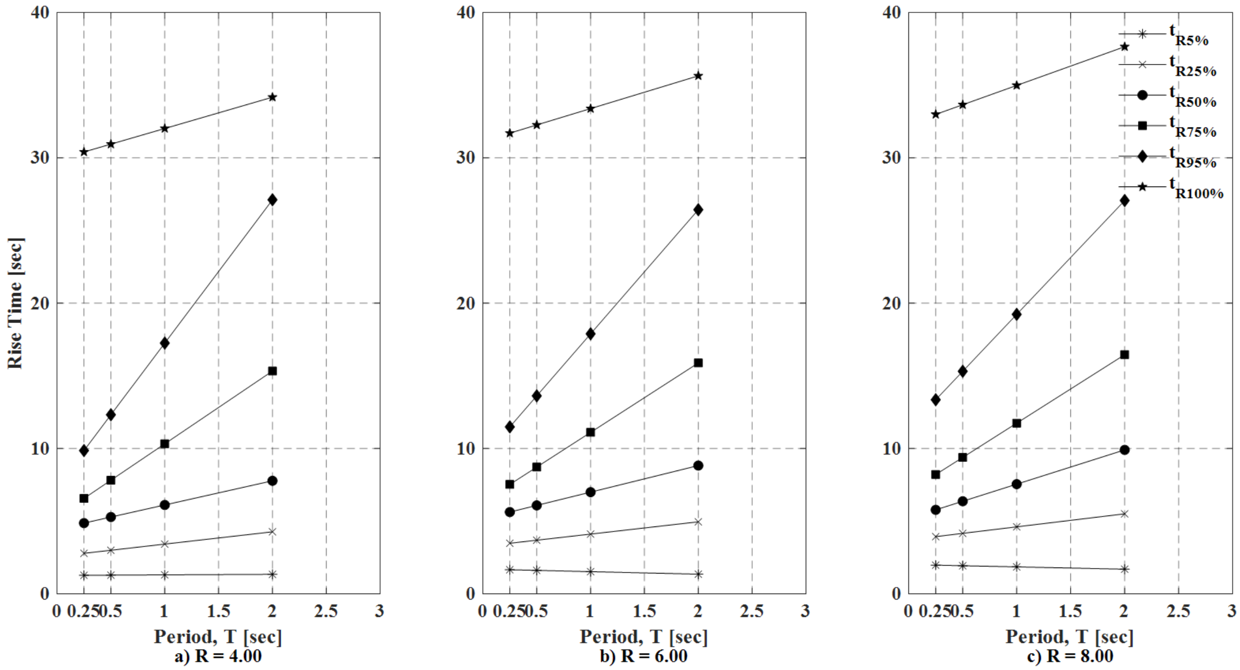

Figure B.7 Proposed fit equations for rise time, t_R when a) R = 4.00, b) R = 6.00 and c) R = 8.00

Appendix C MDOF Systems: Prototype Steel Moment Frame equipped with BRB

C.1 Ground Motions for 3- and 6-Storey Prototype Frame Analysis

Table C.1 Scaled Ground Motions

Event	Year	Station	M_w	R_{jb} (km)	V_{s30} (ft/sec.)	SF	
						3-Story	6-Story
Kobe_ Japan	1995	Kakogawa	6.90	22.50	312.00	2.91	2.98
Kocaeli_ Turkey	1999	Duzce	7.51	13.60	281.86	1.97	1.93
Chi-Chi_ Taiwan	1999	CHY036	7.62	16.04	233.14	1.74	1.68
Duzce_ Turkey	1999	Bolu	7.14	12.02	293.57	1.01	1.00
Imperial Valley-06	1979	El Centro Array #8	6.53	3.86	206.08	1.56	1.56
Yountville	2000	Napa Fire Station #3	5.00	8.48	328.57	1.69	1.71
Northern Calif-03	1954	Ferndale City Hall	6.50	26.72	219.31	2.89	2.75
Victoria_ Mexico	1980	Chihuahua	6.33	18.53	242.05	3.37	3.30
Westmorland	1981	Westmorland Fire Sta	5.90	6.18	193.67	1.44	1.42

Taiwan SMART1(40)	1986	SMART1 O03	6.32	59.74	278.32	2.99	2.90
Coalinga-01	1983	Pleasant Valley P.P. - yard	6.36	7.69	257.38	1.01	1.01
Parkfield-02_ CA	2004	PARKFIELD - VINEYARD CANYON	6.00	4.36	340.45	3.12	3.13
Niigata_ Japan	2004	NIG012	6.63	56.07	229.95	3.68	3.89
Morgan Hill	1984	Halls Valley	6.19	3.45	281.61	3.62	3.64
Chuetsu-oki_ Japan	2007	Kawanishi Izumozaki	6.80	0.00	338.32	1.82	1.82
Chalfant Valley-02	1986	Zack Brothers Ranch	6.19	6.44	316.19	1.36	1.35
Whittier Narrows-01	1987	Bell Gardens - Jaboneria	5.99	10.31	267.13	3.17	3.26
Darfield_ New Zealand	2010	LINC	7.00	5.07	263.20	1.68	1.70
Superstition Hills-02	1987	El Centro Imp. Co. Cent	6.54	18.20	192.05	1.87	1.86
Christchurch_ New Zealand	2011	Styx Mill Transfer Station	6.20	11.24	247.50	2.71	2.67

El Mayor-Cucapah_ Mexico	2010	Westside Elementary School	7.20	10.31	242.00	2.35	2.36
40204628	2007	San Jose; CHP Field Office Junction Ave; 1-story; ground level	5.45	12.55	266.31	4.37	4.48
Northridge-01	1994	Canyon Country - W Lost Cany	6.69	11.39	325.60	1.58	1.57
Managua_ Nicaragua-02	1972	Managua_ ESSO	5.20	4.33	288.77	3.05	3.01

C.2 Floor-wise Energy Distribution

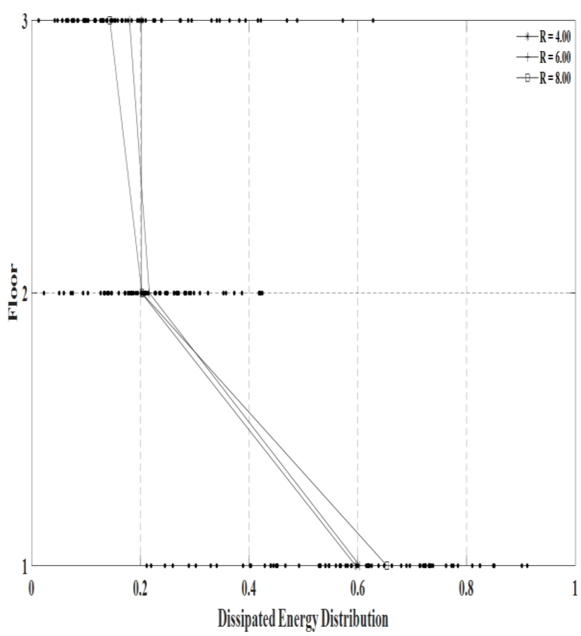

(a)

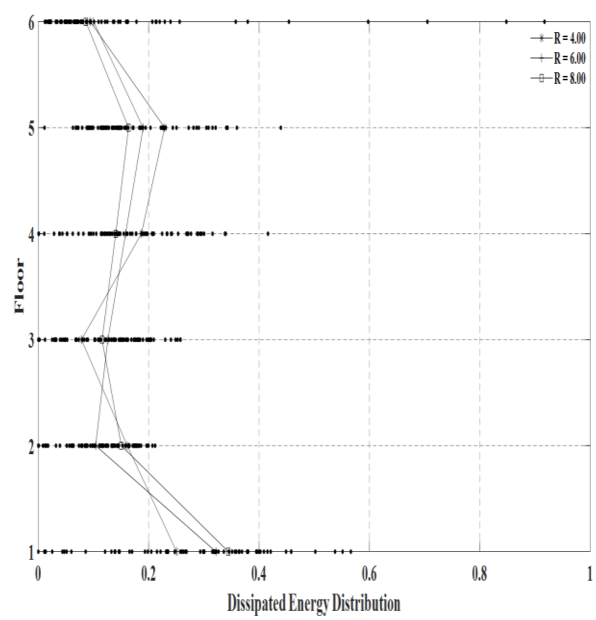

(b)

Figure C.1 Energy distribution in (a) 3-Storey and (b) 6-Storey Prototype Frame

Appendix D 5-Story Prototype Frame equipped with BRB

D.1 Ground Motions for 5-Story Prototype Frame Analysis

Table D.1 Scaled Ground Motions						
Event	**Year**	**Station**	M_w	R_{jb} (km)	V_{s30} (m/sec.)	**SF**
Northridge-01	1994	Playa Del Rey - Saran	6.69	24.42	345.72	2.88
Kobe_ Japan	1995	Amagasaki	6.90	11.34	256.00	1.01
Kocaeli_ Turkey	1999	Yarimca	7.51	1.38	297.00	1.19
Friuli_ Italy-01	1976	Codroipo	6.50	33.32	249.28	4.42
Friuli_ Italy-02	1976	Buia	5.91	10.99	310.68	3.63
Tabas_ Iran	1978	Boshrooyeh	7.35	24.07	324.57	3.65
Chi-Chi_ Taiwan	1999	TCU083	7.62	80.18	354.63	2.91
St Elias_ Alaska	1979	Icy Bay	7.54	26.46	306.37	2.41
Imperial Valley-06	1979	El Centro - Meloland Geot. Array	6.53	0.07	264.57	1.09
Hector Mine	1999	Mecca - CVWD Yard	7.13	91.96	318.00	2.61

Northern Calif-03	1954	Ferndale City Hall	6.50	26.72	219.31	1.50
Chi-Chi_ Taiwan-03	1999	CHY025	6.20	27.88	277.50	2.81
Chi-Chi_ Taiwan-04	1999	CHY015	6.20	50.02	228.66	2.86
Westmorland	1981	Parachute Test Site	5.90	16.54	348.69	1.56
Coalinga-01	1983	Cantua Creek School	6.36	23.78	274.73	1.77
Taiwan SMART1(40)	1986	SMART1 M02	6.32	59.67	306.78	1.78
Taiwan SMART1(45)	1986	SMART1 I02	7.30	56.10	309.41	1.74
Montenegro_ Yugoslavia	1979	Ulcinj - Hotel Olimpic	7.10	3.97	318.74	1.24
Chalfant Valley-01	1986	Bishop - LADWP South St	5.77	23.38	303.47	4.36
Iwate_ Japan	2008	Furukawa Osaki City	6.90	31.07	248.19	1.49
Superstition Hills-02	1987	El Centro Imp. Co. Cent	6.54	18.20	192.05	1.37
Loma Prieta	1989	Sunnyvale - Colton Ave.	6.93	23.92	267.71	1.72
Big Bear-01	1992	San Bernardino - E & Hospitality	6.46	34.98	296.97	3.17
Point Mugu	1973	Port Hueneme	5.65	15.48	248.98	3.72

D.2 Floor-wise Dissipated Energy Distribution

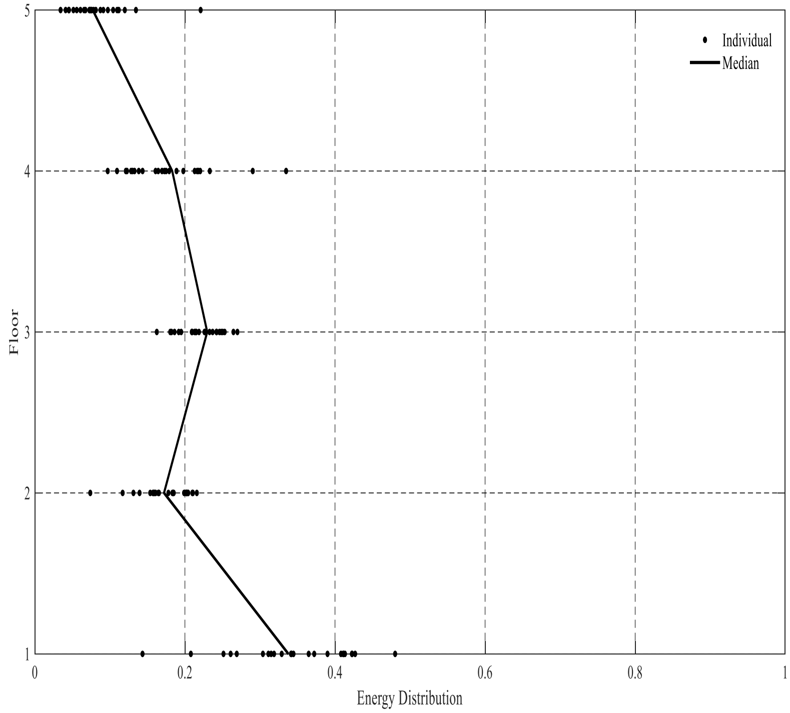

Figure D.1 Floor-wise Dissipated Energy Distribution in 5-Storey Prototype Frame

D.3 Dissipated Energy Time History Comparison

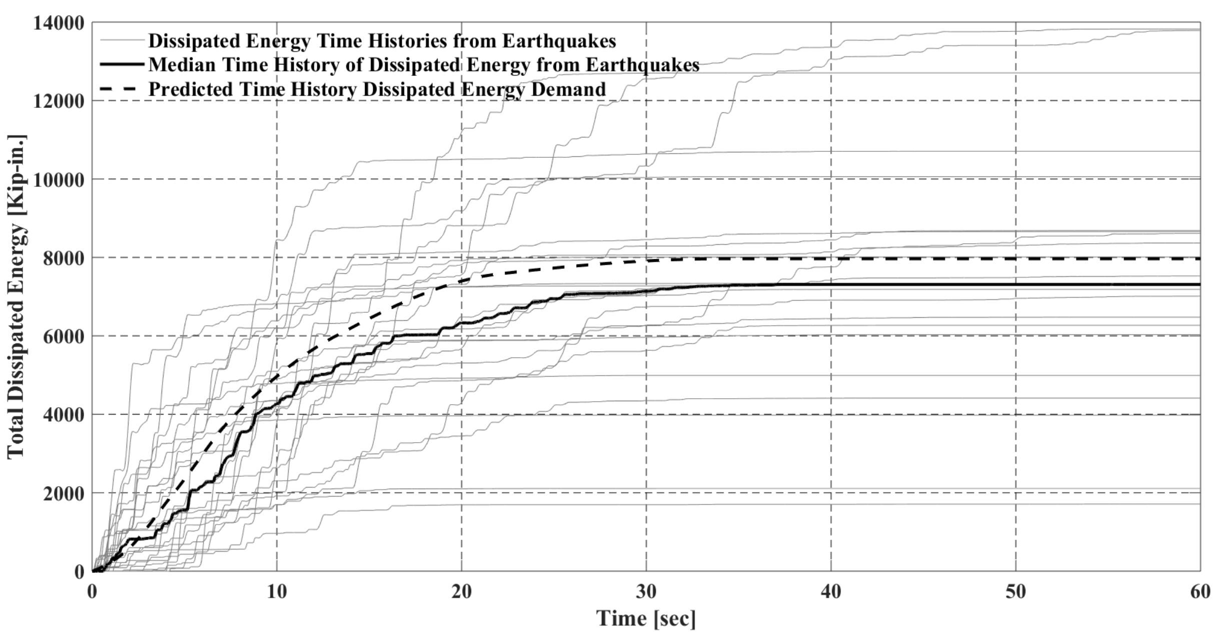

(a)

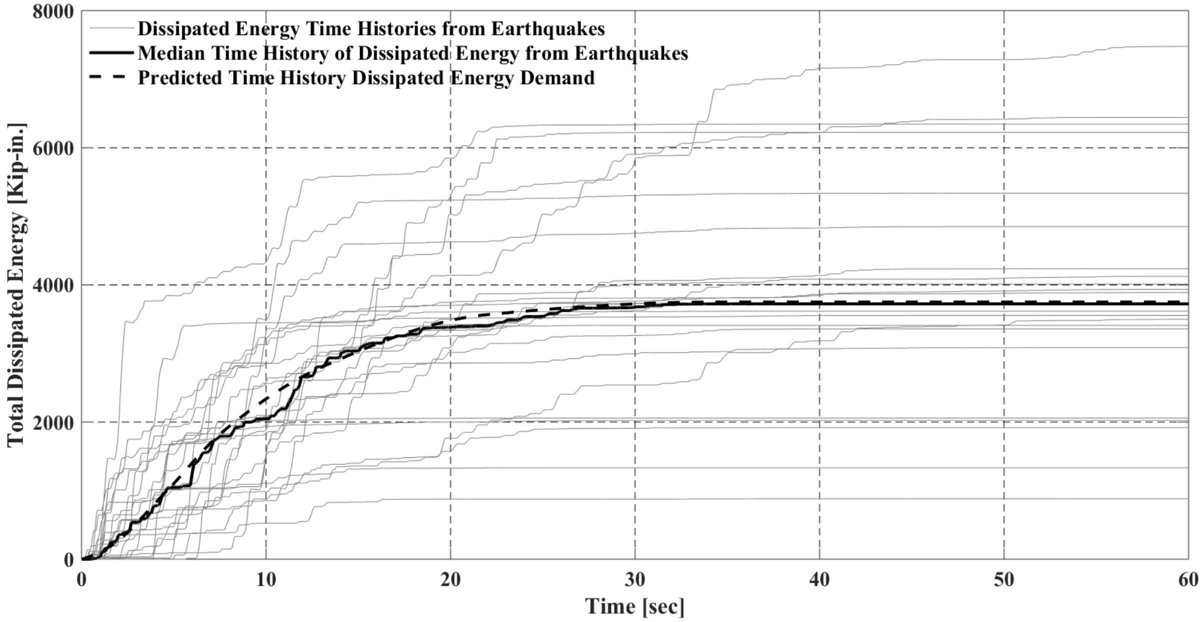
Dissipated Energy Time Histories from Earthquakes
Median Time History of Dissipated Energy from Earthquakes
Predicted Time History Dissipated Energy Demand
Total Dissipated Energy [Kip-in.]
Time [sec]
0
2000
4000
6000
8000
0
10
20
30
40
50
60

(b)

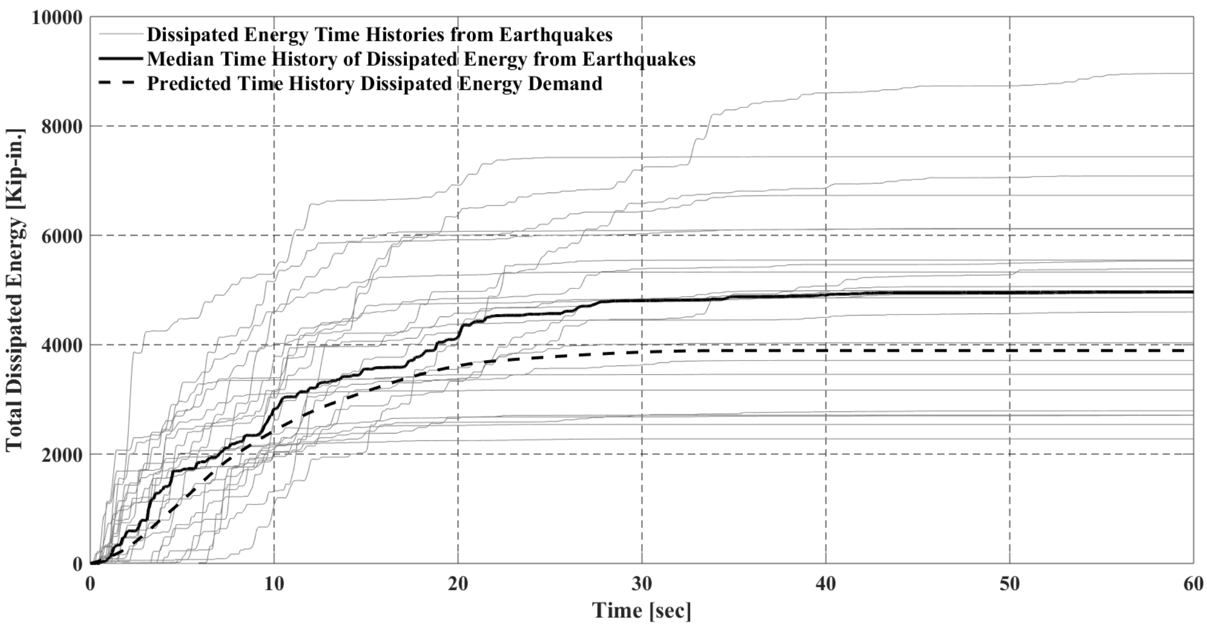
Dissipated Energy Time Histories from Earthquakes
Median Time History of Dissipated Energy from Earthquakes
Predicted Time History Dissipated Energy Demand
Total Dissipated Energy [Kip-in.]
Time [sec]
0
2000
4000
6000
8000
10000
0
10
20
30
40
50
60

(c)

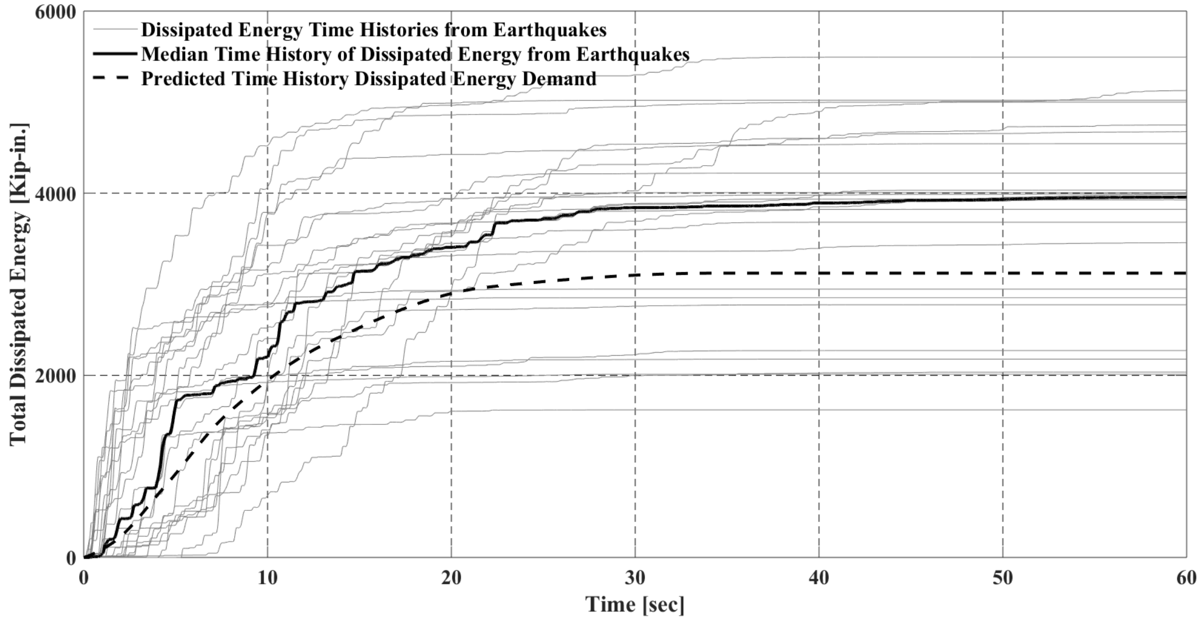

(d)

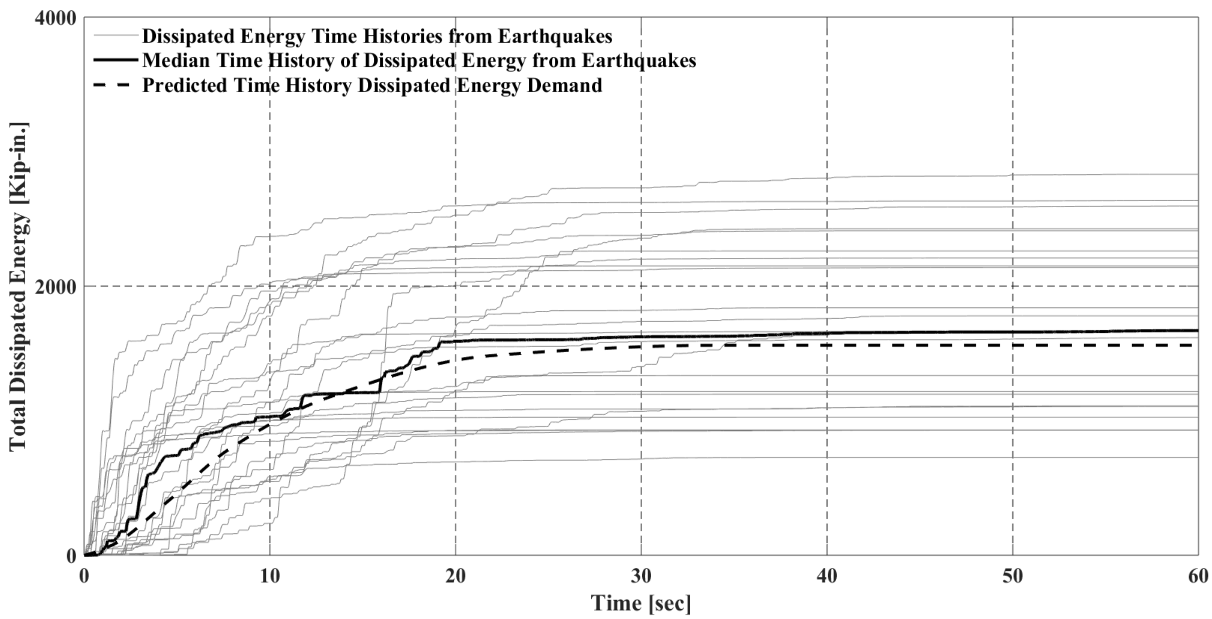

(e)

Figure D.2 Comparison of Dissipated Energy Time History Demand of (a) 1st floor, (b) 2nd floor, (c) 3rd floor (d) 4th floor and (e) 5th floor BRBs